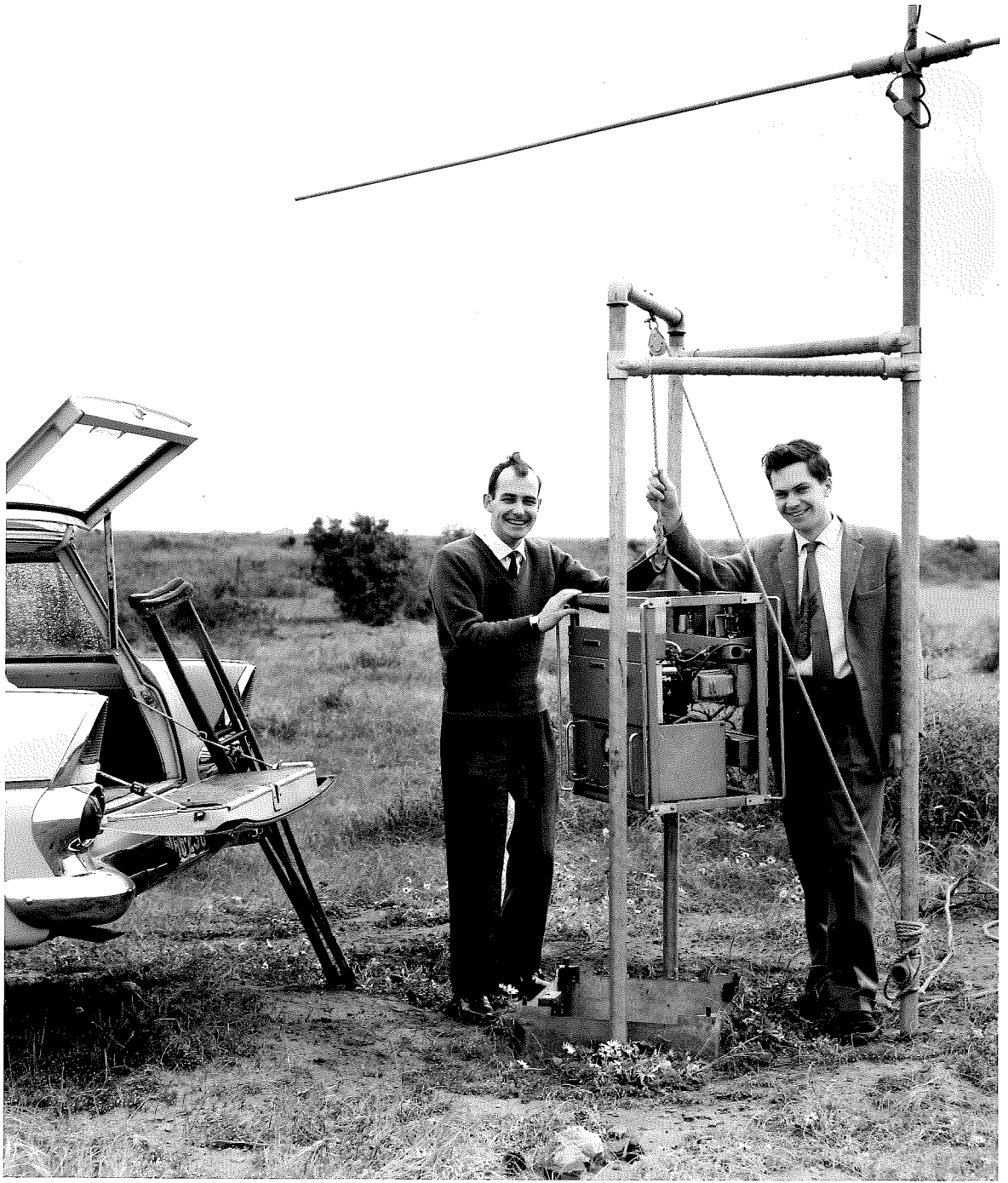# ATMOSPHERIC TURBULENCE

IN THE

METEOR REGION

by

R. G. Roper, B. Sc.

A THESIS

PRESENTED FOR THE DEGREE OF

DOCTOR OF PHILOSOPHY

IN THE

UNIVERSITY OF ADELAIDE.

NOVEMBER, 1962.

CONTENTS

SUMMARY

A re-examination is made of work published by others on turbulence in the upper atmosphere at heights ranging from 80 to 100km. These results are found to be explicable in terms of a modified Kolmogoroff spectrum.

A method is described for obtaining data for the investigation of turbulence in the meteor region from the line of sight drifts of ionized meteor trails as measured by a spaced-station radio technique. The application and limitations of this technique are discussed in some detail.

The results of a thirteen month survey of atmospheric turbulence at meteor heights from December, 1960 to December, 1961 are presented. Direct observations are made on the scales from 100 metres to 3km, and of the characteristic velocity of the energy bearing eddies. The results from this survey are also found to follow the Kolmogoroff law, modified by the effects of a vertical shear and an eddy subrange arising from the action of buoyancy forces. At scales less than 1km the buoyancy subrange predominates. If the measured wind velocity differentials pertaining to this small-scale region are interpreted in terms of a Kolmogoroff spectrum, the turbulent dissipation rate ϵ is found to be approximately 50

ergs/gm/sec, which is of the same order as the 70 ergs/gm/sec found by others from the photographic observations of the diffusion of sodium trails and visual meteor trails (The maximum scale size that can be measured by this photographic technique is limited by visibility to about 1km). Once allowance is made for the buoyancy subrange, the scales to 6km are probably isotropic, and subject to a small vertical shear, while the large scales, whose characteristic size is determined by extrapolation from the scales observed, are distinctly anisotropic, with a vertical scale of 6km and a horizontal scale of the order of 100km.

The turbulent dissipation rate calculated from the change in velocity difference with separation for the scales from 1 to 3km shows a marked seasonal variation, with a maximum of approximately 350 ergs/gm/sec in spring and autumn, and a minimum of about 180 ergs/gm/sec in summer and winter. An attempt has been made to ascribe an absolute value to the turbulent dissipation rate via an expression which involves the height shear. Because of the low echo rate achieved, no information about the diurnal variation in ϵ is forthcoming. However, since the diurnal variation of the characteristic velocity of the energy bearing eddies is of the order of 2:1, a diurnal variation in the turbulent dissipation rate is expected. The dissipation mechanism is

somewhat obscure, since energy is extracted from all scales by the buoyancy subrange. The origin of the large-scale anisotropic eddies is still in doubt, although there is some correlation between the characteristic velocities of these eddies and the diurnal variation of the mean wind.

A preliminary estimate of the turbulence Reynolds number appropriate to the meteor region is given as 7×10^3.

iv

Preface

To the best of the author's knowledge and belief, this thesis contains no material previously published or written by another person, except when due reference is made in the text.

Portions of Chapters III, VI, VII and VIII are claimed as original work, as are Chapters IX, X and XI. The author was responsible for the design and construction of the Three-station Wind Recording Rack and the equipment housed at the outstations, for the design of the main station receivers, for the reading of the three-station wind films, and for the reduction of the data so obtained. All programming of the mean wind and turbulence data for execution on the University's IBM 1620 electronic computer was the work of the author.

This thesis contains no material which has been presented by the author for the award of any other degree or diploma in any University.

Acknowledgements

CHAPTER I.

Turbulence in the Ionosphere

1.1 Historical

Ionospheric irregularities were first studied by Ratcliff and Pawsey at Cambridge some 30 years ago. Recent discussion of turbulence in the ionosphere dates from the discovery about ten years ago of the phenomenon of VHF scatter transmission. Until then, all irregularities were assumed to have a Gaussian distribution of electron density, and to occur in an inherently stable ionosphere. While experiments were being carried out in propagation of radio waves beyond the visible horizon at VHF, scatter from the troposphere was evident; this was readily explained in terms of atmospheric turbulence. Since ionospheric scatter also occurs at VHF, ionospheric phenomena were further investigated in the light of turbulence theory.

1.2 General

Mechanisms of two types can lead to turbulence. The breakdown of primary instabilities in ionization can give rise to turbulent "motions" of the ionization; secondary instabilities can arise from geophysical motions, which will also cause

turbulent motion of the ionization. The first gives rise to apparent motions, these being caused by changes in the ionization density, and not necessarily related to actual physical transportation of the reflecting particles. The second type, which represents a true motion, may or may not be that of the non ionized medium, perturbation of motion being possible if there are strong E or H fields present. In most of the above cases, the appearance of turbulence should be irregular in time, space, amplitude and spectrum.

Available theories treat only turbulent motions that are homogenized, "isotropized", quasi-stationary and associated with a single large scale motion. In forward scatter experiments, the question whether the statistical sampling along the path of the beam of a given wavelength corresponds to the theoretical model remains unanswered. With other causes of electron distribution irregularities besides turbulence (diffusing meteor trails, wave like motions) it does not appear surprising that theoretical spectra and those determined from experiment disagree. Nor is it surprising that there is no agreement amongst workers in the 80 - 100 KM region as to the interpretation of radio data in terms of the velocities of the small scale motions.

It is hoped that the contents of this thesis will help to resolve some of these anomalies in interpretation.

Before proceeding to a detailed discussion of the problems peculiar to the 80 to 100 KM region of the upper atmosphere, a general discussion of atmospheric turbulence is pertinent.

1.3 Atmospheric Turbulence

In recent years there has been an increasing acceptance by meteorologists of the view first put forward by Defant in 1921, that surface phenomena can be explained by an atmosphere which is essentially a quasi-horizontal turbulent flow field. Since 1948, when von Weizsacker and Heisenberg independently extended the theory of turbulence proposed by Kolmogoroff in 1941, considerable interest has been shown by fluid dynamicists in small scale turbulence. In 1953, Batchelor published his "Theory of Homogeneous Turbulence," giving a comprehensive account of the modern theory of homogeneous, and, in most applications, isotropic turbulence. Most of these amplifications of the Kolmogoroff theory were applied to turbulent flows as encountered in aerodynamics and hydraulic laboratories. Here, the turbulence scales were indeed small, their size being dictated by the dimensions of the apparatus. However, McCready (1953) and Taylor (1955) were able to show that much of this work could be extended to the investigation of turbulent fields occuring naturally in the atmosphere. They found that when autocorrelations in horizontal wind velocity

components at two points are measured in the lower atmosphere, they show the particular dependence on the distance between the two points which is characteristic of the inertial sub-range of turbulence scales, up to unexpectedly large separations - often as much as several times the height of observation.

The phenomena of the lower atmosphere have been summarized by Sheppard (1959). In the lower atmosphere, the large scale turbulence increases with height to the tropopause, and then decreases, whereas the small scale turbulence (as measured, for example, on an aircraft accelerometer) decreases with height to the upper tropopause, and then becomes more constant. The pattern of convection is partly responsible for the decrease with height of the small scale turbulence. The Kolmogoroff theory is unable to account for these changing relationships between large and small scale turbulence, and considerable caution must be exercised in inferring the properties of small scale turbulence from observations only on the large scale motions.

1.4 The Stability of the Atmosphere

As pointed out by Stewart (1959), the classical Reynolds number is rarely an important parameter in geophysical motions. By and large it is stability that determines whether or not a given region of the atmosphere is turbulent. It is most un-

usual for the velocity gradient not to be great enough to sustain turbulence, although, of course, the turbulent intensity may be exceedingly low. Thus we may say that, if the atmospheric region under discussion is unstable, or in neutral stability on a large scale, turbulence will occur. Almost never will the velocity gradient be so small that turbulence is inhibited by too low a Reynolds number.

In regions where the structure is stable, as, for example, at altitudes above the mesopause at approximately 80KM, where there is the stabilizing influence of a positive temperature gradient, the inhibition of turbulence is possible, although turbulence will occur if the velocity gradient is great enough. The temperature increase with height will, of course, exert a stabilizing influence only on vertical motions. Large scale horizontal temperature gradients can and do exist, giving rise to geophysical winds that are predominantly horizontal. The magnitudes of these winds are of the order of tens of meters per second, and thus turbulence is expected to be a characteristic of these motions. Because of the vertical stability, the large scale eddies characterizing this turbulent motion would be expected to be distinctly anisotropic, and this has been verified experimentally (see Chapter 3).

1.5 Turbulence at Meteor Heights

To date, the application of turbulence theory to the

atmosphere at meteor heights has met with only diffident suc-. cess.   Some of the apparent inconsistencies are the result of variations in the interpretation of the statistical equations of homogeneous turbulence, and for this reason the derivation of the relationships used in the reduction of the Adelaide wind results is treated in some detail in Chapter II.   The main text of this Chapter is taken from the excellent exposit-ion given by Stanley Corrsin at the Symposium on the Fluid Mechanics of the Ionosphere (New York, 1959).   Material is also drawn from Batchelor's "Theory of Homogeneous Turbulence" (Cambridge University Press, 1953).

CHAPTER II.

Turbulence Theory

2.1 Definition of Turbulence

Unfortunately, there is no universally accepted definition of turbulence. For the purposes of this thesis, a definition of turbulence given by Stewart at the International Symposium on Fluid Mechanics in the Ionosphere (New York, 1959) seems most appropriate.

"A fluid is said to be turbulent if each component of the vorticity is distributed aperiodically in time and space, if the flow is characterized by the transfer of energy from larger to smaller scales of motion, and if the mean separation of neighbouring fluid particles tends to increase with time. This definition excludes all two dimensional flows, as well as such phenomena as vortex sheets, whirlpools, convection cells and internal waves."

The most commonly accepted criterion of the stability of fluid flow is the dimensionless Reynolds number, the ratio of the inertial forces to the viscous forces. If the viscous forces are of the order of, or exceed the inertial forces, then any fluctuation of the mean flow will be quickly damped

out by viscous dissipation. When the Reynolds number exceeds
a certain critical value, the flow becomes unstable for small
disturbances, and so a superimposed flow in the nature of a
fluctuation with characteristic velocity and dimensions is
generated. As mentioned in Chapter I, Section 4, the critical
value of the Reynolds number in the atmosphere depends not
only on the inertial and viscous forces, but also on other
factors influencing the stability e.g. a positive temperature
gradient with height, which severely inhibits vertical motion.

Kolmogoroff (1941) applies the fluctuation principle to
each superimposed flow, so that with increasing Reynolds num-
ber each in turn becomes unstable, generating further disturb-
ances. At sufficiently high Reynolds number, fluctuations of
all magnitudes are present. Further, as the energy of the
larger superimposed flows passes down through the smaller scale
disturbances, the direct influence of the larger scales is lost,
so that all scales smaller than a certain critical size have
statistical properties which, to a large extent, are purely
random. That is, these smaller scales are both homogeneous
and isotropic.

2.2 The Kolmogoroff Turbulence Spectrum

This may be summarized as follows:-

1. <u>The large scale fluctuations</u>, which carry the turbulent
energy extracted from the mean flow. These are included

in the inertial range of scales, the term "inertial" imply-
ing that energy is received from higher scales and trans-
ferred to lower scales with negligible loss.

2.   The isotropic inertial region.   If the Reynolds number
is high enough, a range of scales will exist at the lower
end of the inertial region which does not contribute to the
energy dissipation, but has random statistical properties.
Such an isotropic inertial region rarely exists in wind tun-
nel and hydraulics experiments, because the Reynolds number
involved is usually too low.   However, one may expect to
find such a region in a turbulent atmosphere.

3.   The region of viscous dissipation.   The energy of the in-
ertial region is passed on to these smaller scale fluctuat-
ions, and is dissipated by viscous forces.   The statistical
properties of this state depend only on two parametes, viz.

ϵ, the rate at which energy is handed down from the
larger scales, and

ν, the kinematic viscosity, which determines the rate
at which the kinetic energy of the viscous scales can be
converted to heat.

2.3   The Turbulent Energy Spectrum $\mathcal{E}$

This is the most important property of any turbulent reg-
ion; however, direct measurement of energies is usually not
physically possible, and therefore the energy spectrum is

deduced from the turbulent velocity and scale. To establish
the relationship between velocity and scale, use is made of
the spacial correlation function

$$\mu(\xi) = \overline{u(x) \; u(x+\xi)}$$

2.3.1

where $u(x)$ is the turbulent velocity at x, and $u(x+\xi)$ the
turbulent velocity at a point distance ξ from x. The bar sym-
bol denotes an average taken over a time large compared with
the time constant of the turbulence scale characterized by μ.
This time constant or characteristic time of a turbulent flow
field is the time taken for the turbulent energy carried by
the large scale fluctuations to be passed down through the in-
ertial range and finally dissipated in the viscous region.

Note that μ is compounded from turbulent velocities only;
all mean flow and shear components must be subtracted from the
measured velocity to define the μ field. The energy density
spectrum is the Fourier transform of the spacial correlation
function, taken over all real space. i.e.

$$\mathcal{E}(\kappa) = \frac{1}{8\pi^3} \iiint\limits_{-\infty}^{\infty} \mu(\xi) e^{(-i(\kappa \cdot \xi))} dV_\xi(\xi)$$

2.3.2

Here, the spectral density has been defined in phase
space of dimension κ. It is often convenient, in theoretical
arguments, to refer to the energy associated with an eddy of

size κ^{-1} (Dimension of length in physical space). In the term-
inology of those working on problems in turbulence, an eddy
simply means a volume of fluid moving more or less coherently
with respect to the mean flow. The eddy motion need not be,
and usually is not of a rotating character. The term eddy can
frequently be inter-changed with the more cumbersome expression
"scale of motion".

2.4 Practical Correlation Functions

In experiments conducted on turbulent flow fields, it is
usual to employ the one dimensional lateral and transverse
correlation functions $f(\xi)$ and $g(\xi)$, relating to the turbulent
velocity components parallel and perpendicular respectively to
the separation ξ, where ξ now becomes a one dimensional length.
By definition

$$g(\xi) = \frac{\overline{u(x)\ u(x+\xi)}}{\left[\overline{u^2(x)u^2(x+\xi)}\right]^{\frac{1}{2}}}$$

2.4.1

where u are turbulent velocity components measured normal to
ξ.

The accuracy of such a determination for a given ξ is
given by

$$\partial g = \frac{1-g^2}{\sqrt{(n-1)}}$$

where n is the number of velocity pairs having separation ξ.
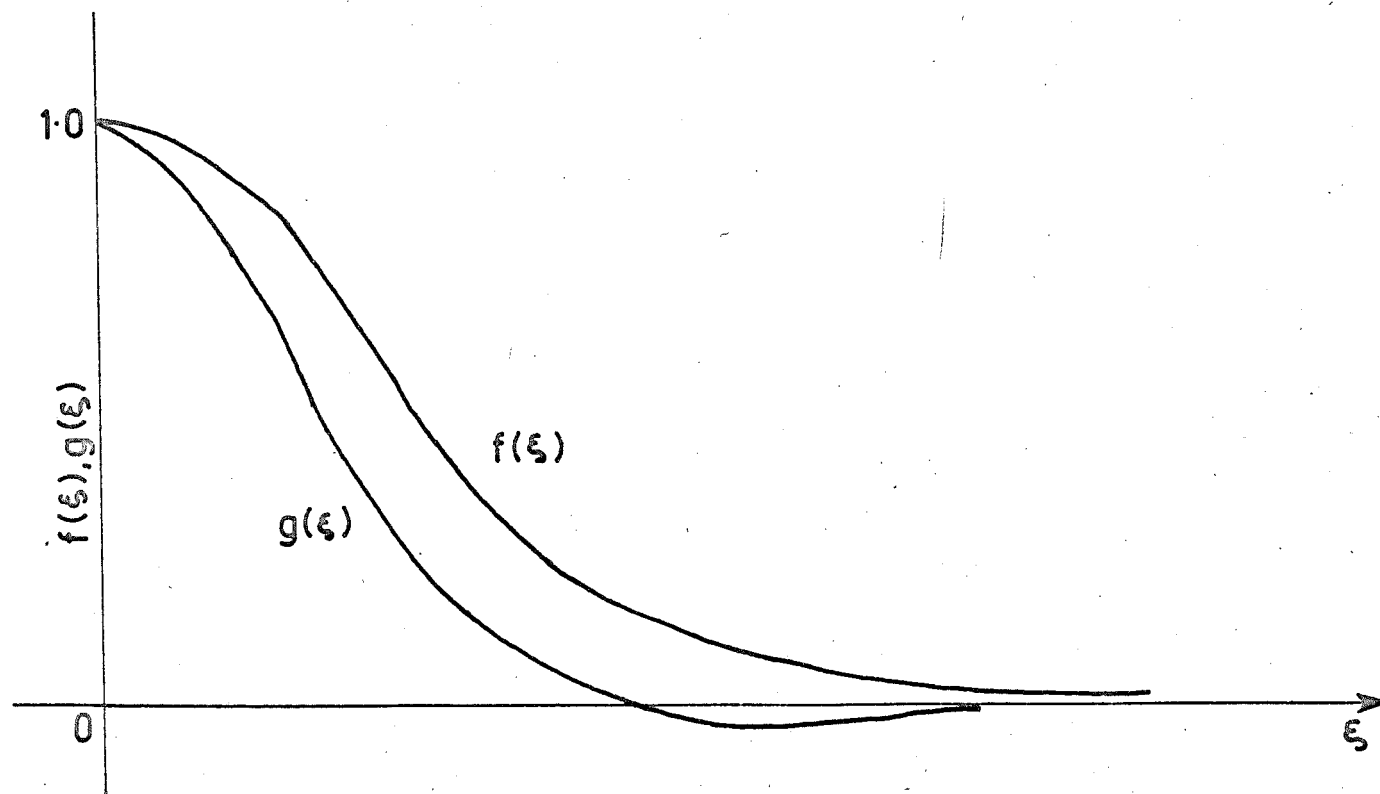
FIG.1 – GENERAL SHAPE OF CORRELATION CURVES.

Similarly

$$f(\xi) = \left[\frac{\overline{v(x)\ v(x+\xi)}}{\overline{v^2(x)v^2(x+\xi)}}\right]^{\frac{1}{2}}$$

2.4.2

for the components **v** parallel to ξ.

The form of these correlation functions is shown graphically in Fig. 1.

For these spacial correlation functions to be readily applied, certain restrictive conditions are necessary. The definition of $g(\xi)$ confines the turbulent velocity vector only to the perpendicular plane, and so the transverse correlation assumes specificity for random sampling only if the turbulent field is isotropic. If the direction of ξ is fixed in space, two dimensional isotropy will suffice. In isotropic turbulence

$$\left[\overline{u^2(x)u^2(x+\xi)}\right]^{\frac{1}{2}} = \left[\overline{v^2(x)v^2(x+\xi)}\right]^{\frac{1}{2}}$$
$$= U_0^2.$$

2.4.3

U_0 is the velocity characteristic of the energy bearing eddies.

The introduction of the equation of continuity for incompressible fluids leads to the relation

$$g(\xi) = f(\xi) + \frac{1}{2}\xi\frac{\partial f}{\partial \xi}$$

2.4.4

between the functions f and g,

or, if the turbulence is isotropic in two dimensions only

$$g(\xi) = f(\xi) + \xi\frac{\partial f}{\partial \xi}$$

2.4.5

[von Karman and Howarth (1938)]

From 2.4.1 and 2.4.2, we have for isotropic turbulence

$$f(0) = g(0) = 1$$

2.4.6

this being the maximum value of f and g.

i.e.

$$\left[\frac{\partial f}{\partial \xi}\right]_{\xi=0} = \left[\frac{\partial g}{\partial \xi}\right]_{\xi=0} = 0$$

2.4.7

2.5 The Characteristic Dissipation Length λ.

Expansion of $f(\xi)$ in the neighbourhood of $\xi=0$ in the form of a Taylors Series yields

$$f(\xi) = 1 + \tfrac{1}{2}f_0''\xi^2 + 0(\xi^4)$$

2.5.1

where the dash symbol denotes differentiation with respect to ξ. Since the dimensions of $f''(\xi)$ is L^{-2}, it is common practice to introduce the length λ, called the characteristic dissipation length, and defined by

$$f_0'' = -\frac{1}{\lambda^2}$$

Thus 2.5.1 becomes

$$f(\xi) = 1 - \frac{1}{2\lambda^2}\xi^2$$

<div align="right">2.5.2</div>

in the neighbourhood of $\xi = 0$.

Similarly, from 2.4.4,

$$g(\xi) = 1 - \frac{1}{\lambda^2}\xi^2$$

<div align="right">2.5.3</div>

near $\xi = 0$.

The significance of the parameter λ, which is a measure of the energy characteristic of the large scale eddies, is treated in more detail in Section 7.

2.6 The One Dimensional Turbulent energy spectrum E.

Using the one dimensional length ξ, we may formulate a one dimensional energy spectrum equivalent to 2.3.2, using $f(\xi)$ and $g(\xi)$ as the velocity correlation functions.

Since

$$f(\xi) = \frac{\mu(\xi)}{U_0^2}$$

the longitudinal one dimensional spectrum function becomes

$$E(\kappa) = \frac{1}{2\pi}\int_{-\infty}^{\infty} U_0^2 f(\xi)\cos(\kappa \cdot \xi)d\xi$$

<div align="right">2.6.1</div>

where κ now defines a one dimensional phase space.
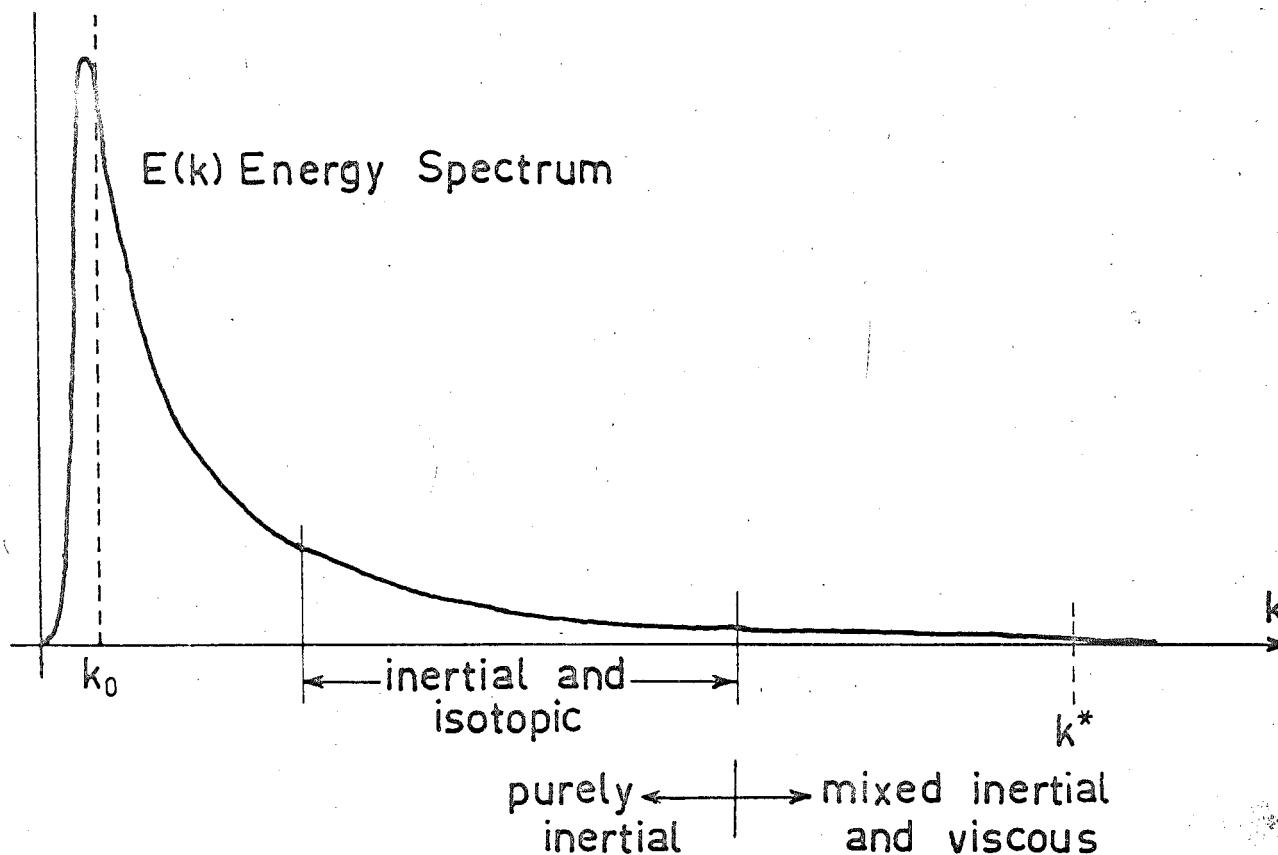
FIG.2 – SPECTRAL RANGES IN TURBULENCE OF MODERATE REYNOLDS NUMBER.

Similarly, the lateral one dimensional spectrum function
is

$$E(\kappa) = \frac{1}{2\pi}\int_{-\infty}^{\infty} U_0^2 g(\xi)\cos(\kappa \cdot \xi)d\xi$$

2.6.2

The form of the one dimensional energy spectrum for moderate Reynolds number is shown in Fig. 2. The peak of the curve occurs at $\kappa=\kappa_0$, and this is the characteristic scale of the energy bearing eddies. G. I. Taylor has defined the size of these energy bearing scales in terms of the characteristic integral scales

$$L_0 = \frac{1}{U_0^2}\int_0^{\infty}\mu(\xi)d\xi$$

Inserting $f(\xi)$ and $g(\xi)$, with regard given to 2.4.4 we have

$$L_0 = \int_0^{\infty} f(\xi)d\xi = 2\int_0^{\infty} g(\xi)d\xi$$

2.6.3

Thus an alternative definition of L_0 is that it is the maximum scale over which velocities are appreciably correlated. Batchelor (1953) has shown that 2.6.3 can be expressed as

$$L_0 = \frac{3\pi}{4}\frac{\int_0^{\infty}\kappa^{-1}E(\kappa)d\kappa}{\int_0^{\infty}E(\kappa)d\kappa}.$$

which rationalizes the term "average eddy of size κ^{-1}" as used

by fluid dynamicists.

At the other end of the turbulence spectrum, at extremely large κ, is the region of viscous dissipation. Kolmogoroff has defined κ^*, the characteristic eddy of this region, as

$$\kappa^* = \left[\frac{\epsilon}{\nu^3}\right]^{\frac{1}{4}}$$

2.6.4

This assumes that at this characteristic eddy size all the energy transferred from the inertial region is being dissipated in purely viscous forces. In physical space, the size of the characteristic eddy of the Kolmogoroff microscale is denoted by $\eta \ (=\kappa^{*-1})$.

If the lower boundary of the mixed inertial-viscous region is at very large κ, there may exist a region both inertial and isotropic. For such a region Kolmogoroff postulated that $E(\kappa)$ depends only on the rate of energy flux through that part of the spectrum. This must equal the total dissipation rate ϵ.

The only form dimensionally possible is

$$E(\kappa) = \alpha\epsilon^{\frac{2}{3}}\kappa^{-\frac{5}{3}}$$

2.6.5

where α is of the order of unity.

Laboratory experiments indicate that this law holds up to wave numbers about as high as

$$\kappa_{\lim} = 0.2\kappa^*$$

2.6.6

If the actual spectrum at extremely high Reynolds numbers is replaced by a purely inertial spectrum as defined (equation 2.5.8) truncated at κ_0 ($= L_0^{-1}$) and at κ^* ($=\eta^{-1} \gg L_0^{-1}$) the total dissipation

$$\epsilon = 2\nu \int_0^\infty \kappa^2 E(\kappa) \, d\kappa$$

2.6.7

can be estimated as

$$\epsilon \approx 2\alpha\nu\epsilon^{\frac{2}{3}} \int_{\kappa_0}^{\kappa^*} \kappa^{\frac{1}{3}} \, d\kappa$$

Neglecting $\kappa_0^{\frac{4}{3}}$ relative to $\kappa^{*\frac{4}{3}}$ we have

$$\alpha \approx \frac{2}{3}$$

This paradoxical estimation of dissipation from a non dissipative form is justifiable as long as the true $E(\kappa)$ decreases sufficiently rapidly for $\kappa > \kappa^*$.

Having determined the form of $E(\kappa)$ for the inertial range of eddy sizes, the form of the correlation function appropriate to this region can now be established.

Since

$$E(\kappa) = \frac{1}{2\pi} \int_{-\infty}^{\infty} U_0^2 f(\xi) \cos(\kappa.\xi) \, d\xi$$

(equation 2.6.1)

it follows that
$$f(\xi) = \frac{1}{U_0^2} \int_0^\infty E(\kappa) \cos(\kappa.\xi) \, d\xi$$

which is, on substitution of 2.5.8 with $\alpha = \frac{2}{3}$,

$$f(\xi) = \frac{2}{3} \frac{\epsilon^{\frac{2}{3}}}{U_0^2} \int_{\kappa_0}^{\kappa^*} \kappa^{-\frac{5}{3}} \cos(\kappa_\bullet \xi) d\kappa$$

and has a solution of the form

$$1 - f(\xi) = a\xi^{\frac{2}{3}}$$

2.6.8

where a is a constant.

Introduction of the relations

$$g(\xi) = f(\xi) + \frac{1}{2}\xi\frac{\partial f}{\partial \xi}$$

(equation 2.4.4)

yields

$$g(\xi) = 1 - \frac{4}{3}a\xi^{\frac{2}{3}}$$

for three dimensional isotropy, or from 2.4.5

$$g(\xi) = 1 - \frac{5}{3}a\xi^{\frac{2}{3}}$$

if the turbulence is isotropic in two dimensions only.

The ratio

$$\frac{1 - f(\xi)}{1 - g(\xi)}$$

2.6.9

is thus 0.75 or 0.60, according as the turbulence is two or

three dimensionally isotropic.

2.7 The Rate of change of Energy ϵ.

Using the dynamical equation first derived by von Karman and Howarth (1938), Batchelor has shown (1953) that the rate of change of energy

$$\epsilon = \frac{d\frac{3}{2}U_0^2}{dt} = 15\nu U_0^2 f_0'' = -15\nu U_0^2/\lambda^2$$

2.7.1

The proportional rate of decrease of energy is

$$\frac{1}{U_0^2}\frac{dU_0^2}{dt} = -10\nu/\lambda^2$$

whence the term "dissipation length parameter" for λ.

2.8 Turbulence Reynolds Numbers.

For the isotropic inertial region there are no character-istic mean flow velocities or lengths, but a turbulence Rey-nolds number may be defined in terms of turbulence parameters. This will be of assistance in determining the scales of the viscous region, since, in the Kolmogoroff theory, the smaller scales see the larger scales as a form of mean motion.

A turbulence Reynolds number due to G. I. Taylor is

$$R_\lambda = U_0\lambda/\nu$$

2.8.1

where U_0 is the velocity characteristic of the energy

bearing eddies, and λ is the dissipation length parameter.

2.9 The Relationships between Eddy Sizes.

From 2.6.4

$$\eta = \left[\frac{\nu^3}{\epsilon}\right]^{\frac{1}{4}}$$

Substituting for ϵ from 2.7.1

$$\frac{\eta}{\lambda} = \left[\frac{\nu^3}{15U_0^3\lambda^2}\right]^{\frac{1}{4}}$$

In terms of the Reynolds number R_λ,

$$\frac{\eta}{\lambda} = \frac{1}{15^{\frac{1}{4}}R_\lambda^{\frac{1}{2}}} \simeq \frac{0.5}{R_\lambda^{\frac{1}{2}}}$$

$$2.9.1$$

A relation between λ and the energy bearing eddies L_0 $(=\kappa_0^{-1})$ can be calculated from the energy spectrum $E(\kappa)$, using a method similar to that employed in the determination of α (equation 2.6.7 et sequ.).

The total energy

$$\tfrac{1}{2}U_0^2 = \int_0^\infty E(\kappa)d\kappa$$

$$2.9.2$$

Substituting 2.7.1 for ϵ, and neglecting $\kappa^{-\frac{2}{3}}$ relative to $\kappa_0^{-\frac{2}{3}}$ gives

$$\frac{\lambda}{L_0} = \frac{8}{R_\lambda}$$

$$2.9.3$$

2.10 The Relationship Between Velocity Differences and Separation in Isotropic Turbulence.

Since velocity differences are the most easily measured parameters of a turbulence spectrum, some knowledge of their behaviour with separation is advantageous.

Batchelor has shown (1953) that, if there exists an isotropic inertial region, then in that region

$$\overline{[u(x+\xi,t) - u(x,t)]^2} = 4\int_0^\infty E(\kappa)\{ 1 - \frac{\sin(\kappa\cdot\xi)}{\kappa\cdot\xi}\}d\kappa$$

This may be written

$$\overline{[u(x+\xi) - u(x)]^2} = 4\int_0^\infty E(\kappa)\{ 1 - \frac{\sin(\kappa\cdot\xi)}{\kappa\cdot\xi}\}d\kappa$$

2.10.1

where the bar symbol now denotes an average over a time large in comparison with the time constant of the energy bearing eddies.

The integrand is suppressed by the small value of $(1-\frac{\sin(\kappa\cdot\xi)}{\kappa\cdot\xi})$ when $\kappa\approx\kappa_0$, and is suppressed by small $E(\kappa)$ for $\kappa\approx\kappa^*$. The behaviour is thus dominated by the inertial range of κ, and thus we may write

$$\overline{[u(x+\xi) - u(x)]^2} = 4\int_0^\infty \tfrac{2}{3}\epsilon^{\frac{2}{3}}\kappa^{-\frac{5}{3}}\{ 1 - \frac{\sin(\kappa\cdot\xi)}{\kappa\cdot\xi}\}d\kappa$$

$$= 9/5 \left[\ \Gamma(\tfrac{1}{3}) [\epsilon\xi]^{\frac{2}{3}} \right]$$

$$= 3.2(\epsilon\xi)^{\frac{2}{3}}$$

i.e.

$$\overline{[u(x+\xi) - u(x)]^2} = 3.2(\epsilon\xi)^{\frac{2}{3}}$$

2.10.2

In terms of the RMS velocity differences $\overline{\Delta v}$,

$$\overline{\Delta v} = 1.8(\epsilon\xi)^{\frac{1}{3}}$$

2.10.3

2.11   The Time Dependent Velocity Correlation Function.

In the single station work of meteorology, the time correlation function $g(\tau)$ is a more convenient quantity than the spacial correlation $g(\xi)$.

By definition, the autocorrelation function

$$g(\tau) = \frac{\overline{v(t)\,v(t+\tau)}}{\overline{V^2(t)}}$$

2.11.1

and similarly

$$f(\tau) = \frac{\overline{u(t)\,u(t+\tau)}}{\overline{U^2(t)}}$$

2.11.2

where v and u are the NS and EW components respectively of the turbulent wind.

The equivalence of the spacial and time correlation functions has provided some contentious arguments in the past, but the experience of meteorologists has been that the equivalence is established for regions sufficiently removed from the effects of orography, and Hutchings (1955) has demonstrated this from radar-sonde balloon readings taken in the upper levels of the lower atmosphere in New Zealand.

A similar power law relating the Eulerian time correlation function and the time of measurement as that determined for spacial correlations and separations has been verified by Hutchings, viz.

$$1 - f(\tau) \sim \tau^{\frac{2}{3}}$$

2.11.3

This relationship assumes, however, that the turbulent velocity is small in relation to the velocity of the mean flow. By a consideration of the one dimensional model of small scale turbulence suggested by von Weizsacker (1948) (reproduced in Section 6), Ogura (1953) has shown that, in the range where the space correlation is given by 2.6.8, $f(\tau)$ may be expressed in the form

$$1 - f(\tau) \sim \tau^{m}$$

2.11.4

m being a complicated function of the mean flow U and RMS turbulent velocity $[\overline{u^2}]^{\frac{1}{2}}$ in the direction of the mean flow.

For

$$U >>> [\overline{u^2}]^{\frac{1}{2}} \qquad\qquad m = \tfrac{2}{3}$$

and for

$$U <<< [\overline{u^2}]^{\frac{1}{2}} \qquad\qquad m = 1$$

Either $f(\tau)$ or $g(\tau)$ may be used in the relation 2.11.4, the general equation being written

$$1 - R(\tau) \sim \tau^m$$

$$2.11.5$$

2.12 The Richardson Number.

In well developed turbulence, the gas is influenced by a force arising from instability associated with the velocity shear.

This yields a turbulent velocity

$$v_t = l_m \left[\frac{d\overline{v}}{dh}\right]$$

where l_m is the momentum mixing length.

If a small volume of air is brought up (or down) over a distance l_h by such turbulent forces, it will descend (ascend) and arrive at its initial level with a terminal velocity

$$v_h = \text{const.} l_h \left[\frac{g}{\Theta}\frac{d\Theta}{dh}\right]^{\frac{1}{2}}$$

where Θ is the potential temperature of the gas.

For turbulent motions of this type to occur

$$v_t^2 \geqq v_h^2$$

A generalized Richardson number Ri^* may be postulated, such that

$$Ri^* = const. \frac{v_h^2}{v_t^2}$$

$$= \left[\frac{l_h}{l_m}\right]^2 \frac{g}{\Theta} \frac{d\Theta/dh}{(dv/dh)^2} = \left[\frac{l_h}{l_m}\right]^2 Ri$$

<div style="text-align:right">2.12.1</div>

where Ri is the normal definition of the Richardson number.

Turbulence will occur when Ri^* is smaller than some critical value.

Considerable simplification of the relation 2.12.1 results from the substitution

$$\frac{1}{T}\left[\frac{dT}{dh} + \Gamma\right] = \frac{1}{\Theta}\frac{d\Theta}{dh}$$

where $\Gamma = \frac{\gamma - 1}{\gamma} \frac{g\mu}{R}$, $\quad \gamma = \frac{C_p}{C_v}$

and μ is the molecular weight.

For a dry atmosphere at sea level $\Gamma \simeq 9.9 \times 10^{-5} {}^\circ K/cm$, and is somewhat less at 100KM. The precise value is not critical in this discussion.

In practice,

$$Ri^* = \left[\frac{l_h}{l_m}\right]^2 \frac{g}{T}\left[\frac{dT}{dh} + \Gamma\right]\left[\frac{d\bar{v}}{dh}\right]^2$$

Theoretically, one expects turbulence to occur for $Ri^* < 1$. In the copious literature on this subject, values from .04 up to 1.0 have been quoted; the lower values usually assume that the momentum mixing length l_m is equal to l_h, which is the characteristic size of the eddies arising from the Richardson type instability. In the theory of homogeneous turbulence, the analogue to the momentum mixing length is the characteristic dissipation length λ; thus

$$Ri^* = \left[\frac{l_h}{\lambda}\right]^2 \frac{g}{T}\left[\frac{dT}{dh} + \Gamma\right]\left[\frac{d\bar{v}}{dh}\right]^{-2}$$

2.12.2

2.13 Turbulence in Shear Flow.

As has been mentioned previously, the meteor region of the atmosphere is stabilized by a positive temperature gradient with height. Such stabilization can produce a stratification of motion, and this in turn can give rise to shear flow. Some knowledge of the modifications of the theories of homogeneous turbulence in the presence of shear could be useful.

Tchen (1954) has investigated the turbulent spectrum associated with shear flow, and his findings may be summarized

as follows:-

For small shear fields, the one dimensional energy spectrum in wave number space is of the form

$$E(\kappa) \sim \kappa^{-\frac{7}{3}}$$

<div align="right">2.13.1</div>

and for large shear

$$E(\kappa) \sim \kappa^{-1}$$

<div align="right">2.13.2</div>

The spacial spectrum $E(\xi)$ thus follows

$$E(\xi) \sim \xi^{\frac{4}{3}}$$

<div align="right">2.13.3</div>

for small shear,

and

$$E(\xi) \sim \ln\frac{1}{\xi}$$

<div align="right">2.13.4</div>

for large shear.

If no preferrential direction is prescribed for ξ, then for small shears the spectrum is usually given by the Kolmogoroff isotropic relation

$$E(\kappa) \sim \kappa^{-\frac{5}{3}}$$

<div align="right">(2.6.5)</div>

i.e.

$$E(\xi) \sim \xi^{\frac{2}{3}}$$

2.13.5

If ξ is the direction specifying the shear, (a vertical shear is defined as a variation of horizontal wind velocity with height), then, for small shear, 2.13.1 and 2.13.3 apply. For large shears, the relations 2.13.2 and 2.13.4 are appropriate for all ξ.

CHAPTER III.

Measurements of
Atmospheric Turbulence at Meteor Heights

3.1 General

The first attempt to apply the Kolmogoroff Theory to turbulent motions in the meteor region was made by Booker in 1956. The results as presented (Booker and Cohen, 1956) were not in accordance with the known behaviour of meteor trails, and the paper contributed little if anything to the understanding of this region. However, it did stimulate the investigation of turbulence at these heights, and resulted in papers by Manning (1959) and Greenhow (1959) which provided an adequate qualitative treatment of the motions of meteor trails subject to random winds. A paper by Greenhow and Neufeld (1959) on work carried out at Jodrell Bank detailed the results of a spaced station radar survey of wind velocity differentials measured from the drift of meteor trail ionization. (For details of the spaced station technique, see Chapter VII). However, several anomalies exist in this paper, and the value derived for ϵ, the turbulent dissipation energy, is almost an order greater than that determined from rocket

and photographic meteor data (see Chapter XII). Their work
is, however, worthy of detailed consideration, especially
that portion dealing with the larger scale motions.

3.2 Discussion of the work of Greenhow and Neufeld.

The analysis of velocity correlations in this paper is
not particularly rigorous. Because of the limitations im-
posed by station separations the maximum height difference
observed was 4.5KM, at which value the correlation function
relating the transverse turbulent velocity to height separat-
ion fell to 0.22 (see Fig. 3). The curve is then extrapol-
ated to zero at 6.5KM, this extrapolation being justified by
Greenhow and Neufeld from results published by Liller and
Whipple (1954), Fig. 4, which show loss of correlation be-
tween the horizontal velocity of points separated by some
6 - 7KM in height. Figure 5 is an actual photograph of a
trail undergoing distortion. However, in general the zero of
the transverse correlation does not determine the scale for
which velocities are no longer correlated. A measure of the
separations over which velocities are appreciably correlated
is given by equation 2.6.3, viz.

$$L_p = 2\int_0^\infty g(\Delta h)d\Delta h$$

(using Greenhow's notation)

From the theoretical shape of the transverse correlation
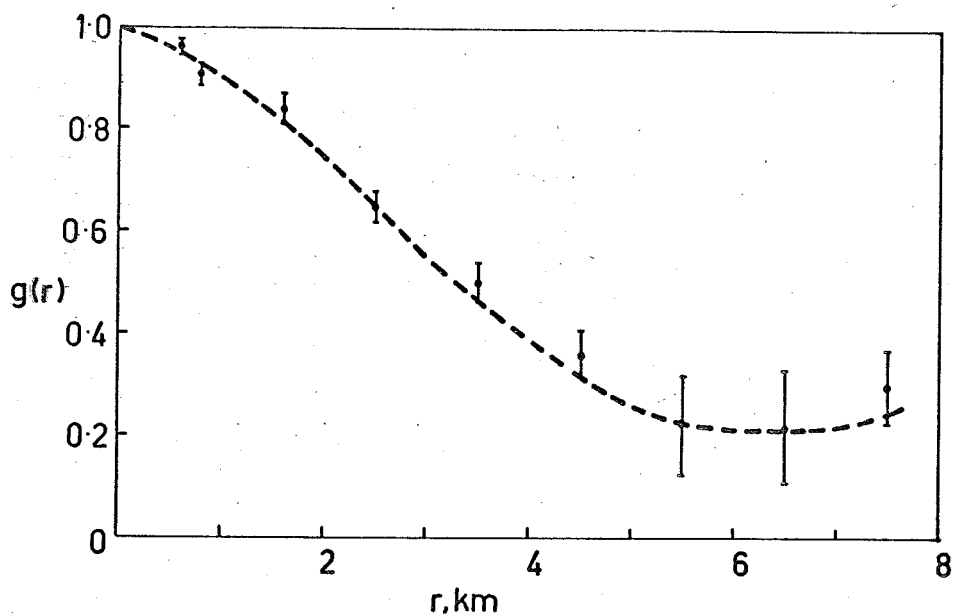
FIG.3a–Variation of velocity correlation g with
spacial separation of the reflecting points r.
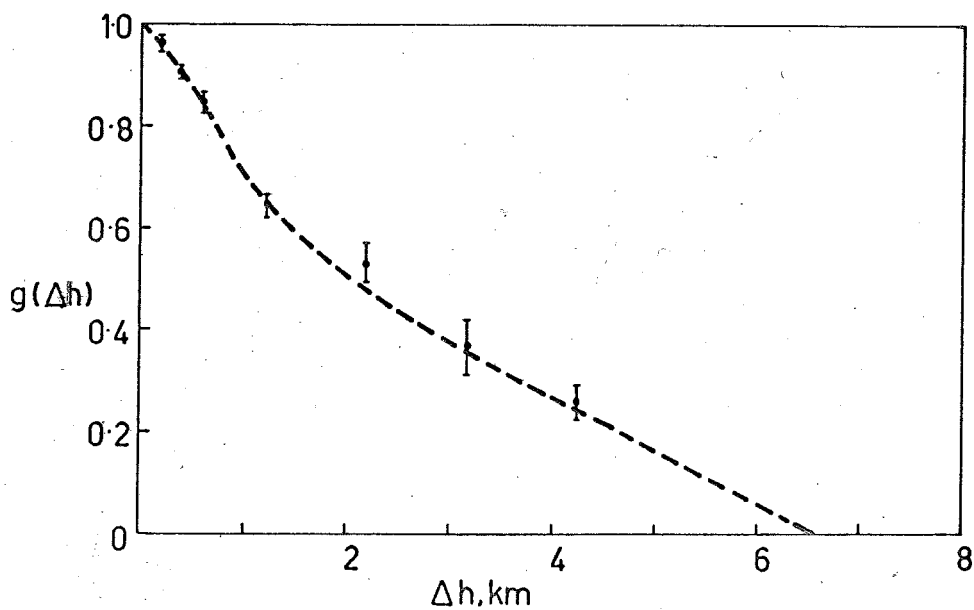
FIG.3b–Variation of g with height separation Δh
of the reflecting points.

curve (see Fig. 1), the area under the curve up to the zero value is an upper limit of the scale of appreciable correlation. By graphing the transverse correlation function of Fig. 3 on squared paper, and counting squares to determine the area under the curve

$$2 \int_0^{6.5 \times 10^5} g(\Delta h) d\Delta h \; = \; 5.0 \times 10^5 \; = \; 5 \text{ km.}$$

This upper limit of appreciable correlation is in keeping with the zero correlation height difference of 6 - 7 KM found by Liller and Whipple. Thus although the scale determined by the zero of the transverse correlation function is not justifiable on theoretical grounds as the scale of zero velocity correlation, it does appear to be a useful indication in this particular application.

The turbulent velocity correlations as derived by Greenhow and Neufeld are not characteristic of the complete flow field, but of the 6KM scale only. To allow for the prevailing and periodic motions of the atmosphere, the mean horizontal wind during any hour was obtained by averaging approximately 100 individual velocities obtained each hour. The turbulent component for echoes in that hour was obtained by subtracting the radial component of this steady wind from each individual echo. One of the restrictions placed on the
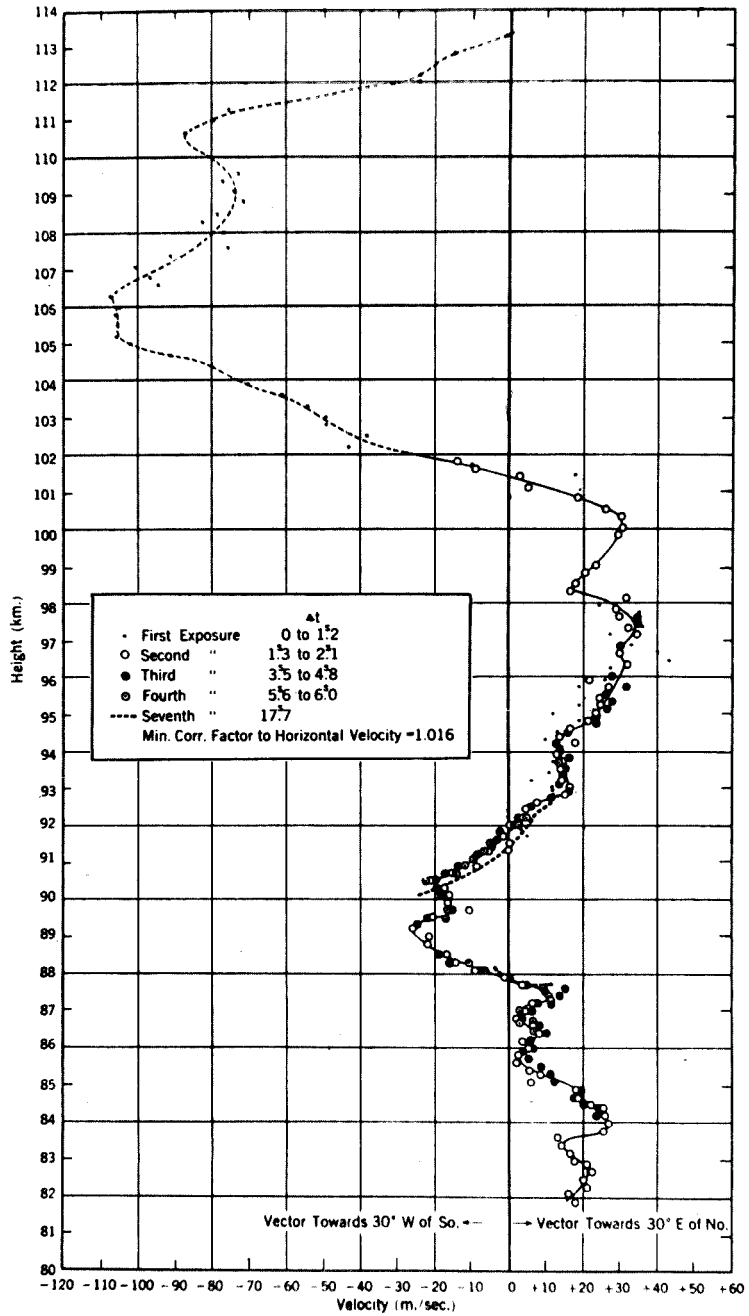
A typical example of meteor train drifts determined photographically at the Harvard Observatory by Liller and Whipple.

FIG 4
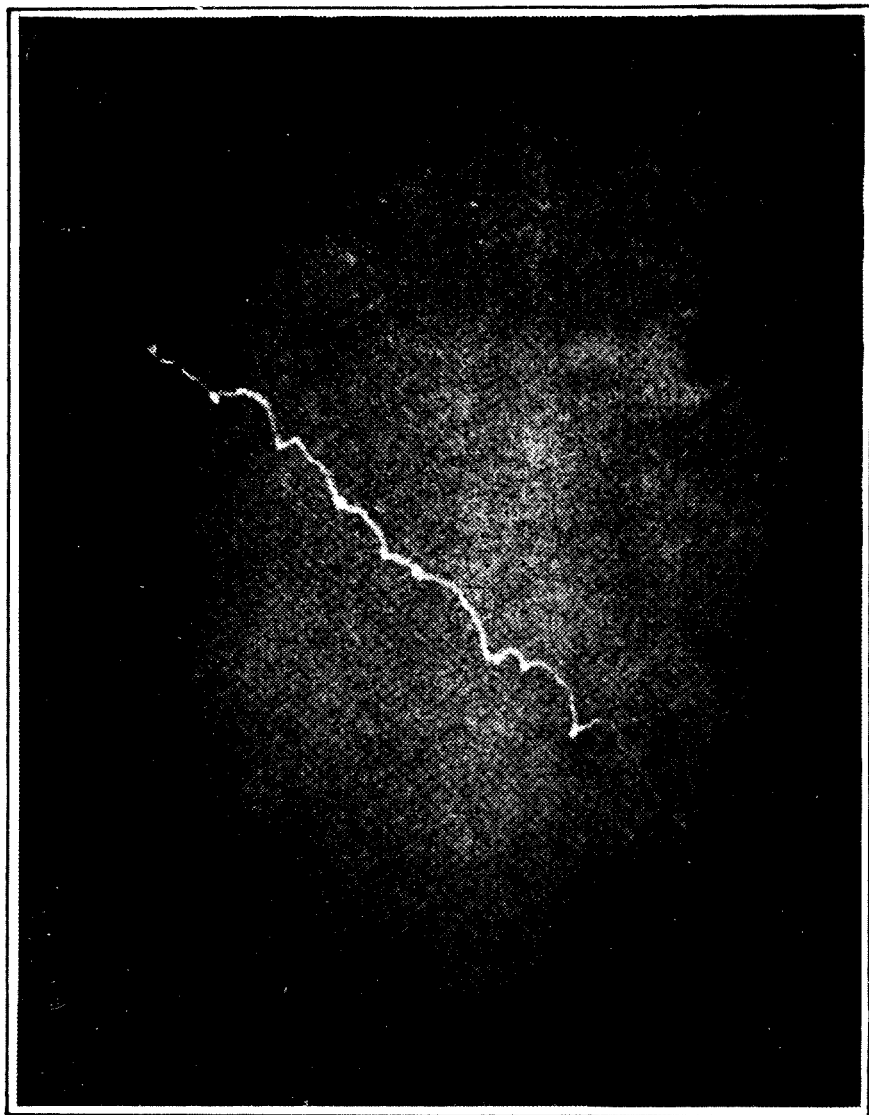
Photograph of a meteor train taken about 60 seconds after passage of the meteor. Length of train approximately 19°. Photo by F. L. Trube, May 3, 1939.

FIG 5

spacial correlation function $g(\xi)$ is that the turbulent velocity components must be averaged over a time large in comparison with the characteristic time of the energy bearing eddies. Greenhow and Neufeld determined this time constant to be 100 minutes (see Section 4 this Chapter). Their averaging interval for mean flow determination is obviously too small, and the correlation function thus determined is not characteristic of the complete turbulent flow. This accounts for the marked effects of the height correlation on the spacial function.

If the correlations of Fig. 3 are graphed according to the relations established in Chapter 2 Section 11

viz.

$$1 - R(\xi) \quad \text{against } \xi$$

Fig. 6 results.

Because of the anisotropic nature of the large scale eddies, the spacial correlation, parameter $VT=\xi$ of which contains components of the horizontal, exhibits the anomalous slope of 1; linear extrapolation of this portion of the curve to "zero correlation" $(1-R(\xi)=1)$ yields a scale of 7KM.

The correlation against Δh, however, exhibits the slope characteristic of the inertial subrange of the Kolmogoroff turbulence spectrum. Extrapolation of this line to "zero correlation" yields a vertical scale of 6KM.
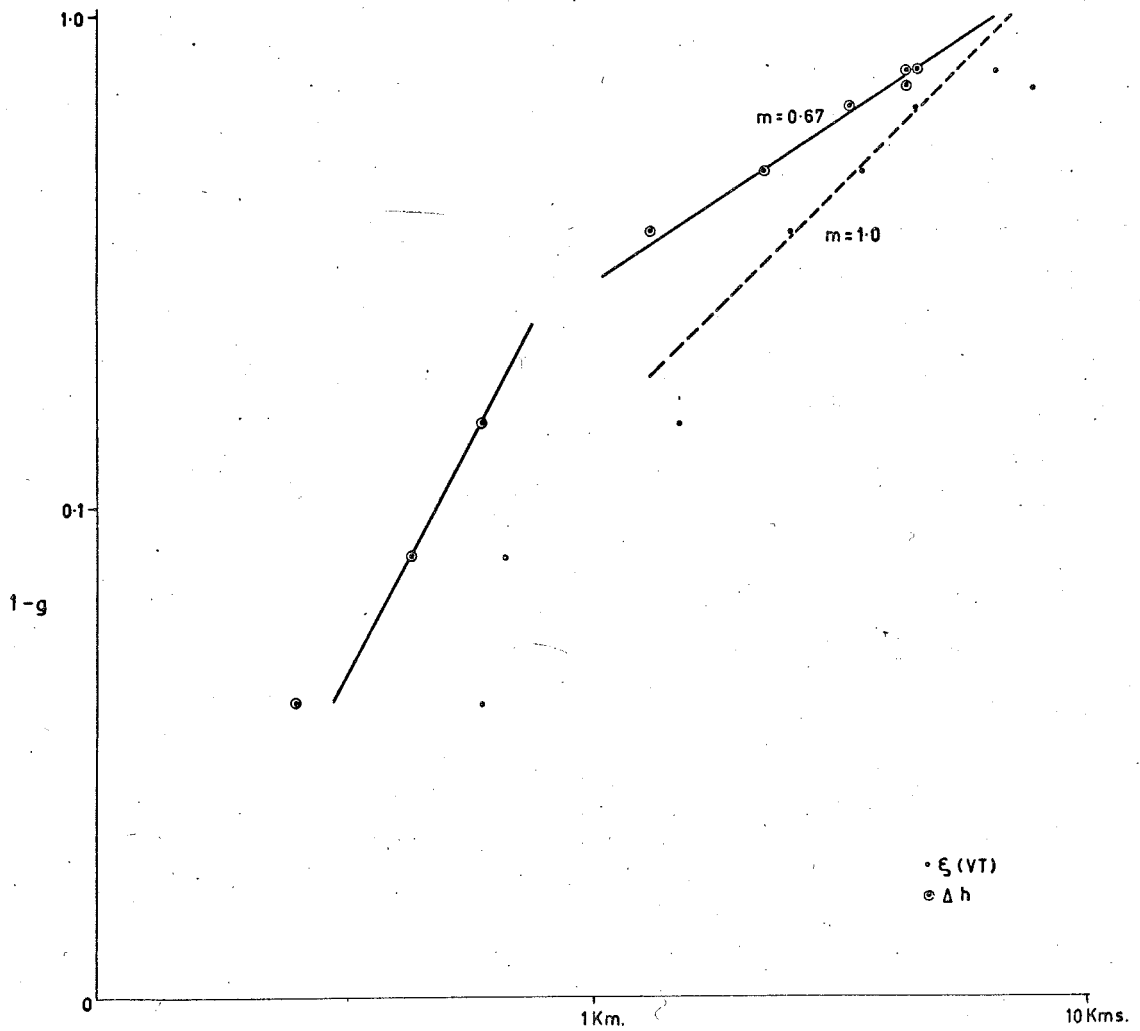
FIG.6 – SPACIAL AND HEIGHT CORRELATIONS
(AFTER GREENHOW)

At separations less than 1KM, the slopes of the correlations change markedly. This breakdown could be explained as due to the onset of viscous dissipation at scales less than 1KM. Since from hydraulics and wind tunnel experiments the spectrum behaviour of the inertial subrange can be expected to hold down to scales five times the characteristic eddy size of the Kolmogoroff microscale (equation 2.6.6), this would indicate a minimum eddy size

$$\eta = 200 \text{ metres.}$$

The error associated with Greenhow and Neufelds' determination of g(0) is of the order of 0.01. This limits the accuracy of direct determination of the smaller scales to some 140 metres.

3.3 Richardson Type Instabilities.

Another explanation for the inertial subrange breakdown at 1KM is the extraction of kinetic energy from the turbulence and its conversion to potential energy by bouyancy forces as suggested by Bolgiano (1959). In this, the generalized Richardson number of Chapter 2 Section 12 is the relevant parameter.

Since the height correlation function appears to follow the Kolmogoroff spectrum, the fitting of a parabola of the form

$$g(\xi) = 1 - \xi^2/\lambda^2$$

(equation 2.5.3)

to the correlation curve in the neighbourhood of $\xi = 0$ should
yield a dissipation length parameter λ characteristic of the
vertical scale of turbulent motion. The value of the dissip-
ation length thus determined is

$$\lambda = 1.4 \text{ KM}$$

Substitution of this value in equation 2.12.2, viz.

$$Ri^* = \left[\frac{l_h}{\lambda}\right] \frac{g}{T} \left[\frac{dT}{dh} + \Gamma\right] \left[\frac{d\bar{v}}{dh}\right]^{-2}$$

using the ARDC (1959) Model Atmosphere in determining T,
$\frac{dT}{dh}$ and Γ and taking Greenhow's figure of 10m/sec/km for $\frac{d\bar{v}}{dh}$
yields

$$Ri^* = \left[\frac{l_h}{\lambda}\right]^2 \times 4$$

For $Ri^* < 1$

$$l_h < 700 \text{ metres}$$

i.e. the scale of eddies arising from Richardson type
instabilities is less than 700 M. Further comments on this
value in relation to the small scale turbulence appear in
Chapter IX.

3.4 The Large Scale Irregularities.

In determining the size of the large scale eddies,
Greenhow and Neufeld (1959 a) used the single station time
correlation function:

$$g(\tau) = \frac{\overline{v(t)v(t+\tau)}}{v^2(t)}$$

Their results as published have been regraphed according to the relation

$$1 - R(\tau) \sim \tau^m$$

(equation 2.11.5)

The best least squares fit line to these points (Fig.7) has slope 0.66, indicating a turbulent velocity less than that of the mean flow (see Chapter 2 Section 11). This is not readily explained since, according to Greenhow and Neufeld, "there was no correlation between the RMS turbulent velocity for any hourly interval and the mean wind speed or mean height gradient in that interval, turbulent velocities of up to 40m/sec being measured even when the mean wind speed was zero." Further comments on this in the light of measurements made at Adelaide appear in Chapter IX.

From the RMS turbulent velocity, measured as 25m/sec, and the time constant of 6 X 10^3 secs (being the time of "zero correlation"), the scale of these eddies is given as some 150KM.

From several time correlations plotted from data obtained over several 24 and 48 hour periods, a minimum scale of 60KM
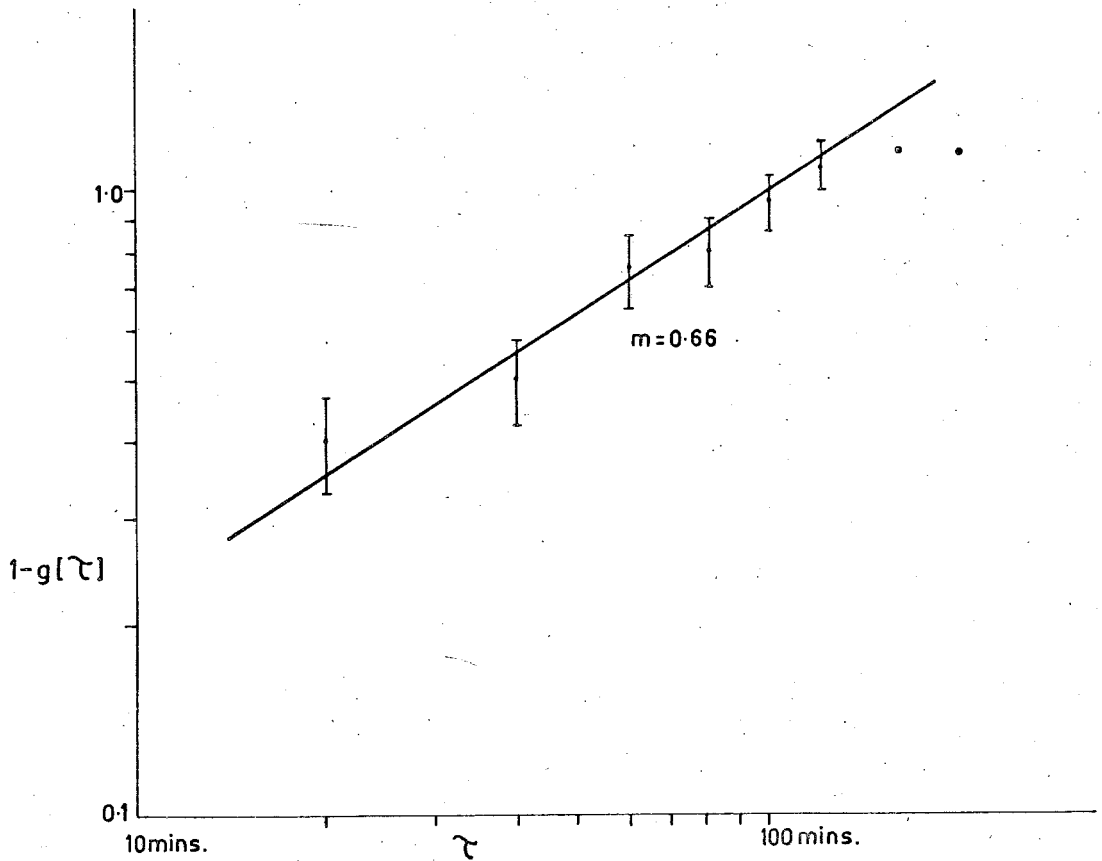
FIG.7 - TIME CORRELATION (AFTER GREENHOW)

and a maximum of 250KM was observed. (Greenhow and Neufeld, 1960). These larger scales are given further consideration in Chapter IX.

3.5 Eddy Diffusion and Photographic Meteors.

The effects of eddy diffusion on meteor trails at heights above 90KM have been investigated by Greenhow by using visual and photographic observations summarized by Millman. The trail radii, defined as the standard deviation r of an assumed Gaussian distribution of intensity across any diameter, were estimated by Greenhow and compared with the theoretical variation of r for various values of ambipolar diffusion and eddy diffusion. The behaviour of such diffusion of trails has been adequately summarized by Booker (1956) as follows. Immediately after trail formation, dispersion proceeds under the influence of ambipolar diffusion, given by

$$r^2 = 4Dt$$

where D is the ambipolar diffusion coefficient.

After a time t_1 , the time constant of the characteristic eddy of the Kolmogoroff turbulence spectrum, the trail radius increases as

$$r^2 = \tfrac{4}{3}\epsilon t^3$$

up to a time t_2 , the time constant of the large scale turbulence. After t_2 the radius once more increases in the

44
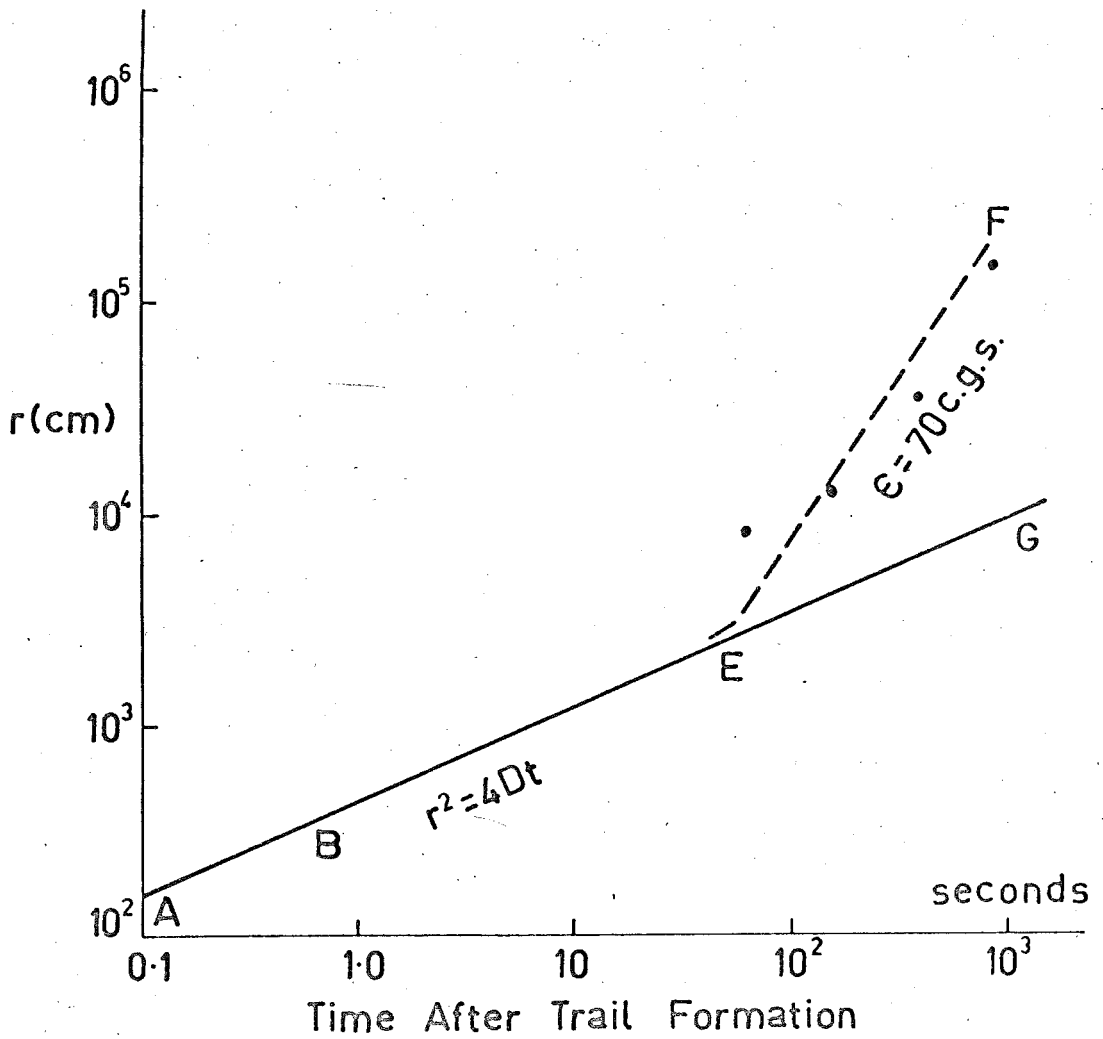
FIG.8 – TRAIL RADIUS r AS A FUNCTION OF TIME.

manner

$$r^2 = 4D_e t$$

where D_e is the eddy diffusion coefficient.

$D_e = VL$, where V and L are the velocity and scale of the large scale turbulence.

Millman's results graphed by Greenhow according to these relations are shown in Fig. 8. AG is the expected growth of trail radius under the influence of ambipolar diffusion alone ($D = 4 \times 10^4$ sq cm/sec at 90 KM). The measured values of r shown on the figure lie about the line EF, for which $r^2 = \frac{4}{3}\epsilon t^3$, and correspond to a turbulence power of only 70 ergs/gm/sec. They give a value of 30 secs for the time constant of the small scale turbulence, far in excess of the value of 0.4 secs determined by Booker and more in keeping with the observed behaviour of radio echoes from meteor trails, which often endure without any observable distortion of reflection for periods of several seconds.

The value of ϵ thus determined is an order smaller than that determined by Greenhow from spaced station observations of meteor trails.

3.6 Rocket Results.

From photographic observations of the diffusion of sodium trails ejected from a Veronique rocket, Blamont and De

Jager (1961) calculated by similar means the turbulent dis-
sipation ϵ to be approximately 70 ergs/gm/sec below 102 KM.
Above this height, the observed diffusion was found to be
completely explained by molecular diffusion. Height strat-
ification of atmospheric motion with dimension 6 KM was also
in evidence, the observed winds being predominantly horiz-
ontal, with a vertical maximum of ±10 m/sec.

Groves (1959) and Rofe (1961) have carried out similar
experiments at Woomera, with both sodium trails and grenades.
The work of Rofe is of particular interest in that small
scale vertical motions are clearly indicated (Fig. 9a). The
presence of such vertical motion is of prime importance in
the explanation of anomalies arising from the application of
the Kolmogoroff theory to small scales at meteor heights
(vide Section 3 this Chapter, and Section 5 of Chapter IX).

3.7 An Examination of Velocity Differentials with Height.

Zimmerman (1962) has applied Tchen's theory of shear
turbulence to the results of the velocity/height different-
ial analysis performed by Blamont and De Jager (1961) from
their sodium trail experiments. Excellent agreement with the
Tchen modifications of the Kolmogoroff theory was obtained.
For preferential specification of ξ as z, the sodium trail
data gives

$$E(z) \sim z^{\frac{4}{3}}$$

* Initial height of glow

Δh(km)

84 km.*

(a)

17.11.60

t(secs.)

96 km.*
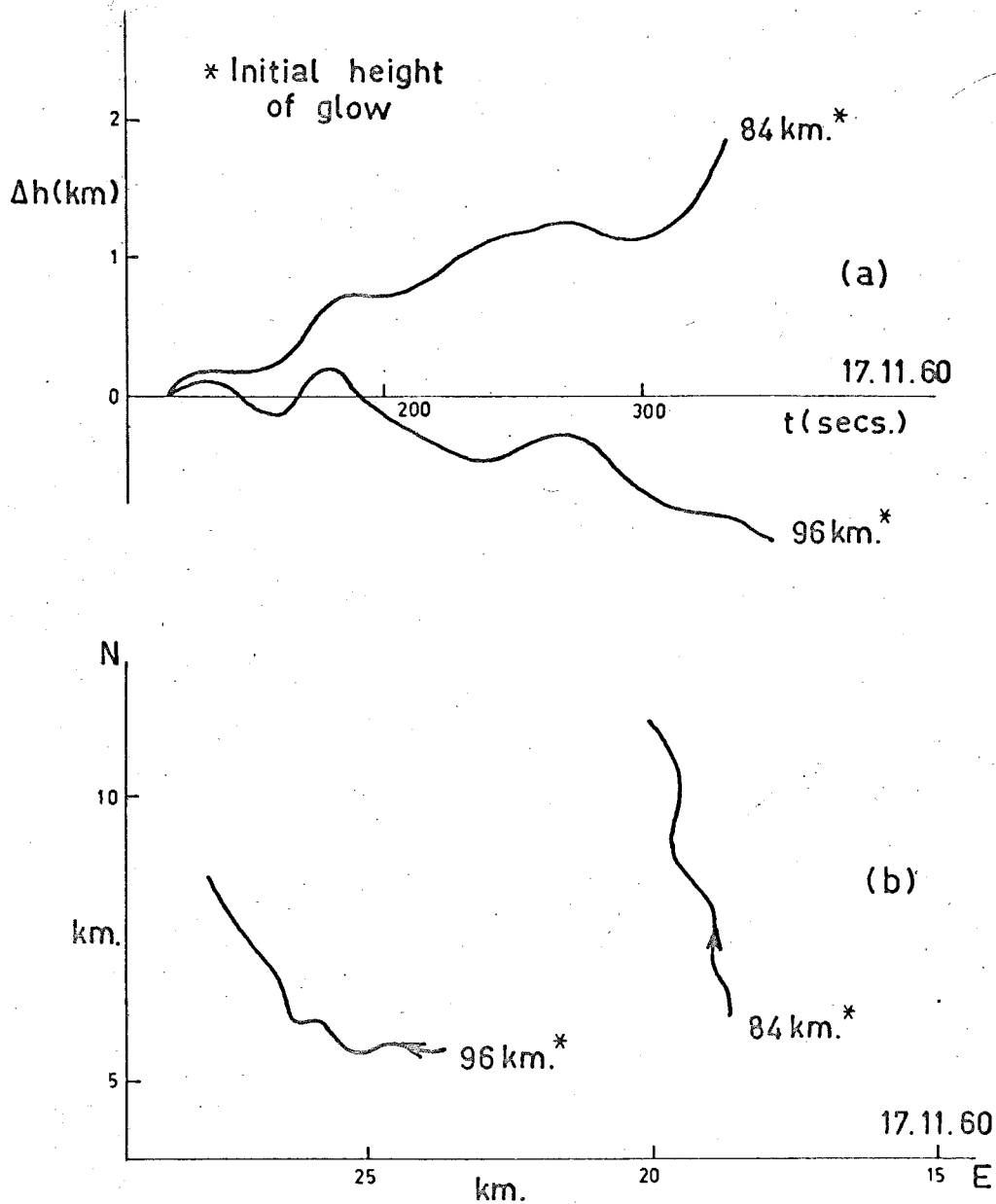
FIG.9 – DISTANCE TIME PLOTS OF GRENADE
GLOWS.   (ROFE, 1961)

up to 6KM height separation, and

$$E(z) \sim \ln \frac{1}{z}$$

for separations greater than 6KM. Zimmerman reforms the height differentials to make the separation ξ isotropic, and finds a Kolmogoroff spectrum

$$E(\xi) \sim \xi^{\frac{2}{3}}$$

pertains up to 6KM separation, with again

$$E(\xi) \sim \ln \frac{1}{\xi}$$

for separations greater than 6KM.

Thus the Blamont / De Jager measurements at 80 - 100 KM are applicable to a region of small shear at separations up to 6KM, with large shears predominating at greater separations.

CHAPTER IV.

Radio Reflections from Meteor Trails

Before the applications and limitations of radio methods of meteor tracking as used to determine atmospheric motions can be fully appreciated, the mechanism of reflection must be understood.

4.1 Historical

When the serious study of the ionosphere began in about 1925, it was discovered that, in addition to the ionization produced by the ultraviolet radiation of the sun, subsidiary sources must exist, particularly in the E region where abnormal increases in ionization occurred during the night.

Skellett (1931) suggested that meteors might be responsible, at least in part, for the E layer anomaly, and, together with Schafer and Goodall (1932) carried out pulse type soundings of the ionosphere during the Leonid meteor shower of 1931. Their results showed that E layer ionization was increased during meteor showers, and that transient increases of up to a few seconds duration sometimes accompanied individual meteors.

In 1941, Chamanlal and Venkataraman in India reported

weak whistles on an unmodulated 7 MCS carrier received at a site located some 10 miles from the transmitter. These whistles lasted approximately a second, usually descended in pitch, and coincided with visual meteors.

With the advances in radio techniques made during the war years, it was possible, in 1945, to begin a systematic study of radio reflections from meteors. The pioneering work in this field was carried out by Hey and Stewart (1947) using a military disposals radar equipment operating on a frequency of 70 MCS. By 1949, radio observations of Meteors were being carried on at Manchester (Lovell, Clegg, Aspinall, Almond, Davies, Ellyet), Stanford (Manning, Villard and Petersen) and Ottawa (McKinley).

More recent developments in this field have already been discussed in Chapter III, and a detailed account of the Adelaide work is given in Chapter VI.

The theoretical discussion which follows is due to Herloffsen, Lovell and Clegg, and Kaiser.

4.2 Theory of Trail Formation.

Because of its high velocity, a meteor in orbit has an energy of the order of several hundred electron volts. As the meteor enters the upper atmosphere, collision with air molecules results in the transformation of some of the kinetic energy of the meteor into heat. The ionized trail is produced

in the 70 to 120 km height range by evapouration of the meteor, molecules leaving the meteor at thermal velocities relative to the meteor of the order of a few electron volts. (Herloffsen 1948)

The rate of evapouration is given by

$$n = (\mu H)^{-1} m \ v \ \cos\chi \ \frac{p}{p_{max}} \left[1 - \tfrac{1}{3}\left\{\frac{p}{p_{max}}\right\} \right]^2 \qquad 4.2.1$$

where

n = number of meteor atoms evapourated per second

m = initial mass of the meteor

μ = mass of an individual meteor atom

v = meteor velocity

H = atmospheric scale height

p_{max} = atmospheric pressure at point of max. rate of
                evapouration

p = atmospheric pressure at point where n occurs

χ = zenith angle of the meteor radiant

(Kaiser 1954)

The electron line density α produced by the meteor is

$$\alpha = \frac{\beta n}{v} \qquad 4.2.2$$

where β is the probability of a single evapourated meteor atom giving rise to a free electron.

Substituting for n

$$\alpha = \frac{\beta}{\mu H} \, m \, \cos\chi \, \frac{p}{p_{max}} \left[1 - \tfrac{1}{3} \left\{ \frac{p}{p_{max}} \right\} \right]^2 \qquad 4.2.3$$

Visual meteors have $\alpha > 10^{10}$ electrons per centimeter.

At formation, the diameter of the trail is of the order of 10 - 100 cm, being a function of the mean free path.

4.3 Decay of Ionized Trails.

After formation, the trail decays under the influence of diffusion, recombination and attachment. Diffusion is the most important; recombination and attachment only assume significance for long duration echoes.

Radial ambipolar diffusion leads to a Gaussian electron density distribution at time **t** of the form,

$$n_e = \frac{\alpha}{4\pi Dt} \, e^{-\frac{r^2}{4Dt}} \qquad 4.3.1$$

where

α = initial line density of ionization

D = ambipolar diffusion coefficient $(D = 2 D_{ionic})$

r = radius of the trail.

4.4 Scattering of Radio Waves by Meteor Trails.   The Radar case.

The classical theory of reflection from meteor trails is that due to Lovell and Clegg (1948). This was subsequently

amplified by Kaiser (1955).

The non-relativistic scattering cross section for a single electron is given by

$$\sigma = \frac{8\pi}{3} \left[\frac{e^2}{mc^2} \right]^2$$

Each electron behaves as a hertzian dipole, with power gain 1.5 over an isotropic radiator. Thus the equivalent echoing area per electron

$$= 4\pi \left[\frac{e^2}{mc^2} \right]^2$$

For an element of trail length $d\xi$, electron line density α, the echoing area becomes

$$dA = 4\pi \left[\frac{e^2 \, \alpha d\xi}{mc^2} \right]^2 = 4\pi \left[\frac{e^2}{mc^2} \right]^2 \alpha^2 \, d\xi^2$$

If P_t is the power output of the transmitter in watts, G the aerial power gain over an isotropic radiator in the direction of the trail, R the range of the echo and λ the wavelength, then the received echo power from element $d\xi$ is

$$dP_r = \frac{P_t G^2 \lambda^2}{(4\pi)^3 R^4} \, dA \text{ watts}$$

$$= \frac{P_t G^2 \lambda^2}{64\pi^3 R^4} \, 4\pi \left[\frac{e^2}{mc^2} \right]^2 \alpha^2 \, d\xi^2 \text{ watts}$$

The total reflected power from the trail is given by integration of the contributions from all $d\xi$ with regard to

the phase of each, and is given in terms of the Fresnel integrals C and S.

Total power of the echo received from the trail is

$$P_r = \frac{P_t G^2 \lambda^2}{64\pi^3 R^4} \, 4\pi \left[\frac{e^2}{mc^2} \right]^2 \frac{R\lambda}{4} \left[C_t^2(\xi) + S_t^2(\xi) \right] \text{ watts.}$$

where $C_t(\xi)$ and $S_t(\xi)$ are the values of the Fresnel integral over the complete trail, whence

$$P_r = \frac{P_t G^2 \lambda^3}{32\pi^2 R^3} \left[\frac{e^2}{mc^2} \right]^2 \alpha^2 \text{ watts}$$

since

$$C_t^2(\xi) + S_t^2(\xi) = 2$$

or

$$P_r = 3.3 \times 10^{-28} \frac{P_t G^2 \lambda^3}{R^3} \alpha^2 \quad \text{watts.}$$

$$4.4.1$$

If separate receiving and transmitting aerials are used (as, of necessity, in the CW method)

$$P_r = 3.3 \times 10^{-28} \frac{P_t G_t G_r \lambda^3}{R^3} \alpha^2 \quad \text{watts.}$$

$$4.4.2$$

An alternative form of this equation, which is more readily applicable to the consideration of the partly formed trail, was obtained by Kaiser by postulating a reflection

coefficient $g = g(\xi)e^{i\phi}$, where ξ is the trail length parameter measuring the distance of the meteor from the t_o or specularly reflecting point, and ϕ is the phase of the reflected wave, such that equation 4.4.2 above becomes

$$P_r = \frac{P_t G_t G_r \lambda^3}{32\pi^4 R_0^3} gg^*$$

Before proceeding further, it is necessary to differentiate between the two types of trail reflection, viz. that produced by underdense and overdense trails. These types are in practice recognized by their echo durations.

4.5   Echo Duration.

Radial diffusion of the trail (Section 3) produces a trail radius r tending to and then exceeding the transmitted wavelength λ. The received power from such a trail is progressively reduced by interference, and the echo decays exponentially with a decay time (duration)

$$\tau = \frac{\lambda^2}{16\pi^2 D}$$

4.5.1

where D is the ambipolar diffusion coefficient.

This is the typical decay pattern of underdense trails. If, however, the initial trail electron line density exceeds a certain critical value, reflection will occur from the surface of an expanding cyclindrical column, and the echo will

persist until the electron line density falls below this critical value, when the echo will decay exponentially as before. Kaiser and Closs (1952) determined this critical electron line density to be approximately 2.4×10^{12} electrons/cm.

If $\alpha \ll 2 \times 10^{12}$ electrons per cm, then

$$g = \pi \alpha \left[\frac{e^2}{mc^2} \right] e^{-4k^2 Dt}$$

$$k = \frac{2\pi}{\lambda}$$

4.5.2

for a fully formed trail.

4.6 The partly formed trail.

If, however, the trail is only partly formed, the reflection coefficient is given by

$$g(\xi) = C \int_{-\infty}^{\xi} F(x) \exp \left[-ik \left\{ \frac{x^2}{R_o} + 2(\xi - x) \frac{u}{v} \right\} \right] dx$$

4.6.1

where $\xi = vt$ ($t = 0$ when meteor is at the specular

reflection point t_o)

$F(x) =$ reflection coefficient of the trail when meteor

is at x relative to the t_o point

$u(x)$ is the line of sight wind component

R_o is the range of the t_o point

v is the meteor velocity

and $k = \frac{2\pi}{\lambda}$ as before   (Kaiser, 1955)

The constant C is chosen so that when $F(x) =$ constant, $u = o$ and $\xi \to \infty$, $g = F =$ value for infinite column of ionization (equation 4.5.2)

i.e.

$$C = \left[\frac{2}{R_0 \lambda} \right]^{\frac{1}{2}} e^{i\pi/4}$$

4.7 The effect of wind shear on reflection.

In the special case where $F =$ constant, $u = u_0 + u'x$ (mean wind plus constant wind shear of gradient u'), and putting $\delta = \frac{2u' R_0}{v}$, equation 4.6.1 reduces to

$$g(\xi) = 2(1-\delta)^{\frac{1}{2}} \exp\left[i\left\{ \frac{\pi}{4} - \theta \right\} \right] I(\nabla) \qquad 4.7.1$$

where

$$I(\nabla) = \int_{-\infty}^{\nabla} e^{-i\frac{\pi}{2}\nabla^2} d\nabla$$

i.e. Fresnel's Integral

This has solution

$$\nabla = \frac{2 - \delta}{[R_0 \lambda (1-\delta)]^{\frac{1}{2}}} v \left[t - \frac{2u_0 R_0}{v^2 (2-\delta)} \right] \qquad 4.7.2$$

$$\theta = k\left\{ u_0 t \left(\frac{2-\delta}{1-\delta} \right) - \frac{\delta^2 v^2 t^2}{4(1-\delta)R_0} - \frac{R_0}{(1-\delta)} \frac{u_0^2}{v^2} \right\} \qquad 4.7.3$$

The phase shift

$$\dot{\theta} = k\left[u_0 \left\{ \frac{2-\delta}{1-\delta} \right\} - \frac{\delta^2 v^2 t}{2(1-\delta)R_0} \right] \qquad 4.7.4$$

corresponds to an apparent time dependent drift velocity.

When compared with the phase of the transmitted wave, the reflected wave will produce a doppler beat of frequency

$$f = \frac{\dot{\theta}}{2\pi}$$

This beat results from the apparent velocity u_a of the trail with respect to the T/R system, where

$$u_a = \frac{f\lambda}{2}$$

i.e.

$$u_a = \frac{\theta\lambda}{4\pi} = \frac{u_0(2-\delta)}{2(1-\delta)} \frac{\delta^2 v^2 t}{4(1-\delta)R_0}$$

4.7.5

If $u' = 0$ (i.e. uniform wind, no shear) then

$\delta = 0$ and $u_a = u_0$

i.e. the apparent line of sight drift velocity of the trail is equal to the line of sight component of the wind. It should be mentioned here that the drift of the trail is that of the neutral air. At this height the influence of the background ionization and magnetic field on the ionized trail is negligible.

If $\delta \ll 1$ i.e. $2u'R_0 \ll v$ which is usually the case, then equation 4.7.5 reduces to

$$u_a = u_0 - u'^2 R_0 t$$

4.7.6

By measuring velocities u_1 and u_2 at times t_1 and t_2 respectively, we can find u' since

$$u_1 - u_2 = -u'^2 R_0 (t_1 - t_2)$$

i.e.

$$u'^2 = -\frac{u_1 - u_2}{R_0(t_1 - t_2)}$$

This gives values of u' in cm/sec/cm. The conventional units used are m/sec/km, and in these units

$$u'^2 = -\frac{u_1 - u_2}{R_0(t_1 - t_2)} \times 10^3 \text{ m/sec/km.} \qquad 4.7.7$$

where u is in m/sec

and R_0 in km.

The significance of this equation is best demonstrated by considering the physical picture. Neglecting the translation due to the mean wind component, the effect on the trail of a linear gradient u' m/sec/km (measured perpendicular to and along the trail) is to cause a rotation ω such that

$$\omega = u' \times 10^{-3} \qquad \text{radians/sec}$$

To maintain specular reflection, the reflection point will, in time t, run along the trail from R_1 to R_2, a distance of $R_0 \omega t$ (see Fig. 10). If the line of sight drift velocity is u_1 at R_1, and u_2 at R_2, then

$$u_1 - u_2 = u' R_0 \omega t = u'^2 R_0 t \times 10^{-3}$$
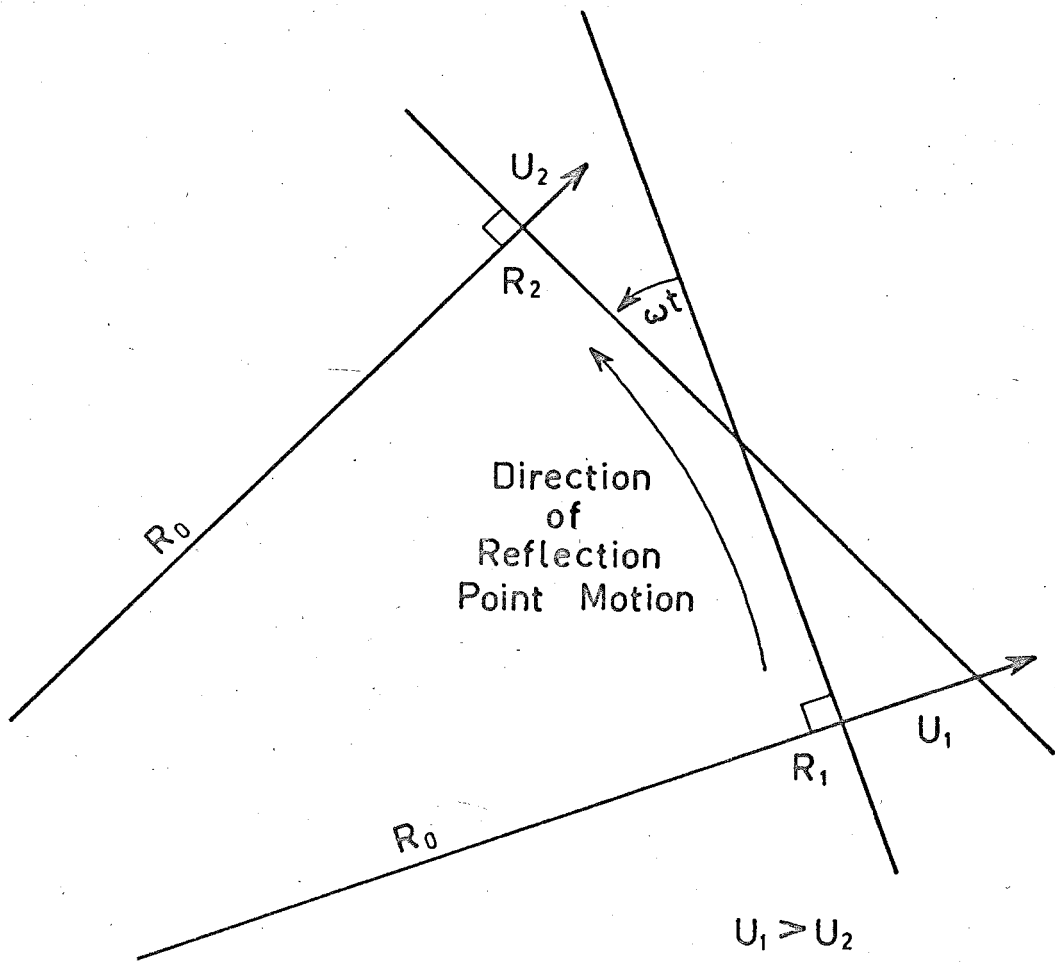
FIG. 10

i.e.

$$u'^2 = \frac{u_1 - u_2}{R_0 t} \times 10^3$$

The rate of motion of the reflection point is given by

$$T = R_0 u' \times 10^{-3} \qquad \text{kilometres/sec}$$

4.7.8

Rao (1958) and Rao and Armstrong (1958) considered this motion of the reflection point to be dependent on the rate of decay of ionization at the reflection point (accompanied by a shift of the reflection point towards the position of maximum ionization α max.) The explanation presented here, which was first proposed by Elford (1954) with different mathematical reasoning, is considered to be more plausible.

4.8 <u>The effect of uniform wind and shear on the measurement of t_0 points.</u>

The amplitude function for uniform wind (no gradient) is given by

$$\nabla = Kv \left[t - \frac{u_0 R_0}{v^2} \right]$$

Kaiser. (See equation 4.7.2)

At the t_0 point, if no wind is present, $\nabla = 0$. However, in the presence of a wind u_0, the measured value of t_0 is delayed by

$$\partial t_0 = \frac{u_0 R_0}{v^2}$$

4.8.1

If the one trail is being observed from three spaced re-
ceiving sites, the property of specular reflection will as-
sign a different t_o point to each station (see Chapter 7 Sec-
tion 1). With a uniform wind, there will be a similar delay
for each reflection point, and thus no overall effect on the
time differences between t_o points at the different sites.

If, however, a linear wind gradient is also present, then
the line of sight component of the velocity will be different
at each t_o point, and will thus produce a different shift in
each point.

This delay at each station is given by

$$\partial t_{o1} = \frac{u_1 R_1}{v^2}$$

$$\partial t_{o2} = \frac{u_2 R_2}{v^2} \qquad \text{In practice,}$$

$$\partial t_{o3} = \frac{u_3 R_3}{v^2} \qquad R_1 \approx R_2 \approx R_3 \approx R_o$$

where u_1, u_2 and u_3 are the line of sight drift veloc-
ities measured at t_{o1}, t_{o2} and t_{o3} respectively.

Thus the true time taken for passage of the meteor from
t_{o1} to t_{o2} is

$$\Delta t_o = \Delta t - \frac{u_1 R_o}{v^2} + \frac{u_2 R_o}{v^2}$$

where Δt is the measured interval.

i.e.

$$\Delta t_o = \Delta t - \frac{R_o}{v^2} (u_1 - \bar{u}_2).$$

But

$$u_1 - u_2 = u'v\Delta t$$

where u' is the wind gradient along the trail.

$$\therefore \quad \Delta t_o = \Delta t \left\{ 1 - \frac{u'R_o}{v} \right\} = \Delta t (1 - \delta/2) \qquad 4.8.2$$

where $\quad \delta = 2u'R_o/v$

This is the same as the expression derived by Kaiser (1955) for the time displacement for spaced stations along a trail x drifting under the influence of a line of sight wind component $u = u_o + u'x$.

4.9 <u>The effect of wind gradients on the measurement of meteor velocities.</u>

As shown in 4.8, a uniform wind affects only the time displacement of the echo, and not the velocity measurement. If a uniform gradient u' is present, however, then from equation 4.7.2 the measured velocity is given by

$$v_a = \tfrac{1}{2}v \frac{2 - \delta}{(1 - \delta)^{\frac{1}{2}}}$$

$$= v \left\{ 1 - \frac{\delta^2}{8} \right\} \qquad \text{for } \delta \ll 1$$

4.9.1

i.e. the effect is small and may usually be neglected.

4.10 Discussion.

The foregoing represents, of course, an idealized set of conditions. Trail ionization is certainly not constant, but increases as the meteor descends through the atmosphere, reaching a maximum only a very short distance before the eventual complete evapouration of the meteor. The meteors with highest velocities will, in general, ionize and disintegrate at higher levels in the atmosphere. Here, the diffusion coefficient is greater, and the trail will therefore decay more rapidly. Because of this limitation in available recording time, there may be some exclusion of faster meteors from our investigation. The simple wind velocity correction applied to t_o measurements is also subject to the limitation that wind gradients may not be linear shears. However, inclusion of this correction does reduce the scatter in radiant for known shower meteors, and is thus worthwhile.

Because of the possible motion of the reflection point along the trail in the presence of wind shears, a limit is placed on the minimum useful separation of reflection points for calculation of wind gradients from separated stations. This is in addition to the uncertainty of location of the reflection "point" within the first Fresnel zone, which makes the maximum contribution to the reflection. These factors

are discussed in greater detail in later chapters, where some results and order of magnitude calculations of these effects are presented.

The theory of velocity determination as presented applies for radar echoes only, and is modified in the CW case by the presence of the coherent ground wave. As shown by Mc Kinley (1949), the continual presence of a reference phase causes a whistle before the t_o point (as in the radar case a post t_o whistle occurs also). Before the meteor velocity can be calculated for such an echo, a knowledge of the relative phases of the sky wave and groundwave is required for all the Fresnel zones used in the calculation. Mainstone (1960) developed a technique for this, utilizing the doppler beat which occurs as the trail drifts (after formation) under the action of atmospheric motion. The minima of the resultant waveform are produced when the skywave and groundwave are π out of phase, and, provided the doppler beat frequency is measurable and constant, the phase can be extrapolated back along the echo.

The presence of the pre t_o whistle is indeed fortunate, since in most cases, the post t_o whistle is lost in the resultant "body doppler" caused by the drift of the trail as a whole.

As shown by equation 4.7.4, the presence of a wind grad-

ient will produce a time dependent velocity of trail drift.
Because of this, a linear extrapolation of doppler phase back
into the pre t_0 whistle can lead to errors in velocity and t_0
point determination. These were estimated by Mainstone as
less than 2%. The present investigation has not seriously
modified this figure.

Note added in proof.

No mention has been made of the meteor particle as a
source of turbulent energy. This question was discussed at
some length at the Symposium on the Fluid Mechanics of the
Ionosphere (New York 1959). The general concensus of opinion
was that whereas the turbulent wake could be of importance
for the larger visual meteors, the contribution of radio met-
eors to the turbulent energy is negligible.

CHAPTER V.

The Adelaide Equipment for Wind Measurement

5.1 General

The original apparatus used for the continuous, auto-
matic tracking of meteor trails at Adelaide was developed in
the early 1950's by Elford, Liddy and Robertson.   The receiv-
ing equipment was installed in a disused ammunition loading
store at Salisbury, the transmitter being operated in the
Physics Department in Adelaide.   Receiver and transmitter
separation was necessary since a continuous wave technique
was used, and the separation of 20KM produced a groundwave at
the receivers of approximately the same level as the skywave
reflected by a typical meteor trail.

By the end of 1957, the site at Salisbury was becoming
more and more unsuitable because of interference caused by
increased industrialization of the area.   Also, the equip-
ment, while still producing worthwhile results, had become
obsolete and required considerable maintenance.   It was
decided, therefore, to build a new receiving station at St.
Kilda, an electrically "quiet" area some 14KM to the west of
Salisbury, and in 1958 the building of equipment for the new

station commenced. The development of a refined technique for meteor velocity determination from CW echoes by Mainstone (1960) about this time initiated a project designed to measure the orbits of individual meteors. This involved the construction and installation of an additional two outstations; these are treated in detail in Chapter VIII. Inherent in the orbit determination is the measurement of the separation distance between the reflection points associated with any two receivers, and this information is utilized in the turbulence investigation (see Chapter VII).

5.2   The Transmitters

The transmitters used for the 1961 survey have been in operation for several years, doing routine wind measurements. The CW transmitter was modified by Mainstone in 1958, and produces an output power of approximately 300 watts at a frequency of 26.773 MCS (wavelength = 11.2 metres). This power is radiated within a cone $\pm 45°$ about the zenith by a three element Yagi array suspended above the Physics building at the University. A similar array is used to radiate the 10KW peak power pulse from the radar transmitter, which operates on the same frequency and is phase coherent with the CW. Pulse width is 10μ sec; repetition frequency 100 pulses per second. The arrays were raised and lowered until a suitable groundwave level (some 8 μv CW) was received at St. Kilda.

MAIN STATION, ST. KILDA

This CW groundwave is used as the reference phase in the drift measurement by the doppler method, and the radar groundwave triggers the range marker generator at the receiving site.

The main receiving station at St. Kilda was operational in July, 1960, and all facilities, including the outstations, were producing results by December of that year.

5.3 The Main Station Mean Wind Measuring Equipment.

The method of determining atmospheric mean motions at meteor heights from the line of sight drifts of trails measured by the doppler shift on CW signals reflected from such trails is due to Manning, Villard and Petersen (1950); as used at Adelaide it contains some modifications in the direction finding and sense of drift determinations. The two basic assumptions, that of aspect sensitive reflection from the trails, and a predominantly horizontal mean atmospheric drift, have been well substantiated both theoretically and experimentally.

The mean wind survey requires the measurement of four parameters for each echo. These are

1) the line of sight drift of the trail

2) the direction cosines of the reflection point relative to NS and EW axes

3) the height of the reflection point
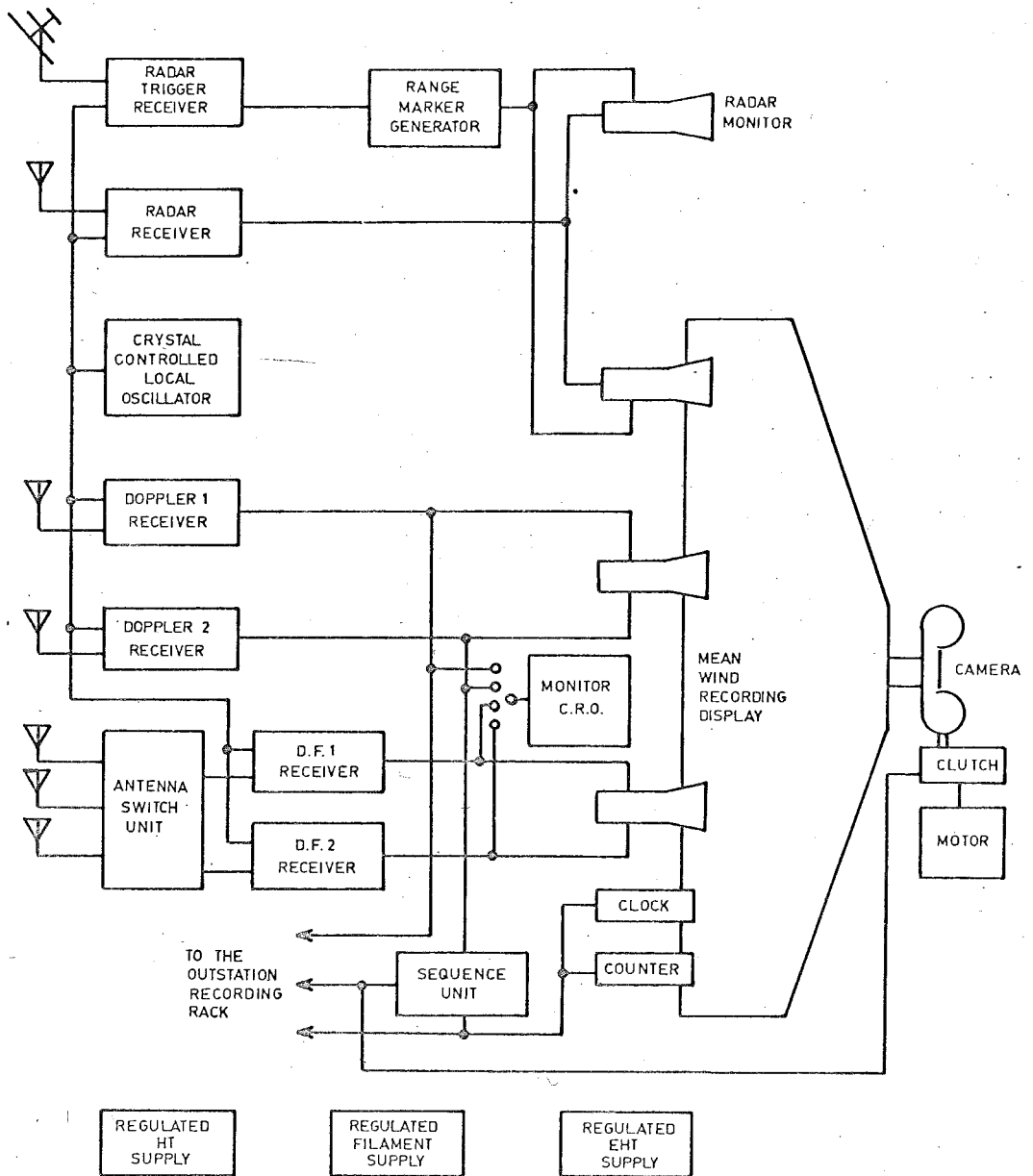
FIG.11 - MAIN STATION MEAN WIND MEASURING EQUIPMENT.

and 4)   the time of occurrence of the echo.

Continuous wave techniques are utilized in the determination of 1) and 2), and 3) is found by using the supplementary pulsed transmitter and radar receiver to determine the slant range of the trail which, together with 2), yields the height of reflection. Fig. 11 is the block diagram of the receiving section of the Mean Wind Measuring Equipment (henceforth referred to as the Wind Equipment).

Five spaced dipoles, each $\lambda/4$ above ground, and four narrow band receivers are used to determine the direction of arrival of the reflected wave. The orientation of these aerials is such that the groundwave always presents a plane wave front to the dipoles. The relative phases of the sky-wave and groundwave are established at the aerials in terms of the relative phases of the low frequency doppler beats. Therefore, there is no necessity to preserve the R.F. phases through the receivers. Two of the receivers, labelled D.F.1 and D.F.2 in Fig. 11, are switched between three of the aerials. Their outputs are D.C. amplified and displayed on a double beam C.R.T in the Wind display. The traces are identified by asymetry of the switching intervals, giving "light" and "dark" traces.

The two Doppler receivers continuously monitor the C.W. level. The sharp rise (or fall) of the signal level which

occurs when a suitably oriented trail is formed in the atmosphere, triggers the sequence unit which is connected to the output of one of these receivers. The sequence unit brightens the oscilloscopes in the Wind display, and energizes the magnetic clutch on the Wind camera. The normal recording interval is of the order of one second. The sequence unit also provides a triggering pulse for the equipment which records information required for turbulence and orbit measurements.

The receivers and D.C. amplifiers are the same as those used in the outstation equipment, and are described in detail in Chapter VIII.

The range of the reflection point is recorded using a conventional intensity modulated A-scope display. A wide band receiver is connected to a sixth dipole, and its output intensity modulates another C.R.T in the Wind display. The time base and range marker generator is triggered by the output of an additional broadband receiver connected to a horizontal three element Yagi array beamed on Adelaide. This ensures that the timebase is always triggered on the groundwave pulse even when the skywave amplitude (as received on a dipole) exceeds the groundwave level.

A clock which is illuminated every quarter hour, and a counter and electronic flash which are fired on each echo

completes the display line-up.

A typical echo as filmed is shown in Fig. 13.

The sense of trail drift (towards or away from the receivers) can be determined from the relative phases of the doppler outputs of the four narrow band receivers, but this is a rather tedious process of elimination, and a much better method which gives the sense of drift on sight from any one output trace was devised by Robertson in 1952. The CW transmitter at Adelaide is phase modulated by a sawtooth wave synchronized with the 50 cycle mains which slowly advances the R.F. phase of the transmitter output and then suddenly retards it by 90° fifty times per second. Normally, this phase modulation produces no receiver output, since the receivers all employ conventional A.M. diode detectors. However, during the presence of an echo the phase retarded groundwave reaches the receivers at St. Kilda about one millisecond before the phase retarded skywave, so that during this brief period the vector triangle RGS in Fig. 12 is replaced by $R'G'S'$ in which G' makes an angle of -90° with G, but the phase of the skywave is unchanged. The brief change from R to R' is recorded as a spike (of duration $\sim$ 1 millisecond) on the doppler beat curve at 1/50 sec. intervals. It can be seen from the record of Fig. 13 that the ends of these spikes trace out a "phantom" beat curve which in this case
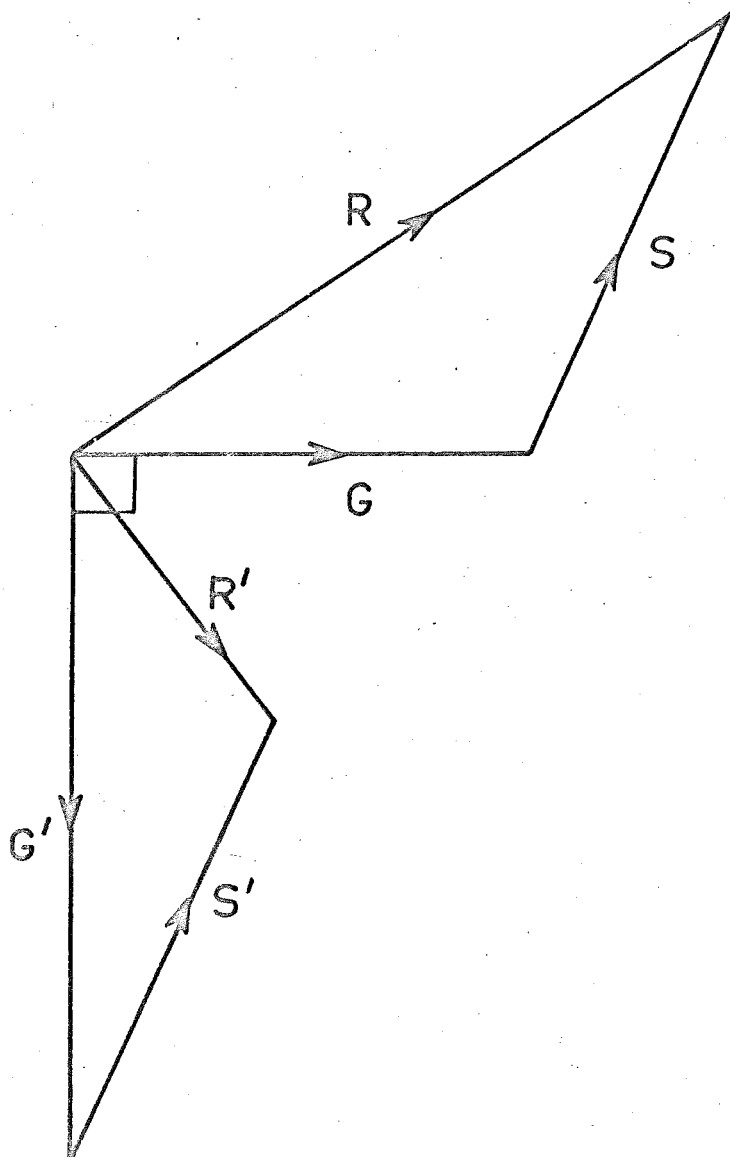
FIG. 12
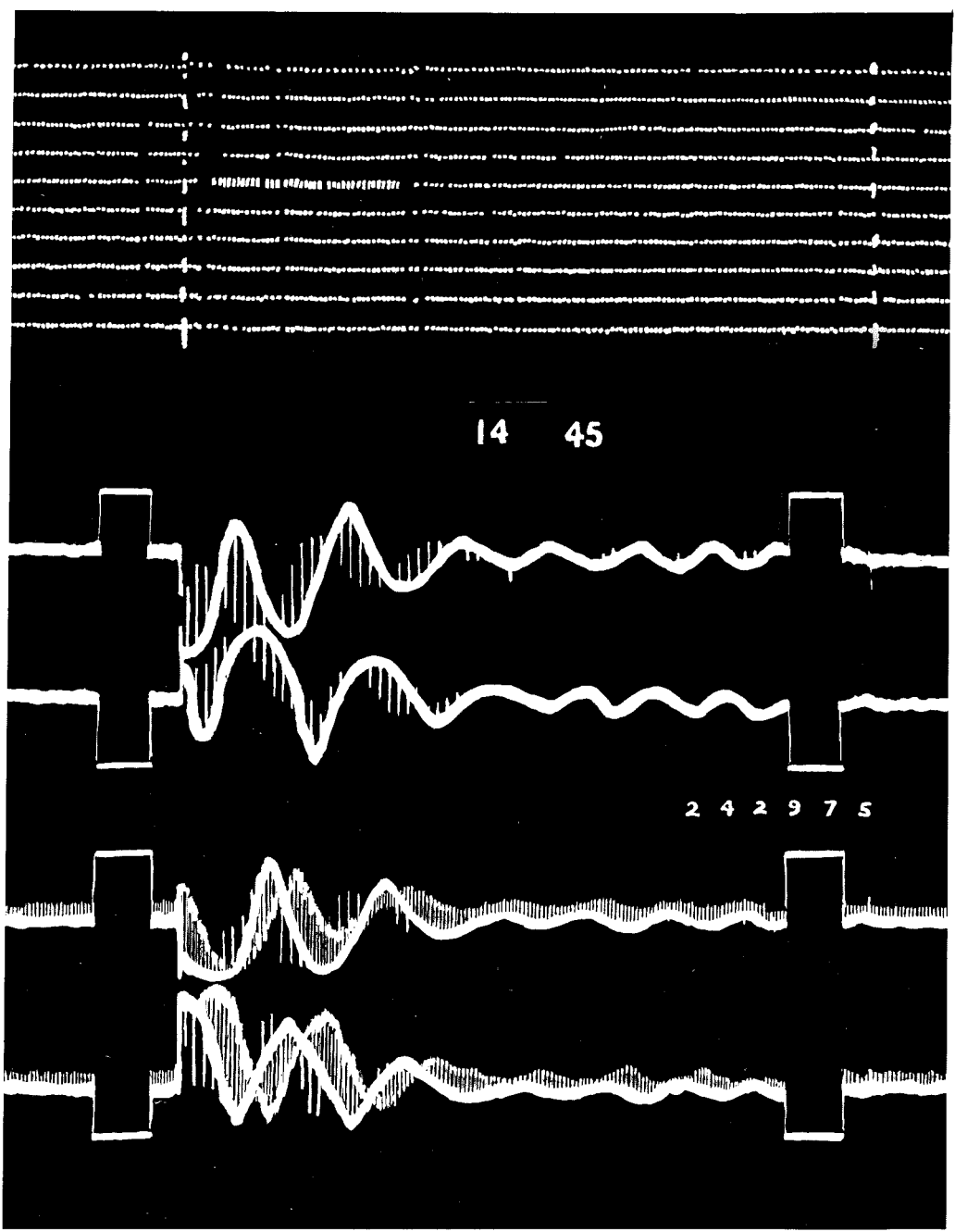
FIG 13- MEAN WIND RECORD

FIG 14 - MEAN WIND RECORDING RACK

leads the main doppler beat curve.

The phase of the phantom beat curve either leads or lags the phase of the main doppler beat curve according as the phase path of the sky wave is either increasing or decreasing. With reference to Fig. 12, if the phase path is increasing, S is rotating clockwise and R is approaching its maximum value as R' is approaching its mean value. Thus R leads R' in phase. Similarly if S is rotating anticlockwise R is approaching its mean value as R' is approaching its minimum value so that R lags R' in phase. In the actual record of Fig. 13, R lags R'. This represents a decrease in the phase path, and the line of sight component of the drift velocity of the meteor is directed towards the T/R system. These sense spikes on the traces also give convenient 20 millisecond time markers by means of which the doppler frequency can be measured.

In the interests of stability, all H.T. power supplies are electronically regulated, and all valve filaments are fed from a constant voltage transformer. The receiver and display power supplies use a highly stable circuit devised by Attree (1955). The output impedance of these supplies is less than 0.1 ohm from D.C. to 50kc, and ripple is less than 10 millivolts at a high tension output of 200ma at 250v.

Fig. 14 is a photograph of the Mean Wind Recording Rack,

housed in the station at St. Kilda.

CHAPTER VI.

Preliminary Investigations at Adelaide

6.1 Methods of Mean Wind Data Reduction.

For the years 1952 to 1962 inclusive, equipment similar to that described in Chapter V has been recording winds in the meteor region above Adelaide. Almost from the commencement of the wind project it was realized that velocity gradients with height existed, and the method of data reduction included arbitrary stratification of the region into three bands 10km thick, centred on 80, 90 and 100km respectively. Stratification with narrower height grouping was contemplated, but was not commensurate with either the accuracy of ranging or the echo rate, and was therefore not implemented.

The echoes are grouped in hourly intervals. Because of the echo rate, it has been necessary to record for several days each month, and to lump the data to give winds for a "typical day" of the month.

For any given height group and time, at least two echoes are required to specify the appropriate mean wind velocity vector, since only the line of sight component of drift can be recorded for each echo. If more than two echoes of the

appropriate height and time are recorded, a least squares fit
to the resultant NS and EW vector components is used to ob-
tain the required wind vector. This analysis is produced in
the Elford et al (1953) paper.

The data read from the wind films is punched onto cards
and processed on an IBM 1620 computer to give the resultant
NS and EW wind components. The appropriate IBM FORTRAN pro-
gramme appears in Appendix I.

The mean hourly winds for a given height range of the
typical day for the given month are then subjected to a
Fourier Analysis to determine the prevailing, diurnal and
semi-diurnal components. This is also carried out on the
1620 computer (programme, Appendix I).

6.2 Random Winds.

An early investigation by Elford et al of trails assum-
ing aspect sensitivity close to the zenith showed that vert-
ical drift velocities were small in comparison with the hor-
izontal drifts, and that the mean motion was confined to
within $\pm 15°$ of the horizontal. Vertical motions of up to 10
metres / second with a vertical mean drift of 1 to 2 metres/
second were found, associated with horizontal winds of 80
metres / second.

One of the most interesting features of the winds as
recorded is the reproduction year after year of the same
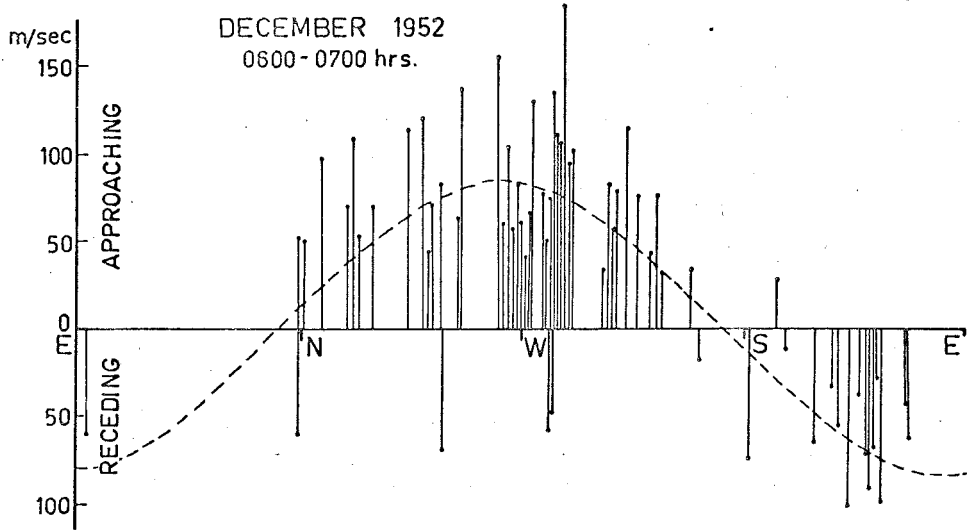
FIG.15a - MEASURED WINDS
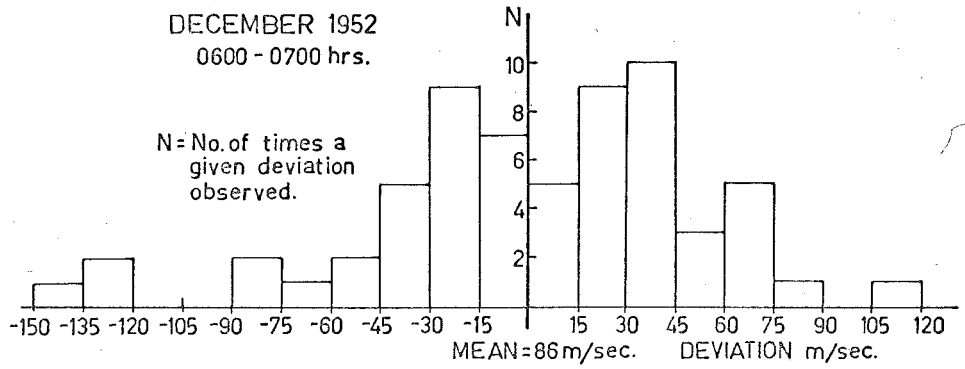
FIG.15b - VELOCITY DEVIATIONS FROM THE MEAN WIND

basic wind patterns for a given month. This leads to the conclusion that turbulent motions, if present, are subjugate to the mean flow.

To obtain some indication of the probable magnitude of the turbulent velocities, the mean wind was extracted from the records for 0600 to 0700 hours, December 1952 (Fig. 15a). The result is the histogram of Fig. 15b. The value of the mean wind at the time was 86m/sec, and the most probable turbulent velocity of the order of 30m/sec. This agrees reasonably well with the RMS velocity of 50m/sec for a mean wind of 100m/sec (Manning, 1959), and also with the 25m/sec turbulent velocity found by Greenhow to be an average regardless of the mean wind speed.

The size of the eddies responsible for this turbulent velocity cannot be deduced from the Adelaide single station observations. A narrow transmitting and receiving beam width is required to determine time correlations (an area of the meteor region small in comparison with the size of the disturbance must be illuminated), and the Adelaide system has always used broad all sky antennae.

6.3   The Effect of Wind Shears on Long Duration Echoes.

The effect on the meteor trail of a linear shear has been shown in Chapter IV Section 7 to produce a rotation of the trail which results in motion of the reflection point

along the trail. Since in the determination of the wind gradients along a trail the separation distance is of prime importance, any factor which may effect reflection point motion is worthy of consideration.

The rate of motion of the reflection point in kilometres/sec is given by equation 4.7.7, viz.

$$T = R_0 u' \times 10^{-3}$$

where R_0 is the slant range of the echo in km and u' is the trail gradient expressed in m/sec/km. The assumption of a linear gradient is, of course, an oversimplification, but it is useful for determining order of magnitude values for the quantity T. If the gradient were truly linear, then there would be no relative motion with time of any two points on the trail, and errors would be incurred only in the absolute and not in the relative drift velocity determinations.

Velocity gradients, when encountered, are characterized by a time dependent drift velocity, observed on the recording film as a doppler beat increasing or decreasing with time.

The actual drift velocity at the t_0 point is related to the observed drift velocity at a time t after the meteor has reached the t_0 point by equation 4.7.6, viz.

$$u_a = u_0 - u'^2 R_0 t$$

If the gradient u' is zero, then the observed drift is equal to the actual drift.

Since by far the greater majority of long duration echoes exhibit this change in doppler frequency with time, it is reasonable to suppose that the trail is always subject to deformation by some form of wind gradient. There is always a finite delay after trail formation before the echo is recorded, and the execution of each doppler cycle in itself introduces a further time interval over which measurement of the doppler is being made. Thus there is always some difference between the measured and actual values of the line of sight drift vector.

To determine the typical order of magnitude of the time dependent drift velocity variation and reflection point motion, 70 echoes for December, 1960, were examined in considerable detail. The average line of sight drift vector for these echoes is 42 metres/sec; the RMS value of the rate of velocity change with time is 9.1 metres/sec/sec. Allowing for an average time after the t_0 passage of the meteor before measurement of 0.1 secs, the average absolute velocity error is only of the order of 1 metre/sec, and is of the same order as the normal film reading errors. However, the rate of reflection point motion is of more consequence. Fig. 16 shows the number of echoes observed with a given reflection point motion (calculated from the doppler variation with time, and assuming a linear gradient). Whereas the average motion of
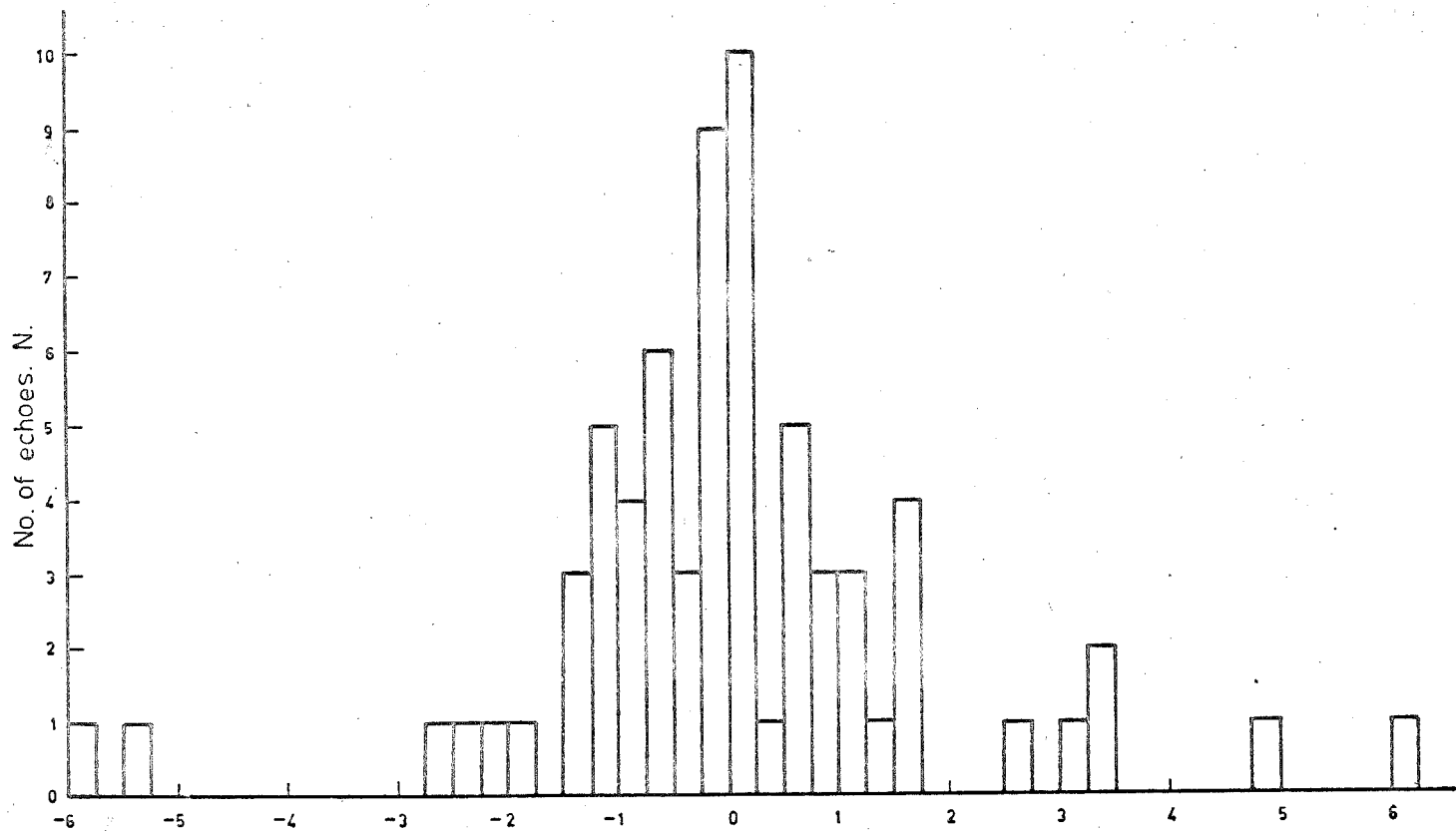
FIG.16 -Motion of reflection point along trail, (km./sec.)

DECEMBER 1960.

the reflection point along the trail is zero, values up to
6 km/sec are found, the RMS value being ~ 1 km/sec. Thus the
drift velocity measured 0.1 sec after time t_o is, on the aver-
age, the drift velocity of a point 100 metres away from the t_o
point. If the wind gradient along the trail is not linear
(which is usually the case, as is shown by reference to Fig.
17a, where the change in drift velocity with time is by no
means constant), then the separation of any two reflection
points on the trail will be highly time dependent. This
places a rather severe limitation on the measurement of trail
shears at small separations (~ 200 metres).

If the echo duration is sufficient, the action of non-
linear shears may cause more than one portion of the initially
straight trail to be normal to the line of sight direction
and hence give equally strong reflections. If these portions
are moving at different relative velocities, interference
between the reflected waves will be observed at the receiver.
This has proved to be a complication for methods of investig-
ation of meteor trails based on the measurement of the pas-
sage over the ground of diffraction patterns caused by re-
flection of radio waves from such trails. The effect is of
little consequence with a doppler method for short duration
echoes.

A typical beat envelope type of long duration echo is
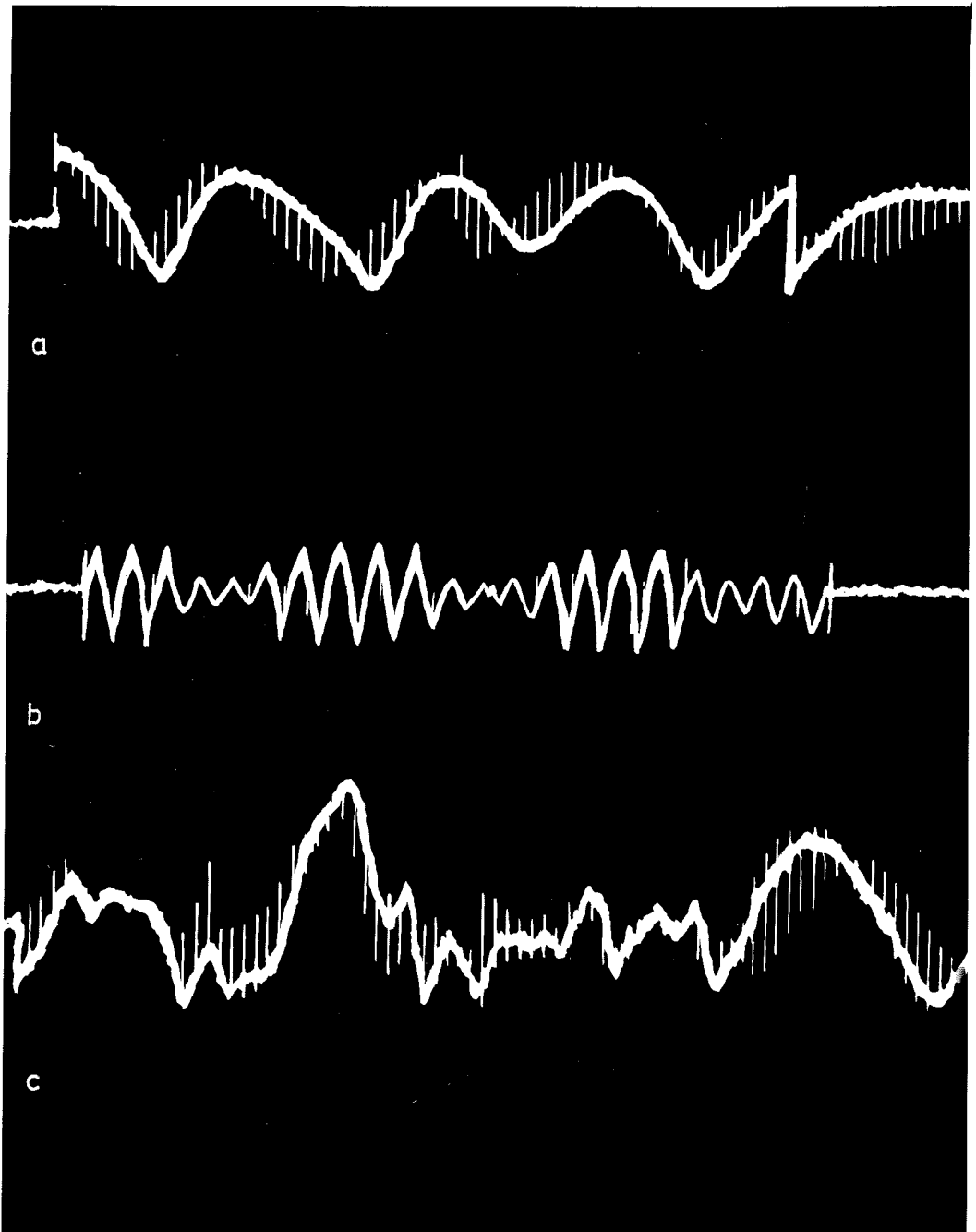
FIG 17- TYPICAL ECHO TYPES

shown in Fig. 17b. This presumably has only two reflecting
centres, moving with small relative velocity. The echo of
Fig. 17c, however, depicts what one might almost describe as
a chaotic situation.

Anomalous echoes can also be caused by the fragmentation
of meteors. This can give rise to blobs of high ionization
lying along the path of the meteor. These regions simultan-
eously produce reflections, and the trail is no longer a line
source. Relative motion of these blobs gives rise to a beat-
ing type echo.

Occasionally, more than one meteor echo will occur at a
given time, the received signal being a combination of the
two doppler beats. This type of echo is usually readily
recognized because of its associated multiple range.

A further investigation of the interesting properties of
long duration echoes is contemplated.
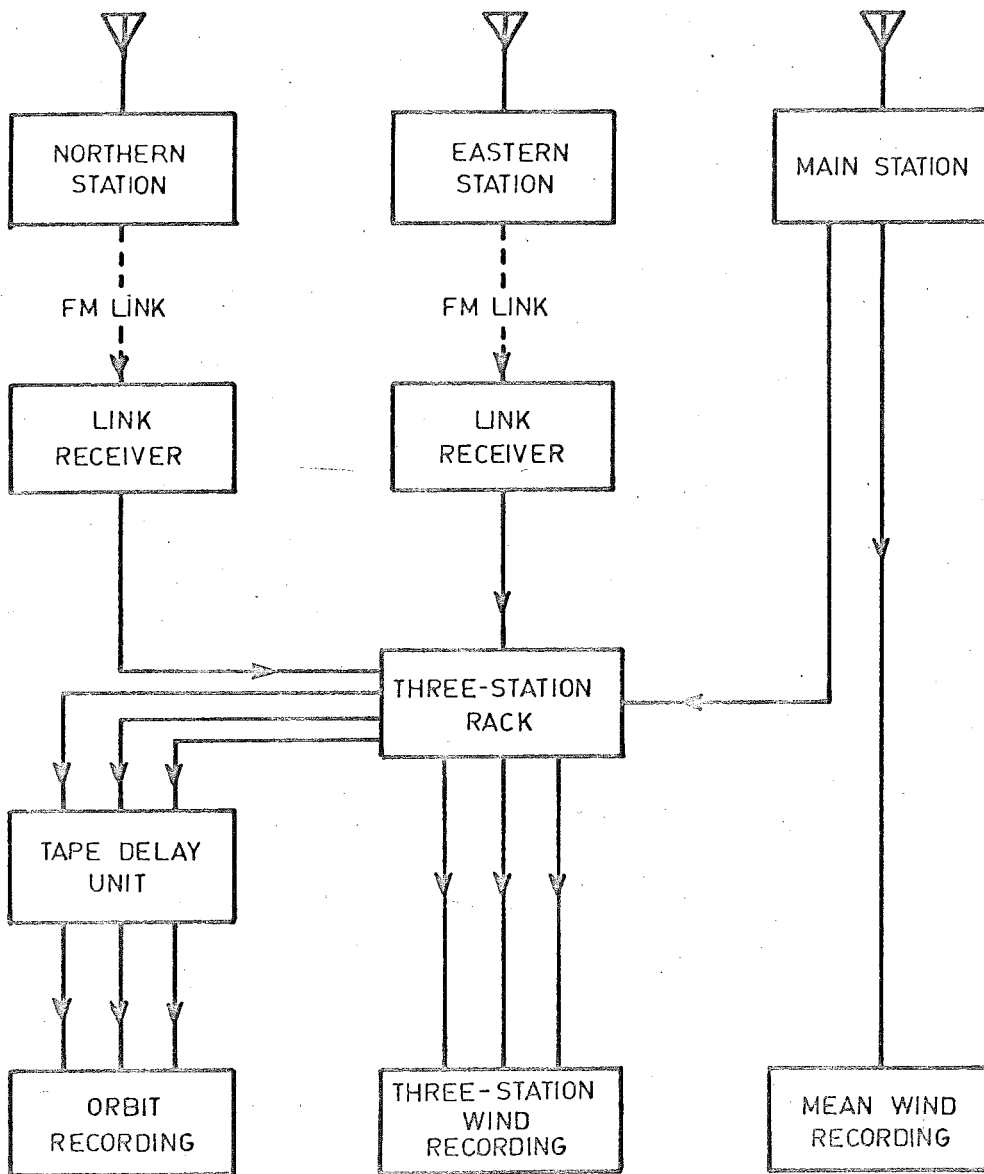
FIG.18 - THE THREE-STATION SYSTEM.

CHAPTER VII.

The Adelaide Three Station System

7.1 General Description of the System.

Since the reflection of radio waves from a meteor trail after formation is, in the first instance, specular, the spacing of receivers on the ground will result in each receiving information from a separate point on the trail. In the Adelaide system three receiving stations are used. The operation of two of these stations is completely automatic in that they run unattended except for routine maintenance, and continuously transmit the signals received back to the main receiving station at St. Kilda.

Fig. 18 is a block diagram of the overall system. One outstation is located at Sheedys' Farm, 4.72 km north of the St. Kilda receiving site, and the other outstation is at Direk, a disused railway siding 4.81 km to the east of the main station (see Fig. 19). For convenience in the specification of the geometry of the system for purposes of data reduction, the transmitting and receiving sites determine a rectilinear system of coordinate axes (see Fig. 20). The transmitters at Adelaide, the St. Kilda main station and the
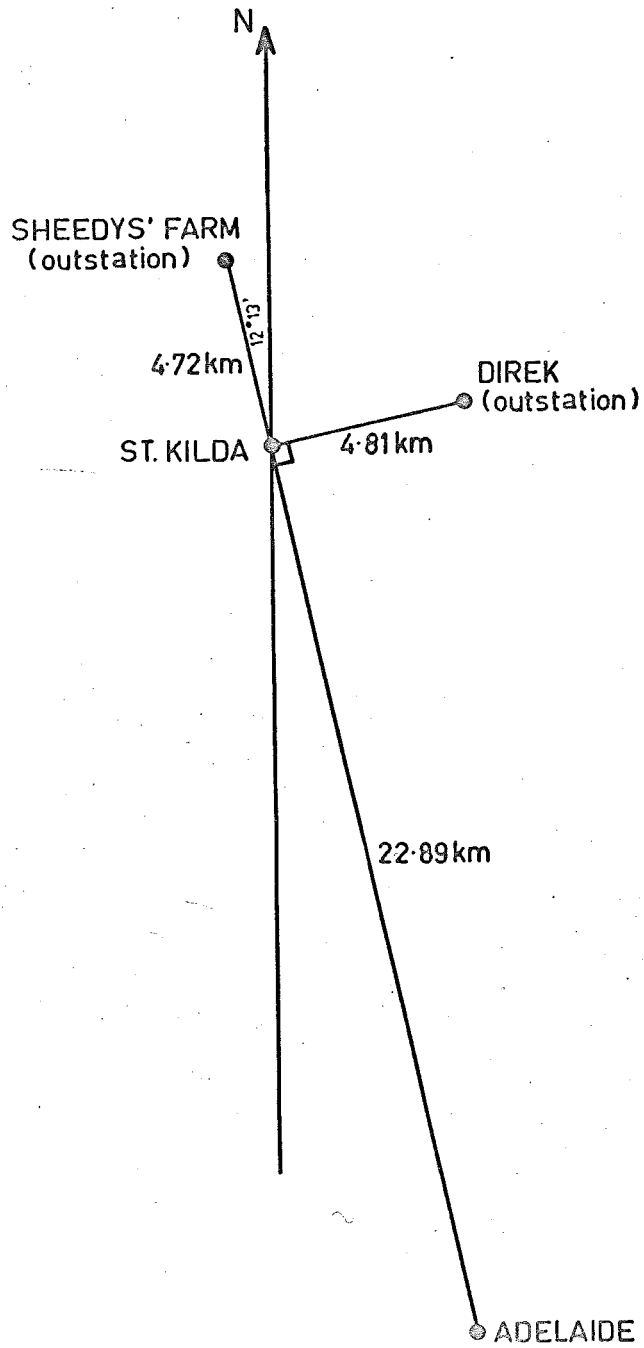
FIG.19 – PLAN of TRANSMITTING and
RECEIVING SITES – 1961.

Sheedys' Farm outstation are colinear, and the St. Kilda - Direk line is perpendicular to this axis.

To simplify the correlation of echoes received at the various stations, all recording is performed at the main station. Three sets of film records are obtained, each concerned with a different aspect of the investigation of the astronomical properties of meteors, and the effects of atmospheric motions on meteor trails.

By recording the initial whistle accompanying trail formation as observed from each outstation, not only can the meteor velocity be determined (from the rate of formation of the Fresnel zone pattern) but also the time of onset of specular reflection, t_o, appropriate to each station can be specified. From the meteor velocity and the different times of commencement of the echo at each station, the spacial separation of the appropriate reflection points is readily calculated. This spacial separation is the parameter ξ, which, together with the line of sight trail drift velocity as determined from the body doppler received at each station, provides the basic data for the turbulence investigation.

As has already been shown in Chapter V, the record taken from the main station receivers uniquely specifies the position of one point on the trail. The coordinates of this point, together with the appropriate ξ values and a knowledge

of the outstation system geometry is all that is required to determine the direction cosines and the position of the meteor trail in the upper atmosphere. From these direction cosines and the velocity of formation of the trail, the orbit of the meteor particle producing the trail can be determined. The basic measurements of meteor velocity and spacial separation of the reflection points were made by a co-worker, Carl S. Nilsson, who completed, concurrent with the turbulence programme, a thirteen month survey of the orbits of shower and sporadic meteors as observed from the southern hemisphere.

7.2   The Choice of the Receiving Station Separations.

For the investigation of atmospheric turbulence from spaced station radio echo observations of meteor trails, there are two main factors which govern the choice of station separation. These are the finite lengths of the trails formed by meteors in the upper atmosphere, and the scale of the turbulence. From the point of view of the orbit project, as large a station separation as possible is desirable, since the accuracy of determination of the direction cosines of the trail increases with increase of reflection point separation. If only a small number of zones of the Fresnel diffraction pattern are discernable on the orbit film record for a given meteor, there is an inherent inaccuracy in the absolute spec-

ification of the t_o points appropriate to each receiving station. If the time difference between the t_o points are large, the effect of this inaccuracy of individual t_o determination on the computed direction cosines of the trail will be small.

The upper limit of station separation is determined by the lengths of the trails formed in the atmosphere. Trail lengths are, on the average, about 20km. If large station separations are used, the number of meteors producing echoes at all three stations will be small. The station separation of 5km used in the Adelaide three station system represents a good compromise between accurate trail direction cosine determination and useable echo rate.

It can be shown geometrically that the maximum separation of reflection points on a suitably oriented trail is half the station separation (See Section 4 of this Chapter). Thus the maximum ξ value associated with a station separation of 5km is 2.5km. Since most of the controversy associated with investigations of atmospheric turbulence in the meteor region has been concerned with the scales of size 1km or less, a station separation of 5km can be regarded as almost ideal for the determination of the properties of small scale turbulence in the height range from 80 to 100km.

7.3 The Use of Shower Meteors in a Turbulence Investigation.

While the turbulence and orbit projects were being developed, it was not altogether certain that the radiants of sufficient meteors would be measured in any one month to give a significant sample for the purpose of turbulence measurements. For this reason, an alternative system was devised, based on the known properties of shower meteors.

The extraction of shower meteors from the sporadic background is made possible by the aspect sensitivity of reflecting trails. A northerly radiant produces trails which assume aspect sensitivity only to the south of the receivers. For a given shower radiant, at any one time the reflection points of such shower meteor trails lie on a horizontal line perpendicular to the radiant direction. (This assumes a flat earth, and that all meteors form trails at the same height, both reasonable approximations). Thus, if the time of occurrence of the echo is recorded, and its reflection point lies on the line appropriate to the radiant at that time, then it is highly probable that the meteor belonged to the given shower. A clock in the wind equipment display records quarter hourly, and this interval is sufficiently small to provide quite accurate grouping. From the time of the echo and the known radiant of the shower, the appropriate trail direction cosines λ, μ, γ can be calculated. To calculate the reflection point

separations, consideration must be given to the geometry of
the trail with respect to the spaced stations.

7.4 <u>The Outstation Geometry.</u> (Fig. 20).

If the trail ξ has direction cosines λ, $\dot{\mu}$, ν, and A_0P_0
is perpendicular to P_1P_0 (specular reflection) then, putting
$q = R_0A_0$

$$(1r_0 + q)\lambda + mr_0\mu + nr_0\nu = 0$$

i.e.

$$r_0(1\lambda + m\mu + n\nu) = -q\lambda \qquad 7.4.1$$

A first order approximation is given by

$$q = + \frac{d}{2}$$

i.e. A_0 is the midpoint of R_0T

This approximation is adequate for the order of accuracy
required in the turbulence investigation. The true solution
is obtained by making the distance $R_0P_0 + P_0T$ a minimum, and
is used in the orbit calculations where a higher degree of
accuracy is required.

Substituting $q = \frac{d}{2}$ in 7.4.1 gives

$$r_0(1\lambda + m\mu + n\nu) = - \frac{d}{2}\lambda \qquad 7.4.2$$

The equation of the trail, in terms of the parameter ξ,
is
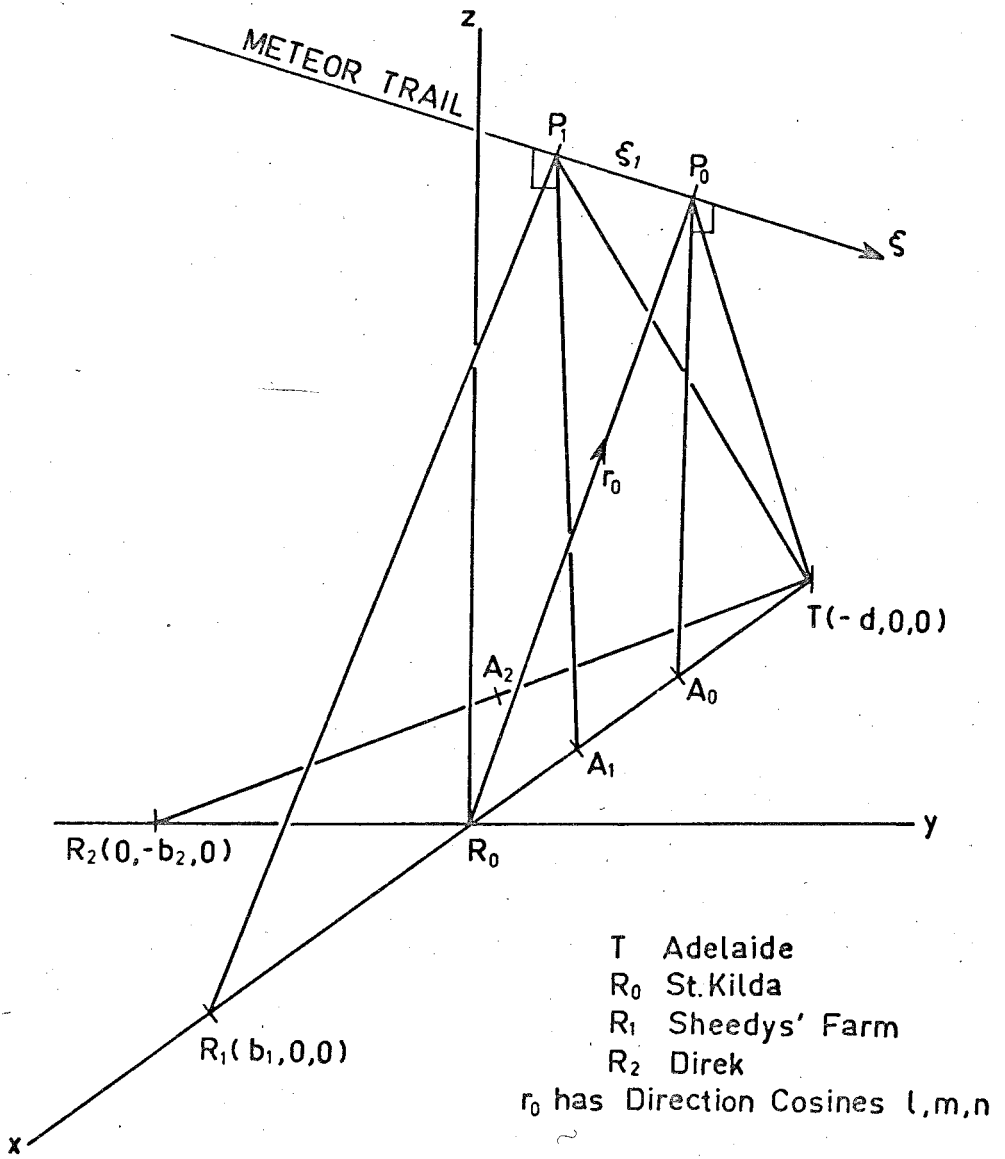
FIG. 20 - THE GEOMETRY OF THE SYSTEM

$$x = lr_0 + \lambda\xi$$

$$y = mr_0 + \mu\xi$$

$$z = nr_0 + \nu\xi$$

For the first outstation R_1

A_1 has coords. $\left(-\dfrac{d-b_1}{2}\right)$, 0, 0

and at $\xi = \xi_1$, the point of specular reflection from T to R_1, the direction cosines of A_1P_1 are

$$\frac{1}{A_1P_1}\left[lr_0 + \lambda\xi_1 + \frac{d-b_1}{2}, \ mr_0 + \mu\xi_1 \ , \ nr_0 + \nu\xi_1 \right]$$

A_1P_1 is perpendicular to the trail

$$(lr_0 + \frac{d-b_1}{2} + \lambda\xi_1)\lambda + (mr_0 + \mu\xi_1)\mu + (nr_0 + \nu\xi_1)\nu = 0$$

i.e.

$$\lambda(lr_0 + \frac{d-b_1}{2}) + \mu(mr_0) + \nu(nr_0) + \xi_1 = 0 \qquad 7.4.3$$

From 7.4.3 and 7.4.2,

$$\lambda\left(\frac{b_1}{2}\right) + \xi_1 = 0$$

i.e.

$$\xi_1 = -\frac{b_1}{2}\lambda$$

For the second outstation R_2

A_2 has coords. $-\dfrac{d}{2}$, $-\dfrac{b_2}{2}$, 0

Specular reflection from T to R_2 requires

$$(1r_0 + \lambda\xi_2 + \frac{d}{2})\lambda + (mr_0 + \mu\xi_2 + \frac{b^2}{2})\mu + (nr_0 + \nu\xi_2)\nu = 0$$

i.e.

$$\lambda(1r_0 + \frac{d}{2}) + \mu(mr_0 + \frac{b^2}{2}) + \nu(nr) + \xi_2 = 0 \qquad 7.4.4$$

From 7.4.4 and 7.4.2,

$$\mu\left(\frac{b^2}{2}\right) + \xi_2 = 0$$

i.e.

$$\xi_2 = -\frac{b^2}{2}\mu$$

The distance b_1 is the distance from the main station at St. Kilda to the outstation at Sheedys' Farm, viz. 4.72 KM; b_2, the distance from the main station to the Direk outstation, is 4.81 KM.

Substitution of the appropriate λ, μ for each shower meteor thus yields the separations ξ_1 and ξ_2.

Because of the reasonably high sampling rate achieved with all orbit information available, this method has not been used to date.

CHAPTER VIII.

The Outstation Equipment

8.1 General

Each of the outstations situated at Sheedys' Farm and Direk is completely self contained, and runs unattended except for routine maintenance. For protection from the weather and possible vandalism, the rack of equipment at each is housed in a steel tank buried in the ground with only a padlocked lid visible (Fig. 21). The 27 mcs $\lambda/2$ receiving dipole is mounted $\lambda/4$ above the ground on a length of two inch waterpipe, and feeds the receiver via a coax cable which runs down the inside of the pipe and underground into the tank. This pipe also serves as an air intake for the blower mounted in the bottom of the tank. Whereas this blower is not strictly necessary, it does help to remove some of the 300 watts being dissipated by the equipment. The warm air is exhausted through louvres under the lid (see Fig. 22).

A.C. power (240v) is conveyed to the rack by an armoured cable which runs underground from the tank for some 30 yards before being connected to the overhead distribution system. This helps to eliminate interference which might be radiated

167 mcs YAGI

OUTSTATION
DIAGRAMATIC SKETCH

27mcs DIPOLE

AIR INLET

GROUND LEVEL

ARMOURED
POWER CABLE

FIG. 21
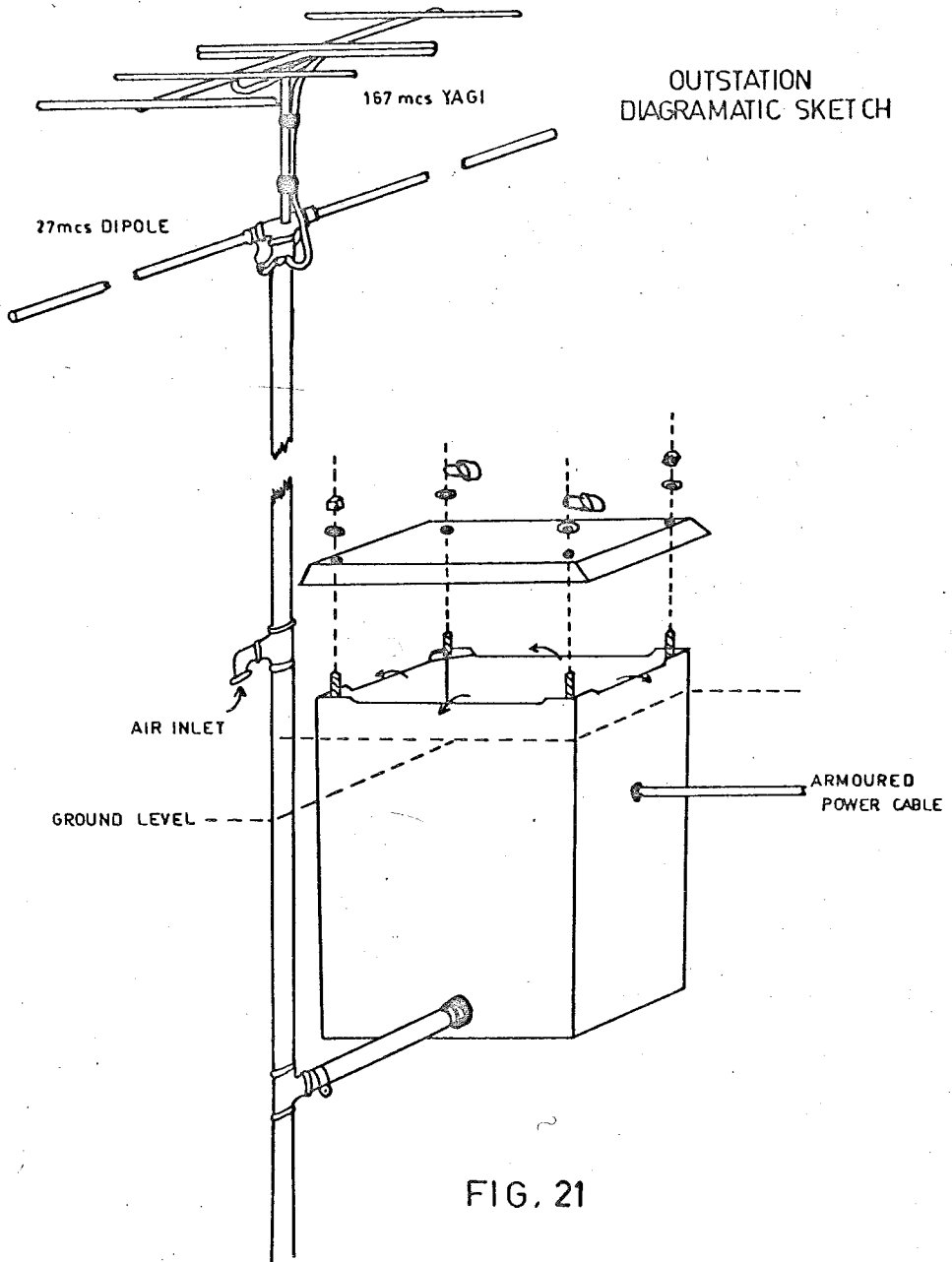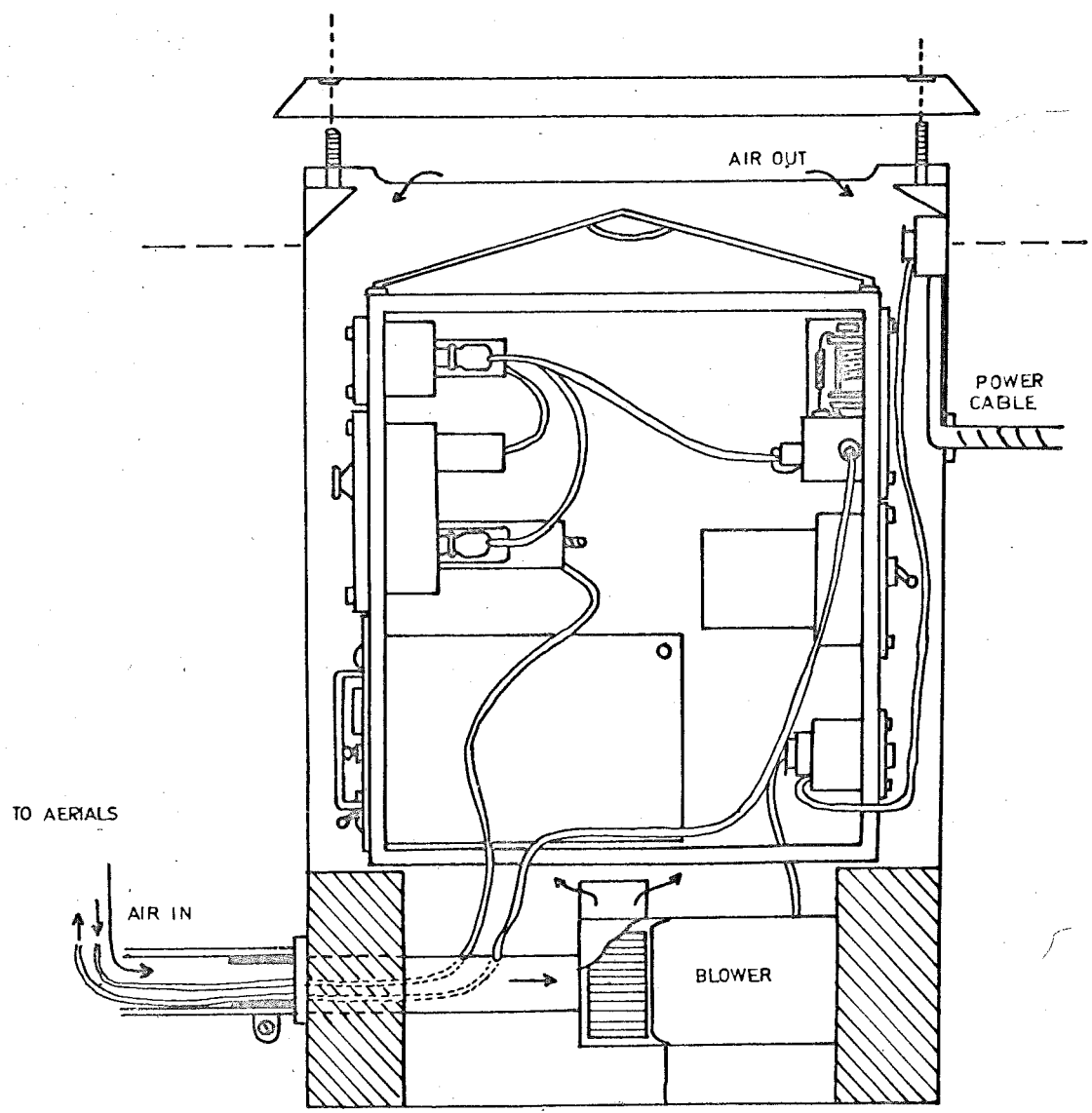
OUTSTATION IN SITU

FIG. 22

OUTSTATION BLOCK DIAGRAM

27 mcs. DIPOLE

167 mcs. YAG1

| NARROW BAND RECEIVER | → | CHOPPER | → | FILTER | → | REACTANCE MODULATOR | → | LINK TRANSMITTER |

XTAL LOCAL OSCILLATOR

-85 V

250 V

400 V

BLOWER

| NEGATIVE REGULATED SUPPLY | STANDARD REGULATED SUPPLY | TX FINAL SUPPLY |

AC LINE
240 V
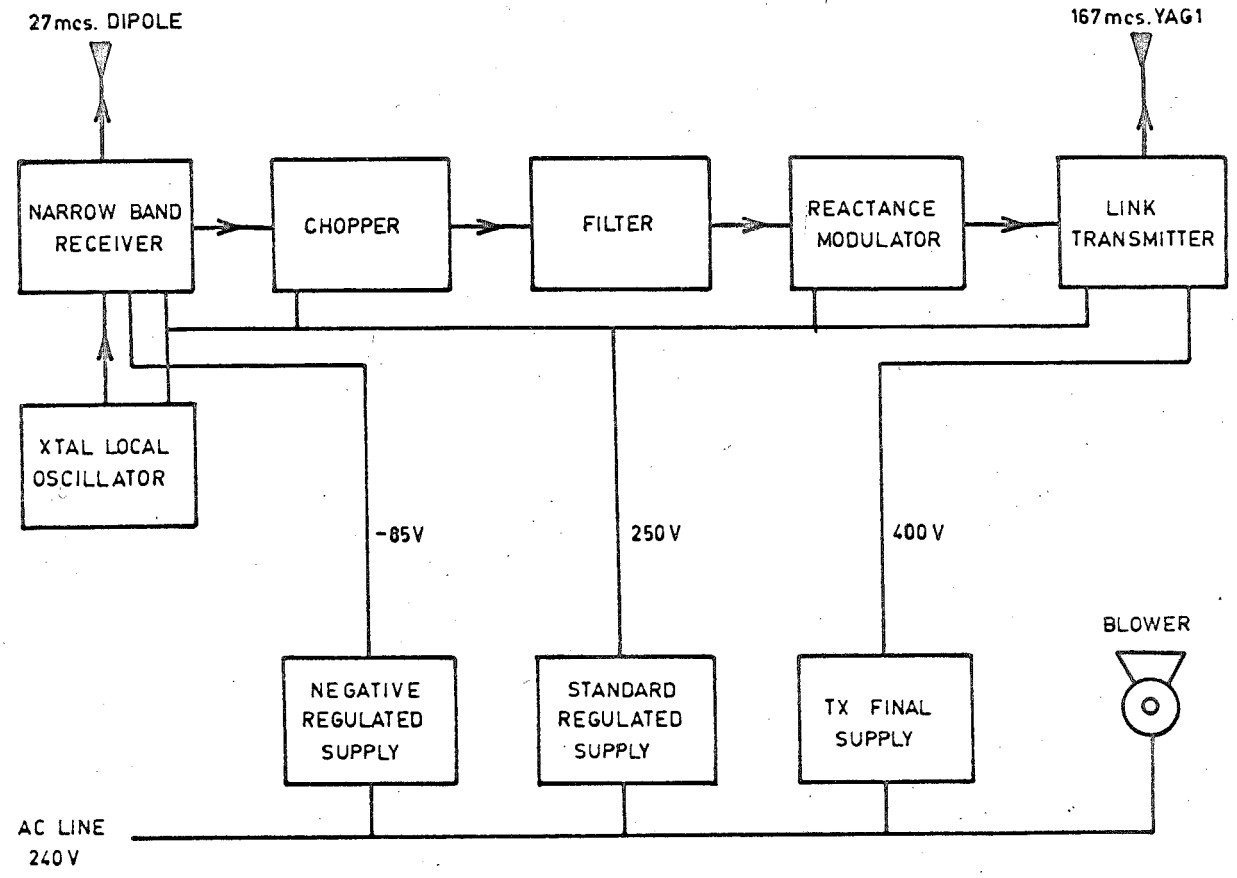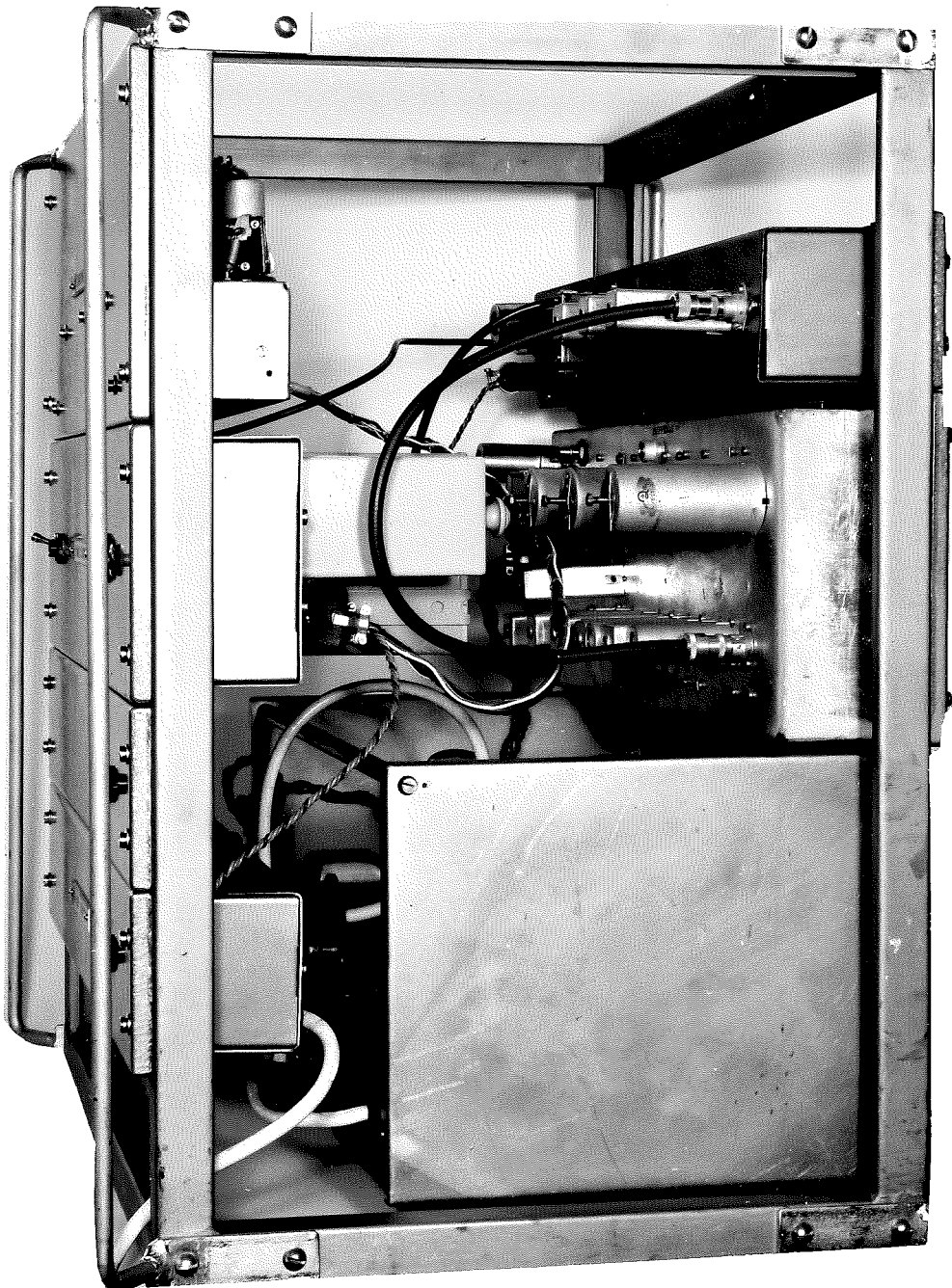
FIG. 23a

FIG 23b - OUTSTATION RACK

by the power wiring, and to minimise distortion of the aerial polar diagram which could occur due to overhead wires in close proximity to the station.

8.2 Detailed Description of the Outstation Equipment.

Each outstation rack (Fig. 23a,b) contains the following:-

(a) a 27 mcs narrow band superhetrodyne receiver, with crystal controlled local oscillator,

(b) a chopper and filter unit,

(c) a frequency modulated 167 mcs transmitter,

(d) associated power supplies.

(a) The 27 mcs Receivers.

As mentioned in Chapter V, receivers of similar design are used in each outstation and at the main station. Since both outstations and main station are almost completely free from man-made interference, considerable time was spent on the design and construction of these receivers to meet the requirements of very low noise figure and high gain and stability.

To reduce the noise figure to a minimum, two stages of radio frequency amplification are used. The first is a cascode employing a triode connected 6AM6 and a 6AQ4; the second a 6AM6 as a conventional pentode amplifier. The pentode mixer, another 6AM6, has cathode bias in the interest of

rapid recovery from high amplitude transients (atmospherics).
Oscillator injection is crystal controlled. Two I.F. ampli-
fier stages (2 X 6BA6) on 1.9 mcs complete the lineup before
detection. Extensive shielding is used between stages; all
filament and HT leads to each stage are bypassed by concentric
feedthru capacitors. The resultant receiver has a noise fig-
ure better than 2 db, image response 72 db down, overall
bandwidth ±4.5kc at the 3 db points, and an overall gain of
180db before detector saturation on input circuit noise.
Normal gain in operation is 120db, a 10 microvolt input sig-
nal producing 10 volts across the detector diode load. Re-
ceiver linearity is excellent up to 30 volts output, with a
smooth overload up to 40 volts out. Either AVC or manually
controlled gain is available. For echo amplitude investigat-
ions a knowledge of both absolute groundwave and skywave is
desirable, and calibration and operation at fixed gain is
necessary. For routine wind and radiant surveys, the const-
ant groundwave output provided by the AVC system simplifies
recording.

(b) The Chopper and Filter Unit.

Under normal quiescent conditions the output of the re-
ceiver consists of a D.C. signal which is a measure of the
groundwave amplitude. In order to transmit this groundwave
level back to the main station, techniques similar to those

employed in carrier telephony are used; the carrier wave which is produced by chopping and filtering the receiver output is in a form suitable for transmission. A heterodyne method had been used previously by Dr. J. S. Mainstone to enable tape recordings of the initial whistle accompanying trail formation to be made for subsequent velocity measurement, but is unsatisfactory for the following reasons. Firstly, a very high order of stability is required not only in the receiver and local heterodyning oscillator, but also in the CW transmitter, if the heterodyne carrier frequency (4kc in the original) is to remain within the passband of the 4kc bandpass filter required to realize the full noise figure advantage of the method. This difficulty could have been overcome by the use of some form of automatic frequency control of the heterodyning oscillator to produce a constant carrier frequency. A second difficulty arises because the heterodyne method is phase coherent. The 27 mcs transmitted wave being phase modulated, severe ringing occurred even in the absence of an echo because of the steep sided bandpass characteristic of the original 4kc filter. This problem has no ready solution. A filter with a bandpass over 6kc wide was eventually used. This reduced the ringing but the echo was degraded by noise.

The chopper method suffers from a 3db increase in noise

over the heterodyne method, but since it is used after de-
tection, the signal is no longer phase coherent in that only
the genuine phase spikes, whistle and doppler resulting from
the groundwave/skywave interaction are present; the 27 mcs
receiver AM detector produces no output other than the D.C.
level from the phase modulated groundwave alone. This means
that the filter bandwidth can be kept down to 1kc (the phase
spikes are normally of the order of 1 millisecond long), with
obvious noise figure improvement.

The circuit of the chopper unit is reproduced in Fig.
24. Stability has proved excellent, being of the order of
±100cps at an output frequency of 5kc (after an initial 12
hour warmup), this being maintained at one stage over a per-
iod of 3 months continuous outstation operation. Switching
transients generated in the diode ring modulator are 60db
down with respect to the filtered signal output.

The output from the filter appears as an amplitude mod-
ulated carrier wave whose frequency is that of the multivib-
rator driving the switching diodes, and whose amplitude is
directly proportional to the receiver detector output.

Different chopping frequencies are used at the two out-
stations, viz. 2kc at Sheedys' Farm and 5kc at Direk. The
choice of suitable chopping frequencies involves considerat-
ion of several conflicting requirements. The whistle accomp-

CHOPPER & FILTER OUTSTATIONS
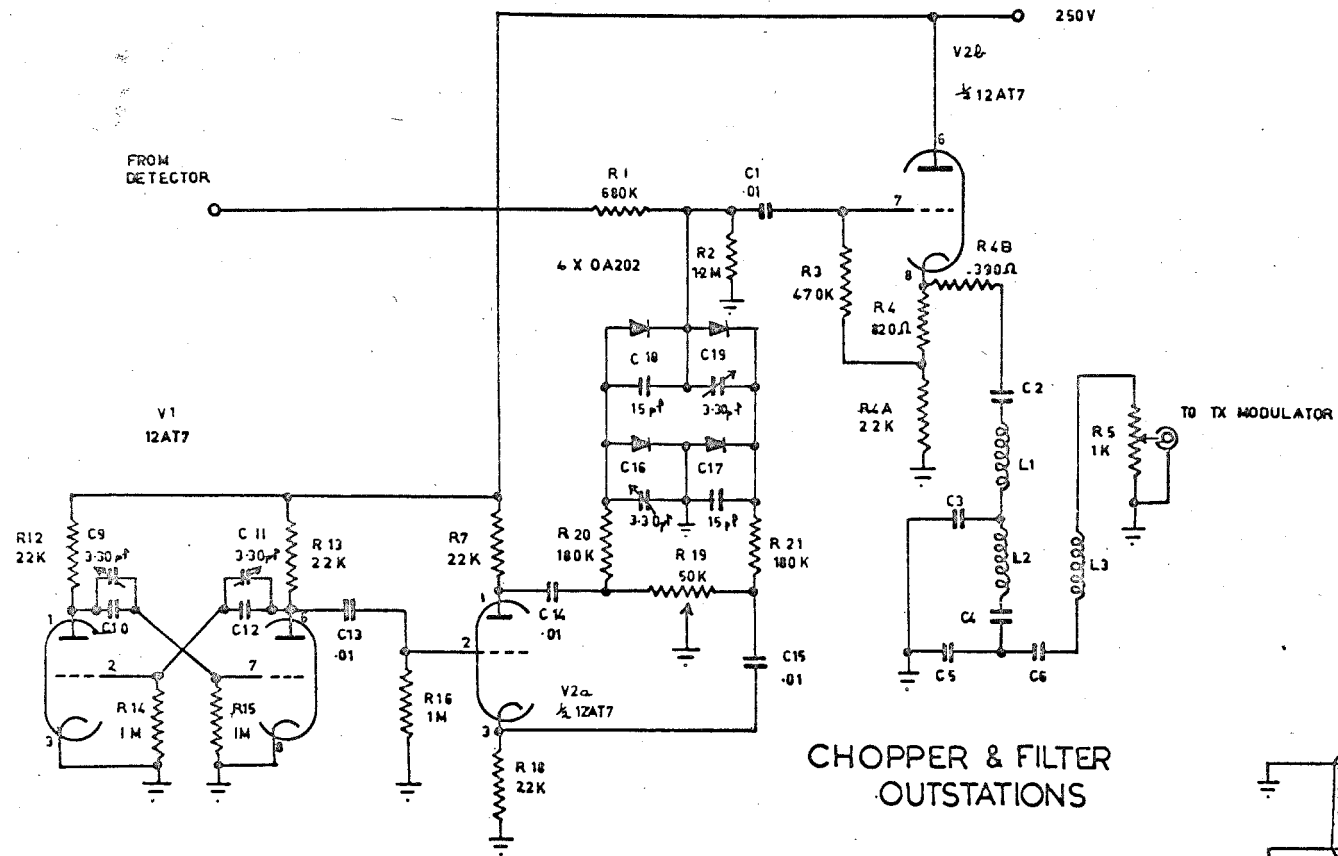
FIG 24

anying trail formation contains frequencies as high as 600

cps for Fresnel zones well removed from the t_o point, and

thus the sampling frequency should be several times this val-

ue. However, the meteor velocity recording technique involves

the storage of information on magnetic tape, which imposes

upper frequency limits at conventional tape speeds. During

storage on tape all signals are mixed and subsequently separ-

ated; if sampling frequencies are harmonically related,

interference between channels can occur. The frequencies

chosen have proved to be a good compromise.

(c) The F.M. Transmitter.

A commercial frequency modulated crystal controlled 167

mcs transmitter (Philips type 1645/02b, now obsolete) is used

to transmit the chopper/filter output back to the main stat-

ion at St. Kilda. The original transmitter, designed for

voice communication, was modified by removal of an input lim-

iting arrangement which would have had a disasterous effect

on the overall linearity of the system, and incorporation of

overload protection devices, deemed necessary since the out-

stations run unattended.

(d) The Power Supplies.

In the interests of stability, the high tension to all

units except the transmitter final amplifier is provided by

an electronically regulated 250v supply, as used at the main

station and described in Chapter V. Negative bias to the receiver manual gain control is also regulated. The transmitter final stage is fed from an unregulated 400v supply; all that is required of this supply is that the output from the transmitter be kept well above the limiting level of the link receivers used at the main station.

Output from the transmitter is conveyed via coax cable inside the antenna pole to a 4 element Yagi array beamed on St. Kilda. The Yagi is mounted 3 feet above the 27 mcs receiving dipole.

8.3 Subsidiary Main Station Equipment.

The transmissions from each outstation are received at St. Kilda on 4 element Yagi arrays, and are amplified and discriminated by 13 valve FM receivers (Philips type 1645/01b, now obsolete. These receivers have been superseded by the manufacturers from considerations of size only. Their performance is quite good). Both outstations are transmitting simultaneously on the same frequency of 167.02 mcs, but the 40db front to side ratio of the receiving arrays ensures that each receiver limits on the required signal. Simultaneous transmissions would not be possible with amplitude modulated signals, because of interference problems. Link noise is 57db down on the information carried; this is due in part to the excellent performance of the bandpass filters connected

RECORDING RACK BLOCK DIAGRAM

YAG1
BEAMED ON
SHEEDY S FARM

DOPPLER 1
ANTENNA

YAG1
BEAMED ON
DIREK

| 167 mcs. LINK RECEIVER | DOPPLER 1 27 mcs. REICEIVER | 167 mcs. LINK REICEIVER |

| 2 KC. BANDPASS FILTER | 3·5 KC. CHOPPER and FILTER | 5 KC. BANDPASS FILTER |

TO VELOCITY EQUIPMENT

CHANNEL DISTRIBUTION UNIT

TRIGGER FROM WIND EQUIPMENT

AUDIO MONITOR

DEMODULATOR and LEVEL MONITOR

SEQUENCE UNIT

STANDARD REGULATED SUPPLY ALL UNITS

DC. AMPLIFIERS

EHT SUPPLY

DISPLAY

CAMERA

FIG. 25

to the receiver outputs. These filters are the same as those used at the outstations to filter the chopped receiver output. Through the use of Ferroxcube potcore inductances a good bandpass is achieved with only two constant k T-sections, and two m-derived end sections.

The signal to noise ratio at the 27mc outstation aerials averages 26db. Low receiver noise figure means that external noise completely governs even weak signal performance, and because the links introduce no measurable degredation, the signal to noise ratio of the filtered FM receiver output is the same as that at the outstation 27 mcs aerial.

The outputs of the link receivers are fed to the channel distribution unit in the Three-station Wind Recording Rack, Figs. 25 and 26. This unit also chops and filters the output from one of the main station doppler receivers. The three carriers thus derived are

2kc transmitted from Sheedys' Farm,

3.5kc output from one main station receiver,

and 5kc transmitted from Direk.

These are in a form suitable for use in the velocity measurement technique.

8.4 The Multi-channel Tape Delay Unit.

Because the Wind Equipments only record information received after the trail is formed, some form of memory circuit

is required to enable the initial whistle associated with the formation of each trail to be recorded.

This is provided by the Multi-channel Tape Delay Unit first designed by Mainstone (1960), but which has since undergone considerable modification and improvement. This was undertaken by C.S.Nilsson, who was also responsible for the reduction of the orbit data.

The original recorder incorporated three separate record and playback head pairs, four erase heads and a highly complicated switching mechanism to automatically effect tape reversal, and thus allow for continuous recording. However, because of the tension differential between heads, simultaneity of time between channels was lost; in addition wow was such that time marker pips on each channel would have done little to improve the situation.

Because of the inherent stability and flexibility of the chopper method of carrier derivation, an alternative recording procedure was devised. The three carriers are mixed (linearly added, so as not to beat together), applied to the one recording head, and picked off the tape approximately 1.5 seconds later by a single playback head. Considerable simplification of the reversal switching mechanism results, and, because of the reduction in the number of heads traversed by the tape, wow and flutter are reduced to negligible proport-
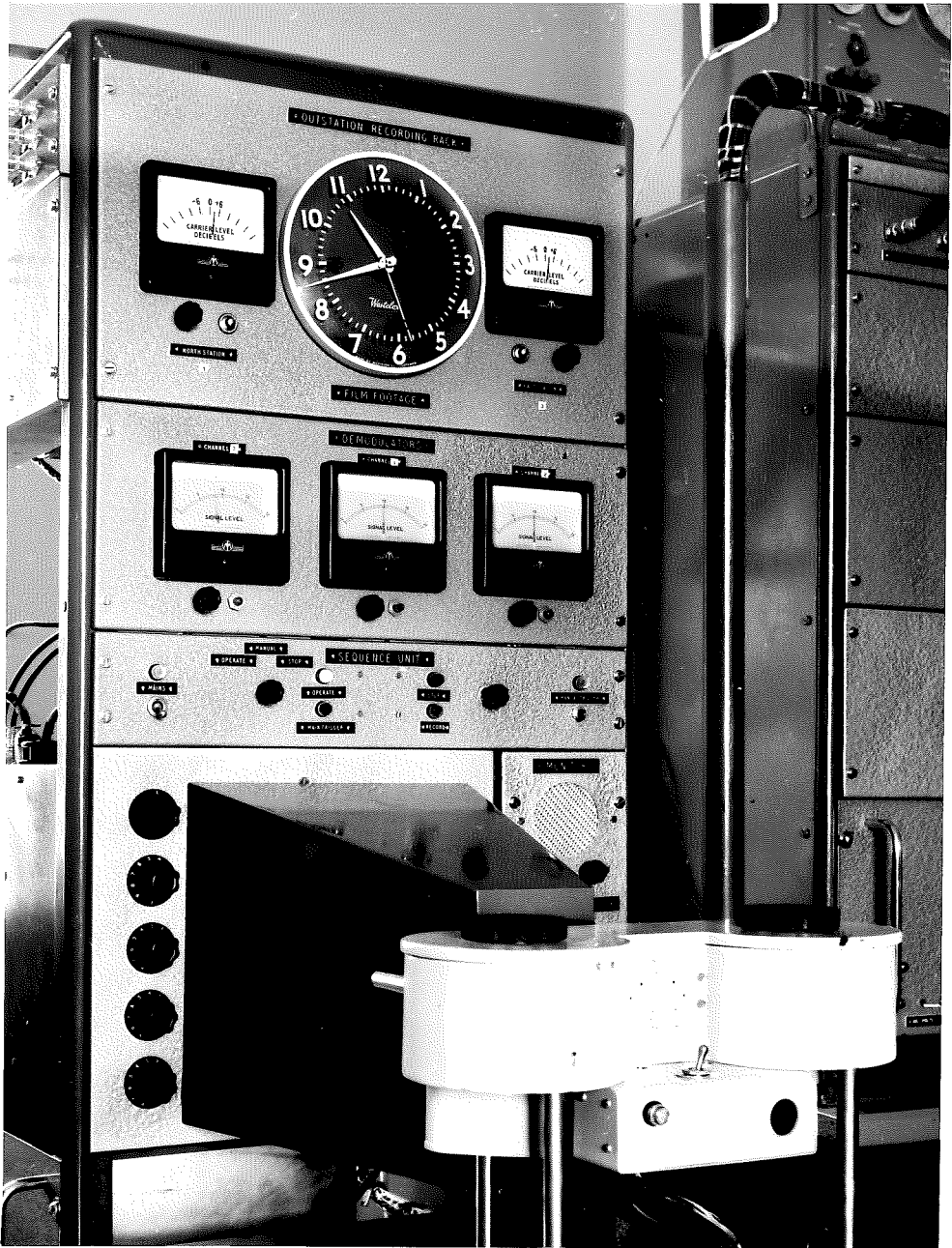
FIG 26 - THREE STATION WIND RECORDER

ions. To unscramble the playback signal, three six section
filters are used, each 1200 cycles wide and centred on one of
the three carrier frequencies. The separate carriers are
then amplified, demodulated and applied to three cathode ray
tubes in the orbit display. If an echo triggers the main
wind equipment, the orbit camera is then set in motion, and
runs for a sufficient interval to record the initial echo in-
formation which has been delayed 1.5 secs by the tape.

Because the whistle amplitude is normally only a few per
cent of the groundwave amplitude, the large body doppler
after the whistle is attenuated by a frequency selective net-
work (the doppler frequency is much less than any component
of the whistle) so that the maxima and minima of the doppler
are recorded without overloading the display amplifiers.

8.5   The Three-station Wind Recorder.

The three outputs from the channel distribution unit are
also applied to the Three-station Wind Display. The records
obtained from this display make possible the measurement of
reflection amplitudes and decay times (the measurement of
diffusion coefficient differential with height is contemplated
as an extension of the turbulence programme) and give a better
overall picture of the post t_o echo than that available from
the orbit display.

The two outstation carriers are amplified and demodulated

by two circuits of the type shown in Fig. 27. The potent-
iometer in the cathode of V_{2b} returns to a negative voltage
supply; suitable adjustment of this potentiometer produces
zero voltage at the output of the lowpass filter $L_{1-4}C_{3-8}$ for
zero carrier input. Presence of carrier input results in
rectification of the signal by the diodes (4 X OA202) and ap-
plication of a positive bias to the grid of V_{2b}. This causes
an increase in current flow through the valve, and a positive
voltage is developed across the filter load R_{13}. The DC vol-
tage output is plotted against peak to peak carrier input in
Fig. 28. The linearity in the 0 to 20v output region is ex-
cellent. The lowpass filter has a frequency cutoff of 1kc,
which is sufficiently high to pass the phase spikes, which
are of the order of 1 millisecond duration, but low enough to
completely suppress the rectified carrier component. Once
again, the use of potcore inductances has produced a filter
of high quality. The filter characteristics are presented in
Fig. 29.

The output from the main station receiver is applied
directly to the appropriate DC amplifier in the cathode ray
tube display, without being chopped, filtered, and then de-
modulated. It is significant that the signal to noise ratio
of the film record obtained from this channel is the same as
that of the outstation records.
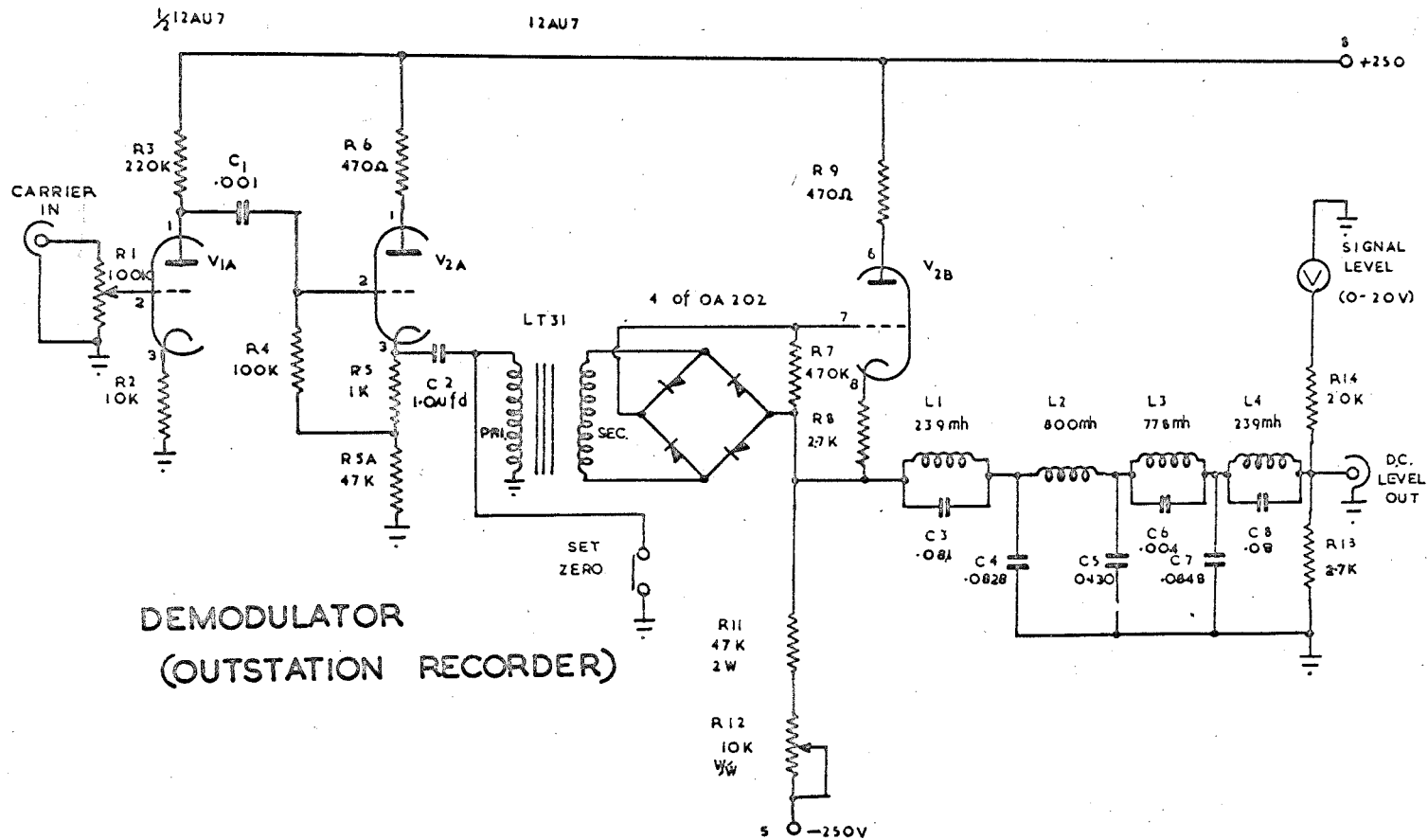
DEMODULATOR
(OUTSTATION RECORDER)

FIG 27

DEMODULATOR CHARACTERISTICS.

$V_{OUT.}$ (D.C.)

V_{IN} (P/P) AT GRID OF V_{1A}.

FIG. 28

LOW-PASS FILTER CHARACTERISTIC.
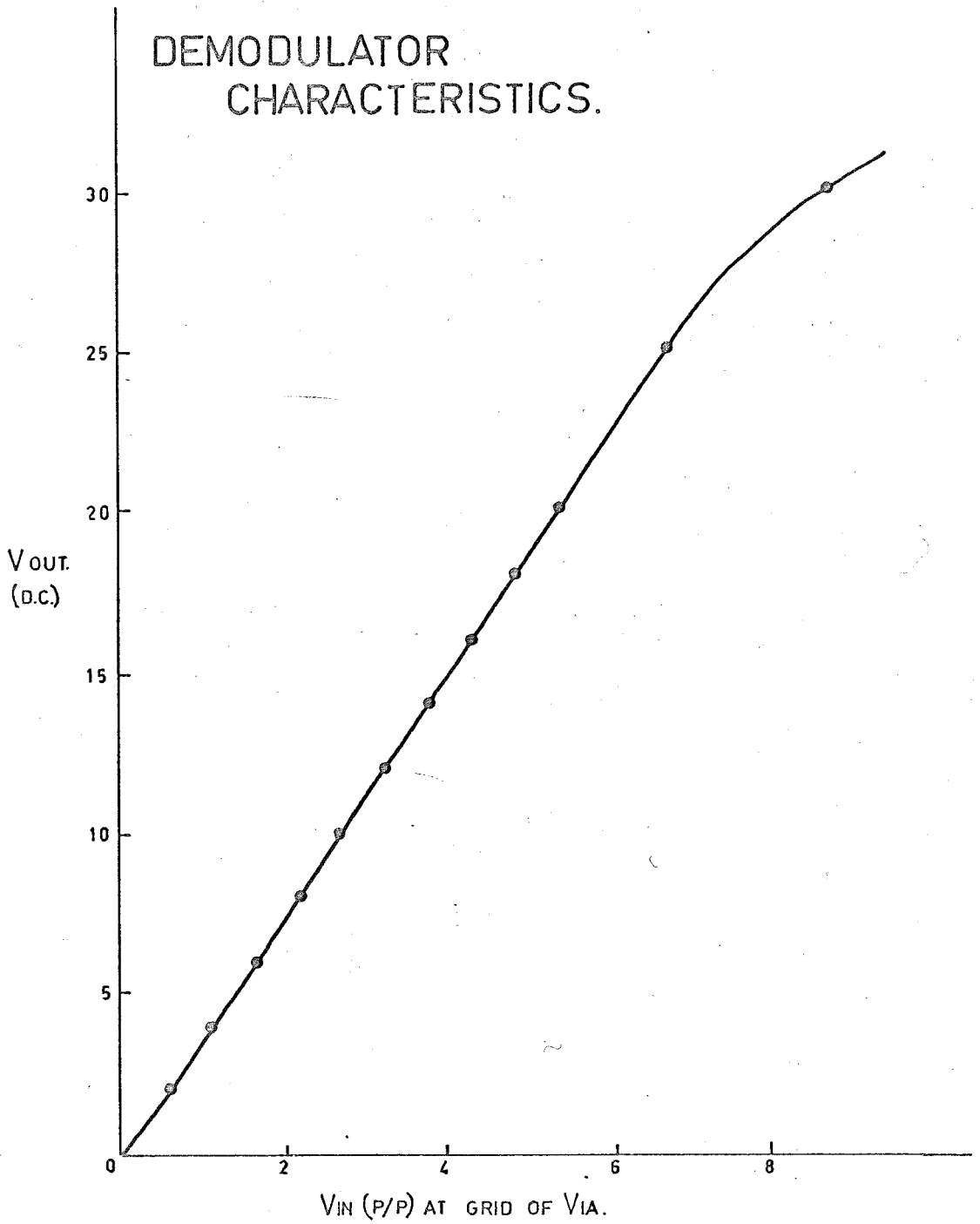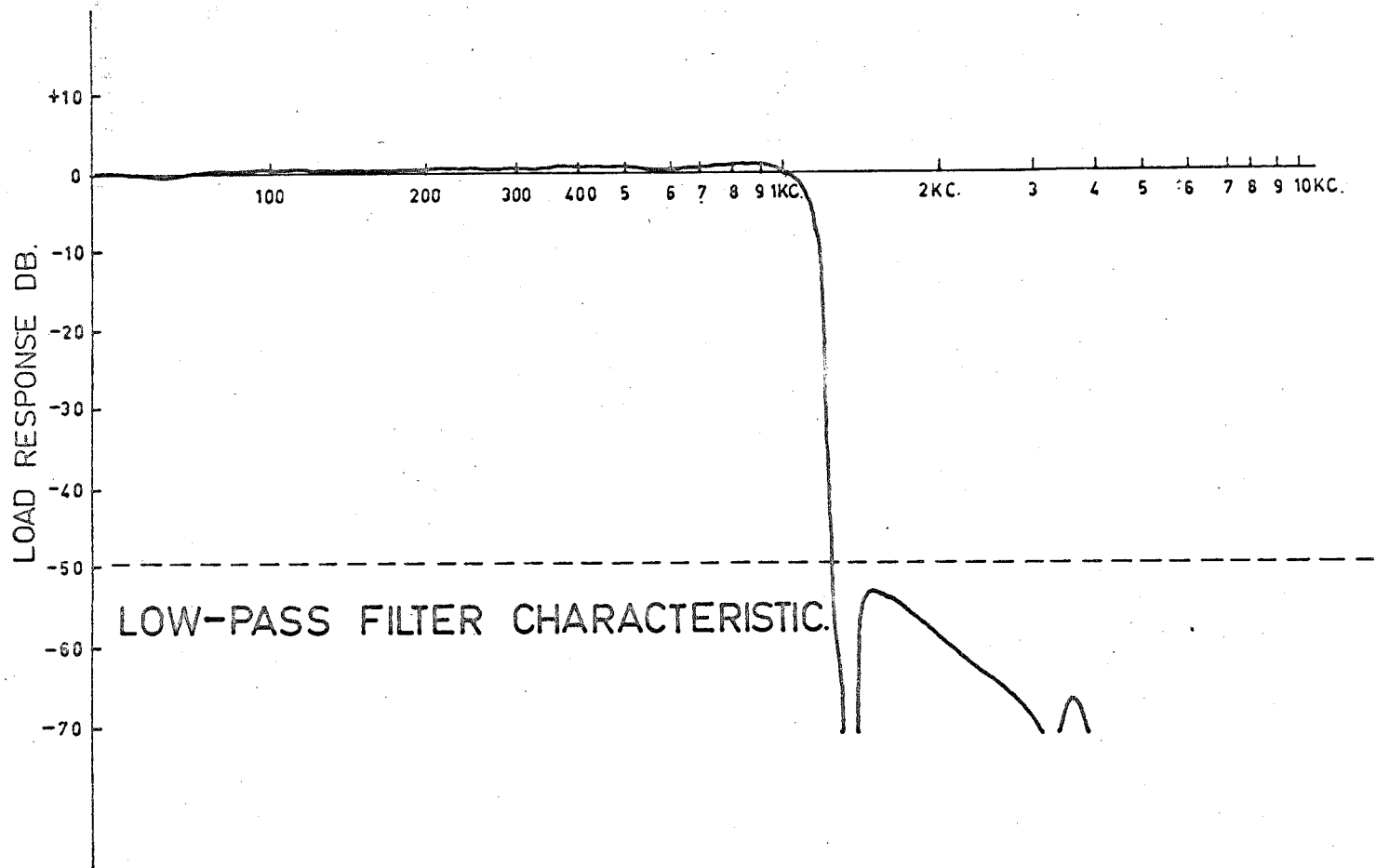
FIG. 29

For monitoring purposes, the signal levels representing the DC outputs of the three station receivers are displayed on three panel mounted meters.

The DC amplifiers in the display were designed for long term stability. A cathode follower drives an anode follower whose plate is connected directly to the appropriate Y plate in the cathode ray tube display. Three such amplifiers are used, two handling the outputs of the outstation carrier demodulators, and the third the output from the main station receiver. These signals are applied to two double beam Cossor 89J C.R.T's. The main station signal deflects the lower trace of the upper cathode ray tube in the display, and also the upper trace of the lower tube. The Sheedys' Farm signal is the very top trace, the Direk signal the very bottom trace (See Fig. 32b). These tubes are certainly not the best for long term photographic recording, but are adequate in this application.

Graphs of the signal level outputs as measured from the film records (normalized to a 10 volt groundwave level) against RF signal microvolts input at the outstation antennae are presented in Fig. 31. The non linearity in the overall characteristic is introduced in the frequency modulation of the 167mc transmitter and subsequent discrimination in the link receiver.

12 AT 7

+250V

R3
470Ω

R9
100K
HI STAB

TO Y PLATE
130V +52VRMS

R7
2.2M
HI STAB

R8
39Ω

10V+7VRMS

R2
47Ω

R1
1M

+14.5V

R4
1K
HI STAB

+13

R6
100K
HI STAB

-2.3V

R10
220K
HI STAB

85A2

R5
10K
HI STAB

R12
18K
2W

-250V

D.C. AMPLIFIER

R11
100K
Y SHIFT

TO Y SHIFT POTS
ON OTHER D.C. AMPS.

FIG 30

119

OVERALL CALIBRATION, SHEEDY'S.
31/8/60.

FIG. 31a

OVERALL CALIBRATION, DIREK.
31/8/60.
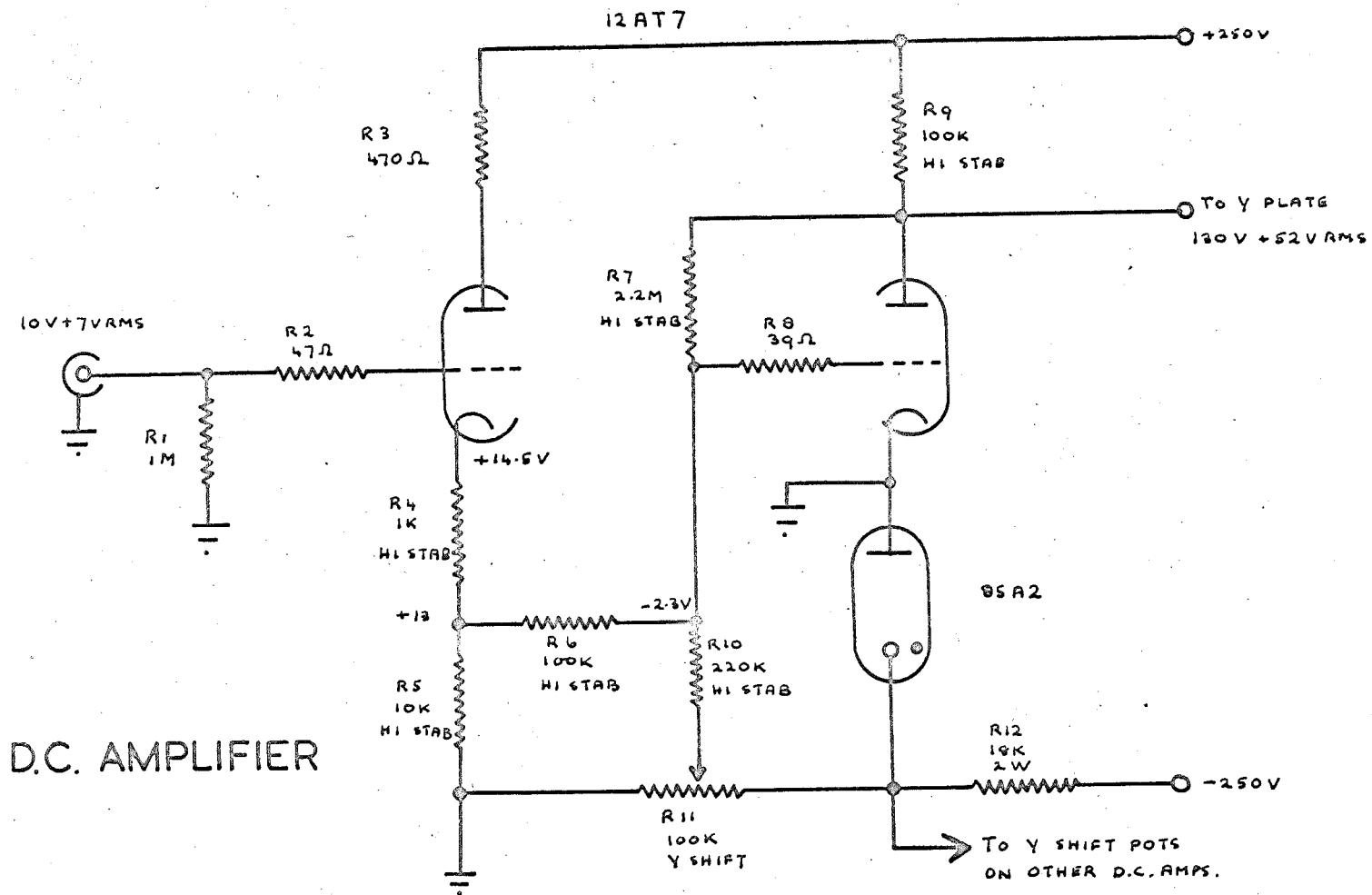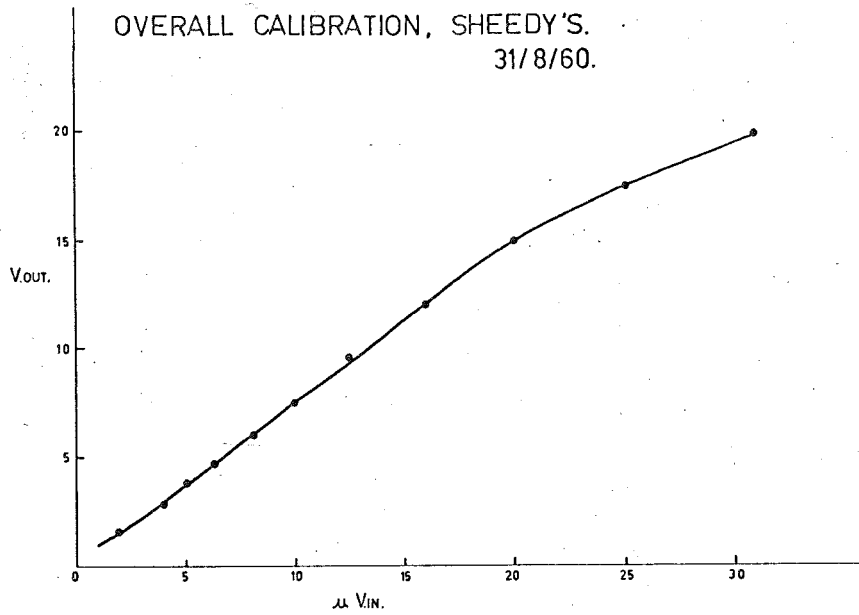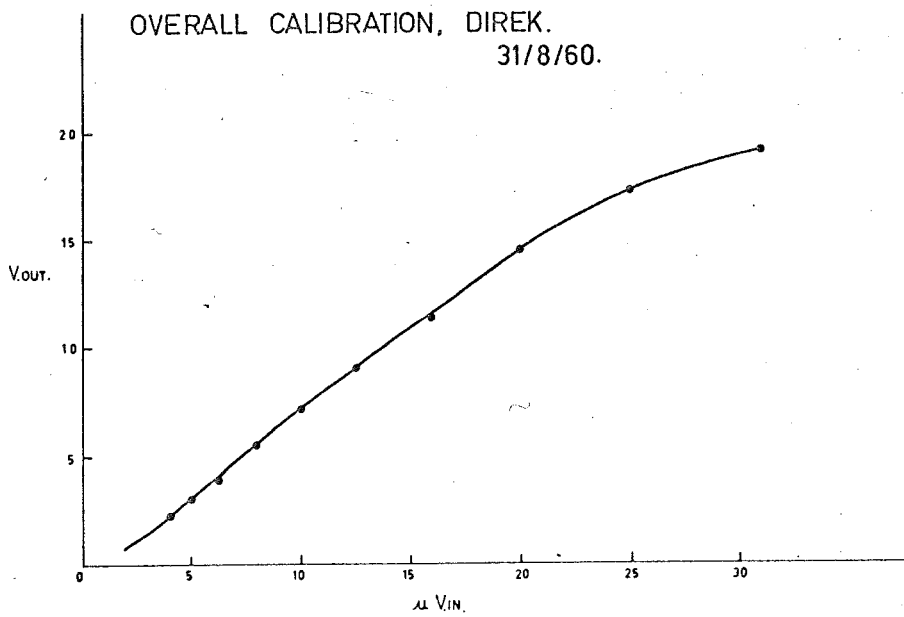
FIG. 31b

The recording camera is a Shackman, which has been modified by including a magnetic clutch between the motor and the film drive. The motor operates continuously and the film is brought into motion by applying a voltage to the clutch from the sequence unit. Gear ratios are such that the 35mm film travels at 0.38 inches/sec when the clutch is actuated. Thus, at the shortest recording duration of 1.4 secs, each echo occupies about half an inch of film. Film is daylight loaded in 100 foot lengths; the sporadic echo rate is such that one film normally lasts 36 hours.

For film correlation purposes, an electronic flash and a six digit counter are mounted in each of the three displays (orbit, mean wind, and three-station wind). The counter and flash are operated during each echo by trigger pulses from the mean wind recording rack sequence unit.

The magnetic clutch actuating the three-station camera is wired in parallel with the mean wind equipment clutch to minimise delay in the commencement of recording, but once the film is in motion control by the wind equipment is removed and the three-station sequence unit takes over. This unit contains several relays and an electronic timer, the duration of the run being set by a switch on the front panel. Recording intervals from 1.4 secs minimum to 30 seconds maximum can be selected. Most of the routine running is done with the

shortest duration in the interests of film economy, but, for observations of long duration echoes, times up to the maximum have been used occasionally. Manual triggering of the clutch and sequence unit is also available for testing purposes.

8.6 The Film Records.

The films from the orbit display (a), three-station wind display (b) and mean wind display (c) are shown in Fig. 32 for echo number 54746. The whistle patterns of 32(a) show that the echo was first received at the Main Station (middle trace), then at the Direk Outstation (bottom trace) and finally at Sheedys' Farm (top trace). The time scale is indicated by the phase spikes which are quite evident on the slow body doppler at the end of each echo. These spikes are 20 milliseconds apart.

The record of 32(b) shows the presence of wind shear. The initial whistle does not appear, since it precedes the main echo which triggers the camera. Taking the traces in the order of reflection point occurrence as determined from 32(a), the line of sight drifts are

27 metres/sec at the main station (centre two mirror image traces)

40 metres/sec at Direk (bottom trace)

and 55 metres/sec at Sheedys' (top trace).

The first reflection point always occurs at the greatest
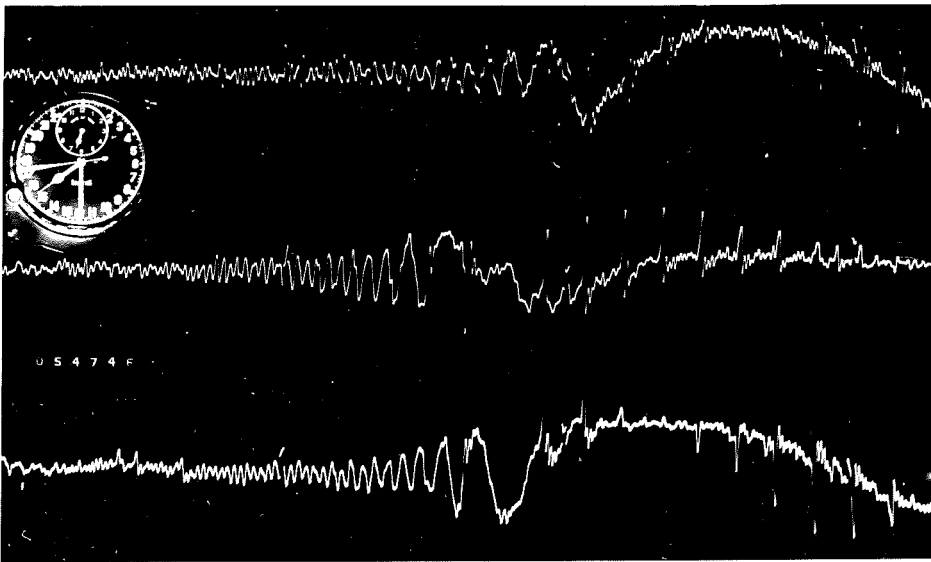
a ORBIT
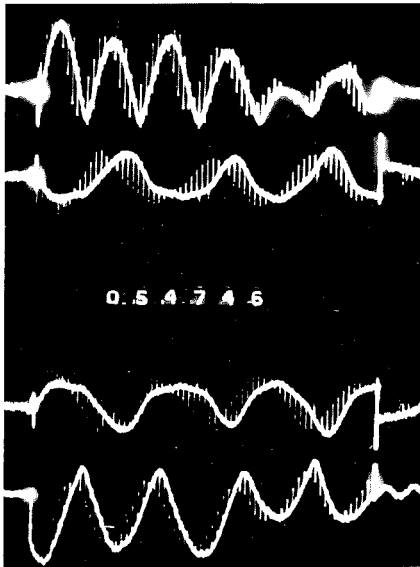
b 3-STATION WIND
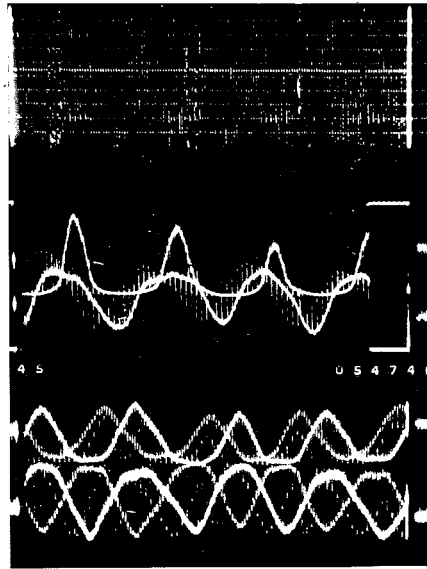
c MEAN WIND

FIG 32

height; thus this echo shows the presence of a negative wind gradient with height.

Before the meteor velocity and separation distances can be determined from 32(a), a knowledge of the range and direction cosines of at least one reflection point are required. This information is furnished for the main station echo by the film 32(c). The upper trace is a conventional radar scan, the equispaced dotted horizontal lines being 20km range markers. The range at 108km is clearly visible. The next two traces are the outputs of the two doppler receivers. Unfortunately the magnitude of the echo was such that receiver overload occurred. However, the doppler minima are still well defined; because of the nature of the beat waveform $(\cos^2 t)$, the minimal cusps are always used for measurement. The spikes on the trace caused by the phase modulation of the transmitter are clearly visible. Since the wave traced out by these spikes leads the doppler beat, the trail drift is towards the observer.

Local time is recorded by the clock in the orbit display. Films are correlated by means of the electronically flashed counters.

CHAPTER IX.

The Methods of Data Reduction
as Applied to the Results For December 1960

9.1   The Mechanics of the Turbulence Data Reduction.

At the commencement of the orbits and turbulence pro-
jects in 1958, it was appreciated that considerable time would
be involved in data reduction, since any worthwhile orbit
survey and turbulence investigation would necessitate record-
ing for at least twelve months.   The design and construction
of the completely new St. Kilda receiving station and the two
outstations took until mid July, 1960, and the whole system
was operating reasonably satisfactorily by December of that
year.   For the first few months, until the end of April,
1961, equipment reliability was not good, and the rate of
echoes suitable for reduction suffered.   However, for the
rest of the survey, which terminated at the end of December,
1961, very little equipment maintenance was necessary, and re-
duction of the data already obtained was commenced.   This
proved to be a most tedious process, six months of graphing,
curve fitting and desk machine calculation being required to
produce the final results for only one month, viz. December,

1960. Fortunately, early in 1961 the Weapons Research Establishment at Salisbury installed and made available to University users an IBM 7090 digital computer to ease the load on their digital/analogue computer WREDAC. From the research viewpoint, the 7090 is one of the best computers in the world. Not only is it quite fast in operation, but it is relatively easily programmed via the IBM FORTRAN language; programmes are written in an elementary algebraic form, which is translated by the machine itself into the highly complicated binary coded machine language.

Programmes to expedite some aspects of the orbit reduction were first run by C. S. Nilsson early in 1961, but the complete orbit reduction programme was not finalized until the beginning of this year (1962). The first turbulence programmes were run in January, 1962, and underwent considerable addition and modification until the installation, in April, 1962, of an IBM 1620 computer in the University's Computing Centre. Although considerably slower in operation than the 7090, and having a very much smaller storage capacity, the 1620 has the most decided advantages of personal operation by the user, 24 hour a day availability, and no charge for research use. Because of programme complexity and large storage requirements, the orbit reductions were carried out on the 7090 at W.R.E., and the information for each echo relevant

to the turbulence programme was punched onto cards by this
machine. All subsequent reduction was then performed on the
University's 1620. The FORTRAN programmes appropriate to
each portion of the data processing appear in Appendix II.
No attempt is made to translate these programmes directly
into conventional mathematics, since the method is adequately
detailed in subsequent sections of this Chapter. The lists
given of variables used in the programmes are not complete in
that many of the variables used within the programmes are
concerned only with machine manipulation, and the lists are
therefore confined mainly to quantities used as input and
output.

9.2   The Formulation of the Turbulent Velocity Field.

Before any application of the theories of homogeneous
turbulence can be attempted, all mean velocities and mean
gradients must be eliminated from the total flow field. As
detailed in Chapter V, the Adelaide method of mean wind meas-
urement involves the hourly grouping of wind velocities meas-
ured over several days. This represents a time average over
an interval which is certainly long compared with the time
constant of 100 minutes for the energy bearing eddies determ-
ined by Greenhow and Neufeld. The annual repetition of the
pattern for a typical day of a given month lends weight to
the assumption that the motion as determined is, in fact, a

true mean.

The first assumption made in the preliminary data reduction as applied to the turbulent motions is that these are isotropic. Although this radical assumption is not true (other workers have clearly demonstrated the anisotropy of turbulent motion at these heights), it simplifies the initial approach, and enables an eventual estimate of the possible vertical component, and thus a clue to the degree of anisotropy.

The data available from each record for turbulence measurement consists of

a) the line of sight motion at three points on the meteor trail,

b) the spacial separations of these three points,

c) the line of sight direction cosines and the height above ground of one of these three points,

d) the direction cosines of the meteor trail,

and e) the time of occurrence of the echo.

Accurate determination of the line of sight drift requires measurement of at least two cycles of the body-doppler beat immediately after trail formation. This corresponds to a line of sight drift of one wavelength at the transmitted frequency of 27 mcs; i.e. 11.2 metres. Even if another of the measured points on the trail was subject to zero wind

drift, the deformation of the trail during the interval of measurement is small since reflection point separations are of the order of hundreds of metres. Thus the trail may be assumed linear.

The sampling method involves the measurement of velocities perpendicular to the separation parameter, and is thus of the form specified for the transverse correlation of Chapter II, Section 4.

To perform the mean wind extraction, the NS and EW mean wind components for each of the three height groups centred about 80, 90 and 100km are tabulated hour by hour. A linear interpolation is used to determine the mean gradient for each hour above and below the 90km level. All subsequent reduction utilizes the velocity components at the 90km level, and the appropriate gradient, depending on whether the reflection point lies above or below this height. The height of the echo received at the main station is computed directly from the wind records (see Chapter V). The height of each out-station echo is calculated relative to this height, from the direction cosines of the trail itself, and the separation of the reflection points. The information for this purpose is obtained from the orbit data. Whereas the main station reflection point determination is subject to errors of the order of ±3km, the height differentials are measured to ±20

metres. The mean wind velocity appropriate to the mean solar time of the echo is then calculated for each of the three reflection points. The line of sight components of the mean velocities are then subtracted from the line of sight drifts as measured from the Three-station Recorder film to give the velocities of the turbulent flow field. The RMS value of the turbulent velocities for all echoes in a given month is taken as the velocity characteristic of the energy bearing eddies.

9.3 Turbulent Velocities as a Function of Separation.

The two important quantities which can be related to separation are the turbulent velocities and velocity differences.

The transverse correlation function given in 2.4.1 is

$$g(\xi) = \frac{\overline{u(x)u(x+\xi)}}{[\overline{u^2(x)} \ \overline{u^2(x+\xi)}]^{\frac{1}{2}}}$$

This can be redefined as

$$g(\xi) = \frac{\Sigma u(x)u(x+\xi)}{[\ \Sigma u^2(x) \ \Sigma u^2(x+\xi)]^{\frac{1}{2}}}$$

since, in forming the means for a given ξ, the number of echoes of that separation is common to both numerator and denominator. In practice the summations are made over discreet intervals of ξ in 200 metre steps, commencing at a separation of 100 metres; all reflection point velocities with separat-

ions ξ less than 100 metres fall in the first group, all with separations of more than 100metres but less than 300 metres in the second and so on.

The RMS turbulent velocity differences for a given separation are found for similar intervals from

$$\left[\frac{\Sigma \ (u_i - u_j)^2}{N} \right]^{\frac{1}{2}}$$

where u_i, u_j are the line of sight turbulent velocities measured at reflection points i and j of separation ξ, and N is the number of observations with this value of ξ.

To illustrate the method, the results for December, 1960, the first month of the survey, are presented in detail. The transverse correlation has been graphed (Fig. 33) according to the relation

$$1 - R(\xi) \sim \xi^m$$

<div align="right">(equation 2.11.5)</div>

A line of slope $\frac{2}{3}$ is superimposed.

Very little significance can be attached to the variation of the velocity correlation function with separation. The scatter of Fig. 33 can be explained in terms of the distinct anisotropy of the energy bearing eddies, the time dependent nature of the turbulent flow, and the perturbation of the small scale spectrum by the eddies of the buoyancy sub-
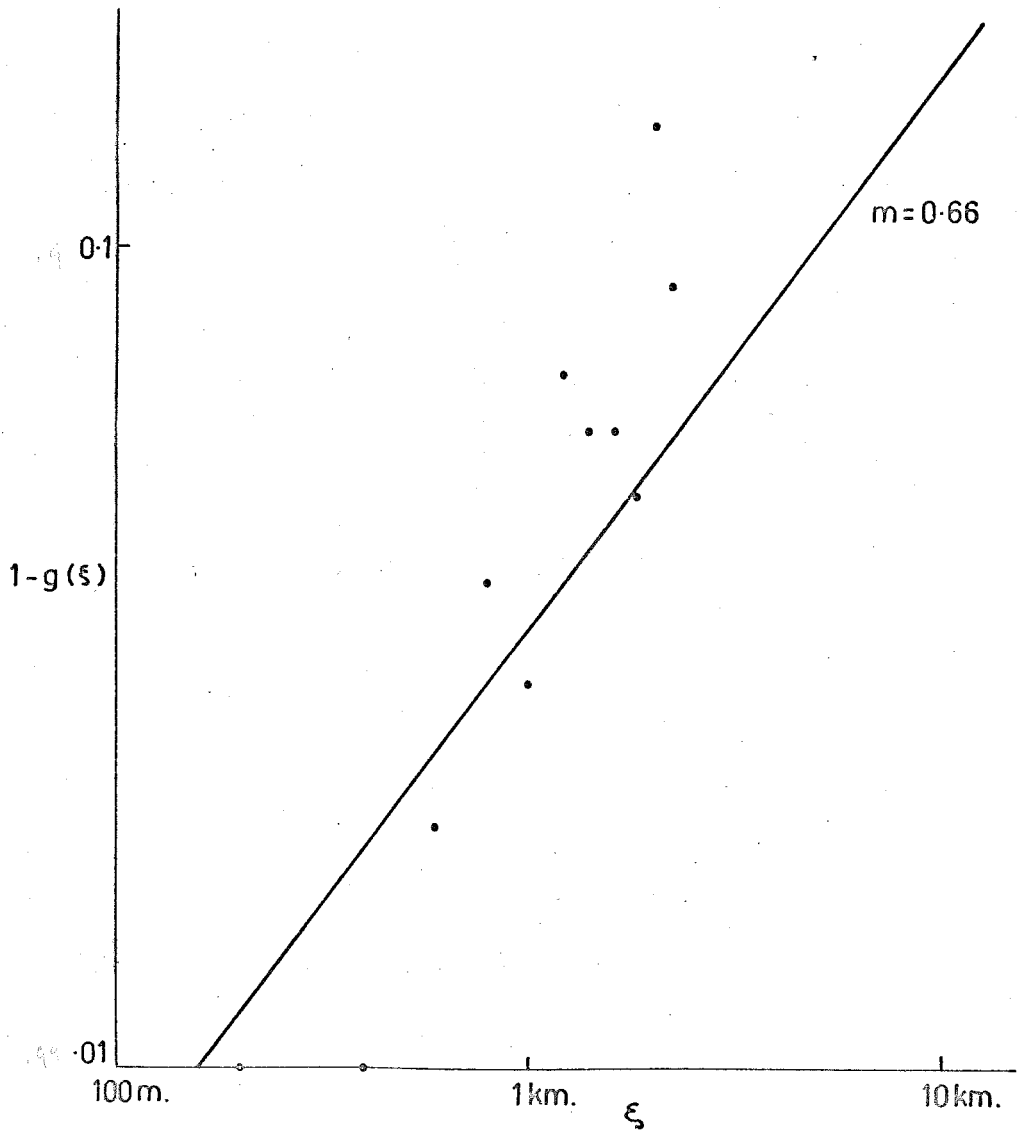
FIG. 33 – The transverse velocity correlation, December 1960

range. These factors are considered in detail later in this chapter.

The velocity differences of Fig. 34, however, do prove to be of some consequence. To relate the RMS velocity differences to the Kolmogoroff spectrum, use is made of equation 2.10.3, viz.

$$\overline{\Delta v} = 0.83(\epsilon \xi)^{\frac{1}{3}}$$

where ϵ is the rate of dissipation of the turbulent energy.

Various values of ϵ were substituted until the Δv curve fitting most of the measured velocity differences was derived. During this curve fitting process, it became quite obvious that there existed a distinct anomaly at the smaller scales, in particular those less than 500 metres. Whereas the overall best fit was obtained for a value of ϵ of approximately 300 ergs/gm/sec., the smaller scales were better represented by a rate of dissipation of energy of less than 100 ergs/gm/sec. This is of considerable interest in that optical measurements of the expansion of soduim and meteor trails, which are limited by the visibility of the trail to scales less than 500 metres, have produced ϵ values of some 70 ergs/gm/sec (see Chapter III Section 6).
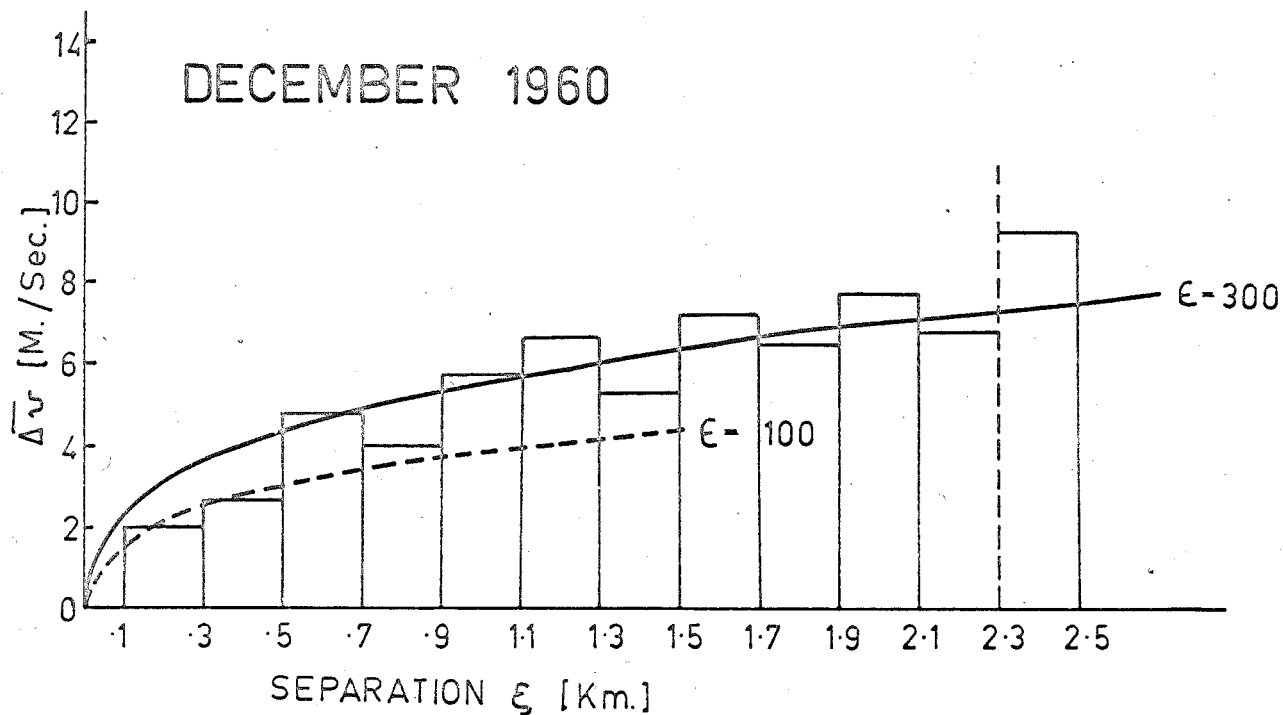
FIG.34-Variation of velocity difference with separation.

9.4   The Anomalous Velocity Differences at Small Separation.

One of the axioms of the Kolmogoroff theory is that all scales of the inertial subrange are characterized by the same value for the turbulent dissipation parameter ϵ.   The breakdown of 9.3 is explicable in terms of the Kolmogoroff theory only if the scales less than 500metres are no longer inertial, but comprise the region of viscous dissipation.   The size of the eddy characteristic of the viscous dissipation subrange is given in 2.6.4 as

$$\eta = \left(\frac{\nu^3}{\epsilon} \right)^{\frac{1}{4}}$$

where ν, the kinematic viscosity, is of the order of 10^5 cms /sec at 95km.

For $\epsilon = 300$ ergs/gm/sec.,

$\eta = 13$ metres.

Since the characteristics of the inertial subrange are expected to hold down to some five times this scale (vide 2.6.6) the onset of viscous dissipation should not be apparent until separations less than 100 metres are reached.   It would appear that some other source of energy extraction is required to account for the anomaly.

Examination of Fig. 34 in greater detail brings out some other features.   While the anomaly in the velocity differences is most marked below 500 metres, there does appear to

be an overlying periodic variation at larger separations, with period between minima in the velocity differences of approximately 700 metres. As has been previously mentioned in Chapter III Section 3, the presence of a buoyancy subrange can extract energy from all scales of the turbulent flow field. These buoyancy effects become most important when the buoyancy potential energy per unit mass is of the order of the turbulent translatory kinetic energy per unit mass.

The buoyancy potential energy per unit mass is given by

$$P_\epsilon = L_\beta^2 \, \frac{g}{\Theta} \, \frac{d\Theta}{dh}$$

where L_β is the eddy size characteristic of the buoyancy (or Richardson type) instabilities, and Θ is the potential temperature of the gas.

From Chapter II Section 12

$$\frac{1}{\Theta} \frac{d\Theta}{dh} = \frac{1}{T} \left[\frac{dT}{dh} + \Gamma \right]$$

At a height of 95km

$$g = 950 \ \text{cm/sec/sec}$$

$$T = 180 \ ^\circ A$$

$$\Gamma \simeq 10^{-4}$$

and

$$\frac{dT}{dh} \equiv 2.5 \ ^\circ A/\text{km}$$

$$\therefore \quad P_\epsilon = 0.6 \times 10^{-3} \, L_\beta^2$$

By equating this to the total turbulent translatory kinetic energy per unit mass,

$$\tfrac{1}{2}U_o^2 = 0.6 \times 10^{-3} \, L_\beta^2$$

where U_o is the velocity characteristic of the energy bearing eddies.

i.e. $\quad L_\beta \cong 25U_o$ $\qquad\qquad\qquad\qquad\qquad$ 9.4.1

For the December 1960 results,

$U_o = 25$ metres/sec

$L_\beta = 625$ metres.

In all probability, the motion observed at scales less than 600 metres is not that of the small scale regions of a Kolmogoroff spectrum but is due to the vertical displacement of gas brought about by the turbulent shears. Since this motion has a preferred direction, and involves potential as well as kinetic energy, the mode of energy dissipation would be expected to be modified, and not to proceed as for the Kolmogoroff spectrum.

Although the possible presence of these buoyancy scales is considered to provide the best explanation of the small scale anomaly, two other factors inherent in the meteor method of turbulent velocity measurement should not be overlooked.

The first factor is involved in the idealized notion of discreet reflection points. In actual fact theory shows that the majority of the radio frequency energy reflected from the trail comes from the first half Fresnel zone about the specular reflection point. The length of this half zone is given by

$$1 = \tfrac{1}{2} \sqrt{R_0 \lambda}$$

(Kaiser)

where R_0 is the midpoint range of the echo, and λ is the radio frequency wavelength of the transmitted energy. For an average range of 150km, and a λ of 11.2 metres,

$$1 = 700 \text{ metres.}$$

If the trail remains straight in terms of line of sight distortions of less than $\lambda/4$, the relative motions of points separated by 700 metres will not be resolved. However, once distortion exceeds this rather small figure, lengths of trail of only a few wavelengths will give rise to echoes of amplitude very little less than that from the whole half zone. This effect has been demonstrated most conclusively by Greenhow and Neufeld (1959b) using a precision radar with a resolution of the order of better than 10 metres at a range of 200km. The effect places a lower limit on "discreet" echo separation of some 50 - 60 metres.

The other factor, that of reflection point motion along the trail under the influence of wind shears, has been treated

in detail in Chapter VI Section 3. This effect has been shown to place a lower limit of some 200 metres on the measurement of reflection point separations.

Since both these limits are associated with scales much less than those affected by the observed anomaly, the presence of the buoyancy subrange with a scale of a few hundred metres seems reasonably well substantiated.

9.5   The Large Scale Irregularities.

In any attempt to extend the turbulent flow field to scales outside the range of measurement, considerable caution must be excercised.   However, the good agreement obtained between theory and experiment over the 1km to 2.5km region, coupled with the experience of meteorologists obtained at lower heights, does inspire some confidence in an extrapolation to the size of the energy bearing eddies.

The relation between the scales of the inertial subrange is given in terms of the turbulent dissipation energy ϵ by

$$\epsilon = A \frac{U^3}{L}$$

9.5.1

(Batchelor, 1953)

where U is the velocity of the eddies of scale L. A is a constant (of order unity) whose value depends on the definition of L .

If the scale of an eddy is defined as the distance over which the velocity of that eddy falls from its characteristic

value to zero, the velocity difference relation of 2.10.3
(which has been shown to apply to measurements made in the
meteor region at separations up to 2.5km) may be used to det-
ermine **L**.

Rearrangement of 2.10.3 yields

$$\epsilon = \left[\frac{1}{5.7} \right] \frac{U^3}{L}$$

9.5.2

with Ł replacing the separation length ξ.

From the December 1960 results, the velocity of the en-
ergy bearing eddies was 25m/sec, and the turbulent dissipat-
ion rate 300 ergs/gm/sec. Substitution in 9.5.2 gives the
scale of the energy bearing eddies as

$$= 95 km.$$

This is comparable with the scales of 60 to 250km for
the energy bearing eddies as measured from their time correl-
ation by Greenhow and Neufeld (see Chapter III Section 5).

For eddies of velocity 25 m/sec and scale 150km, as
measured at Jodrell Bank, 9.5.2 gives a turbulent dissipation
of 200 ergs/gm/sec, which is of the same order as the Adelaide
results.

The reason that the expression 9.5.2 seems to be more
consistent than 9.5.1 with **A** unity, which latter is well sub-
stantiated in measurements of laboratory turbulence, probably

arises from the anisotropy of the turbulent flow field under
investigation and the redefinition of the characteristic
scale involved in its application. For the purposes of this
thesis the relation 9.5.2 is used as an empirical tool;
further work on its derivation is contemplated at a later
date.

9.6 Further on the Degree of Anisotropy.

Three values of line of sight turbulent velocity are ob-
tained from each meteor trail observed. These values of tur-
bulent velocity have been grouped for all echoes in the month
according to the zenith angle Z of the main station reflect-
ion point; because the separation of reflection points is
less than 3km at an average range of 150km, there is only a
small variation in the zenith angles of arrival of the sig-
nals associated with each echo as received at each of the
three stations.

The RMS turbulent velocities for intervals of cosZ of
0.05 are plotted in Fig. 35. The velocities decrease with
decreasing zenith angle, until, for echoes nearly overhead,
a value of approximately 10 m/sec is observed.

If the height correlation interval of 6.5KM observed by
other workers in this field is taken as the characteristic
eddy length in the vertical direction in the equation 9.5.2,
then, for a turbulent dissipation of 300 ergs/gm/sec., the
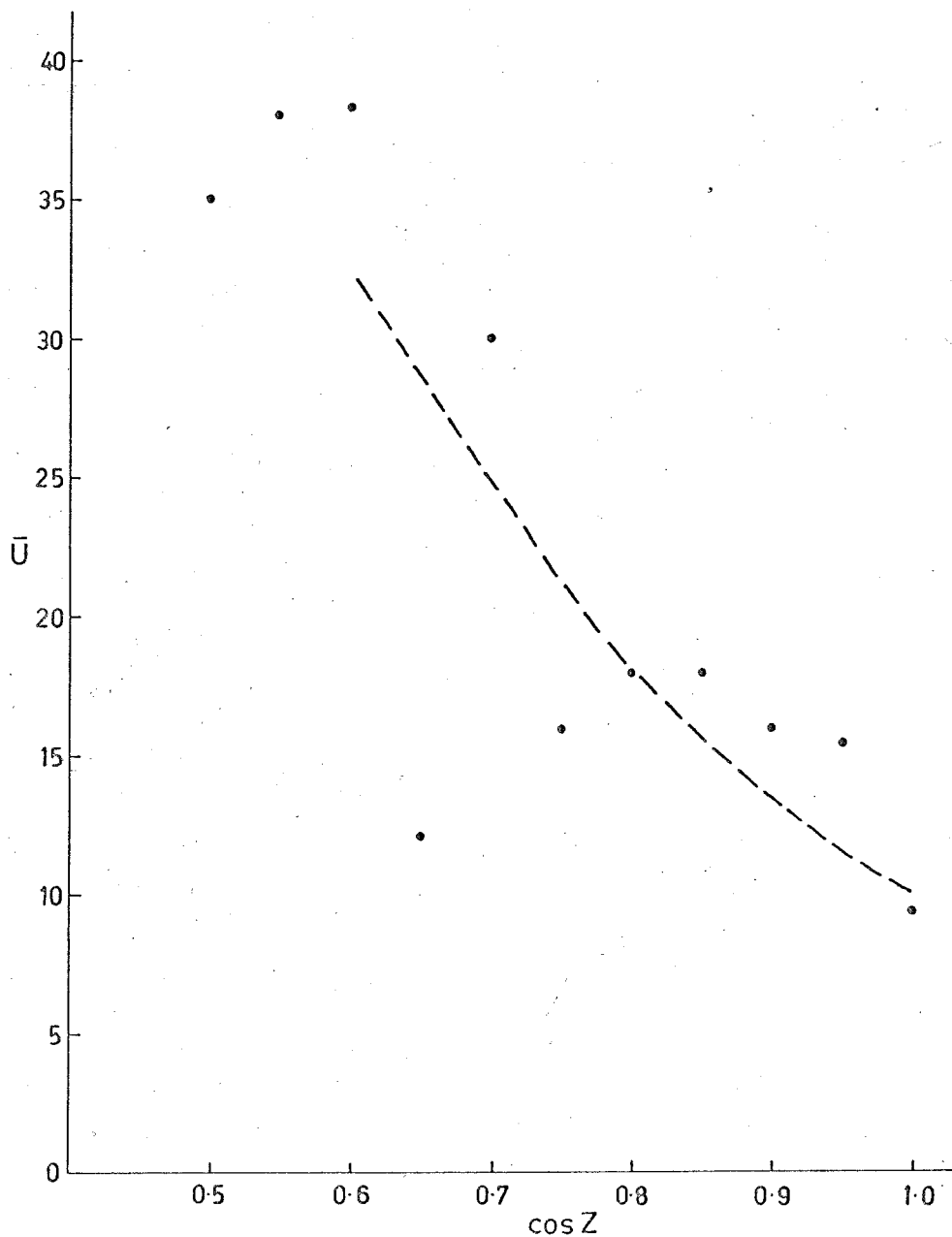
Variation of RMS Turbulent Velocity with
Zenith Angle.
FIG.35

characteristic velocity of such an eddy is 10 m/sec. If
9.5.2 is considered, as originally derived, as the velocity
difference/separation relation for an isotropic, inertial
eddy subrange, the scales to 6.5km could belong to such a
subrange.

The characteristic velocity of the turbulent flow field
(considered as isotropic) has been determined as 25 m/sec;
the RMS vertical velocity is 10 m/sec; thus, regardless of
whether or not a Kolmogoroff spectrum is assumed, anisotropy
of the large eddies with the maximum dimension horizontal is
certainly well established.

9.7 The Variation of the Velocity Difference with Height
Difference.

To investigate the relation between turbulent velocity
difference and height difference, the analysis for spacial
separation was repeated, using height differences as the
length parameter, regardless of the actual spacial separat-
ion. To obtain a measure of the variation of the spectrum
function $E(\Delta h)$, the logarithm of the squares of the velocity
differences has been plotted against the logarithm of the
height differences Δh. The result is shown in Fig. 36. The
best fit line of slope 4/3 is also plotted. While there is
considerable scatter, agreement is generally good. The
height differentials would appear to be indicative of a tur-
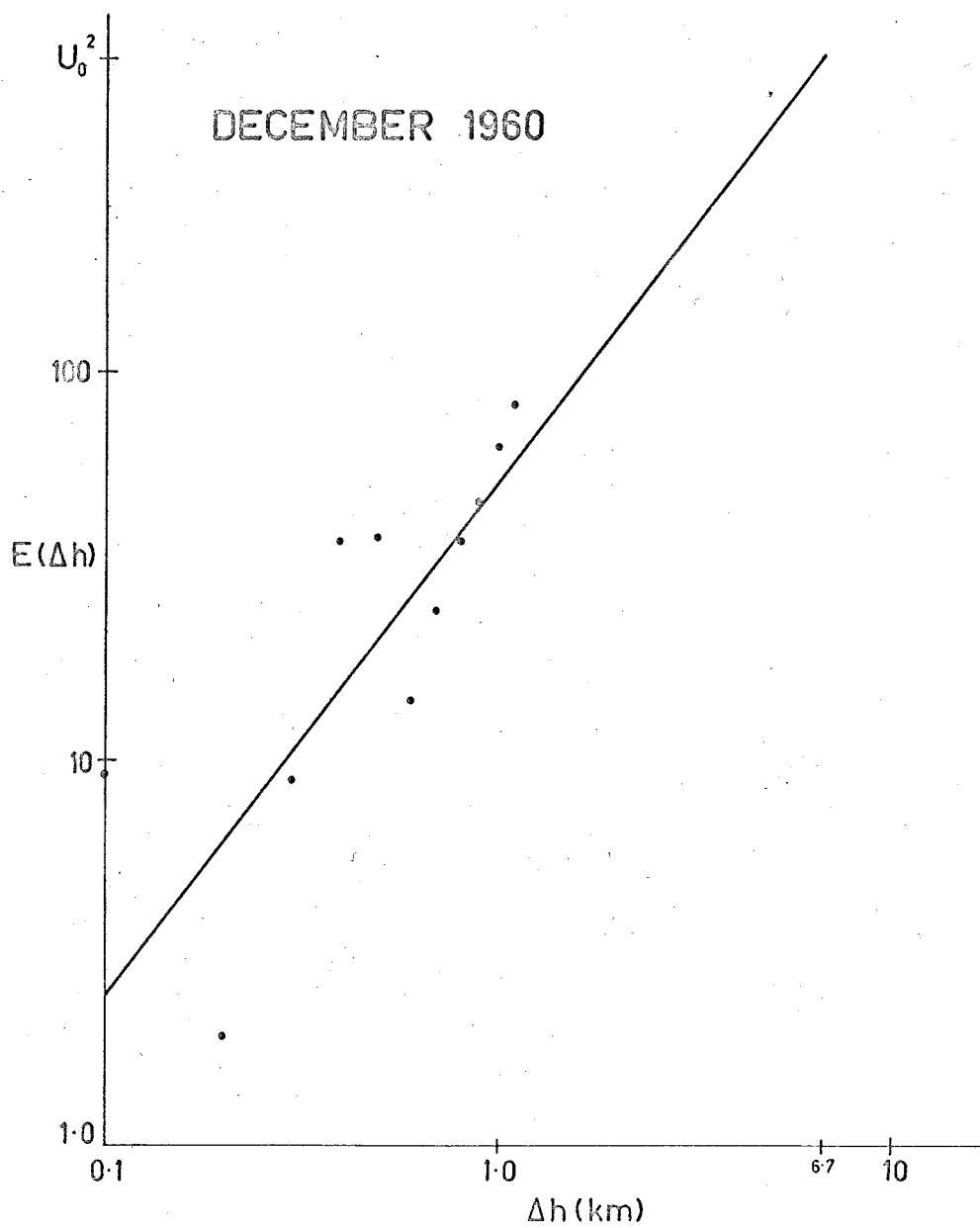
FIG. 36

bulence subjected to shear.

Extrapolation of the best fit line to a value of
of 625 (corresponding to the characteristic turbulent veloc-
ity U_0 of 25 m/sec.) yields a scale of 6.7km. Since the
spacial separations follow the isotropic Kolmogoroff spec-
trum, the 4/3 power law for the height differentials per-
tains to a region of small shear, which, if the extrapolation
to the characteristic velocity is valid, should hold up to
6km.

9.8   The Variation with Time of the Characteristic Velocity of the Energy Bearing Eddies.

To determine the variation of the magnitude of the char-
acteristic velocity of the turbulent flow field throughout a
typical day, the turbulent velocities for each echo are sub-
jected to an analysis similar to that used to derive the mean
wind. There is, however, the added complication of the vert-
ical motion which must be considered in any attempt to resolve
the turbulent velocities in the NS and EW directions. This
problem does not arise in the mean wind analysis since mean
vertical motion is very small relative to the horizontal vel-
ocity.

The effect of the vertical motion (taken as 10 m/sec)
was removed by subtracting from the magnitude of each turbul-
ent velocity measurement the component of the vertical motion

in the line of sight direction. The resultant was assumed to
be the line of sight component of a horizontal turbulent mot-
ion. The radical assumption is now made that the azimuth of
the line of sight is as likely to be the true direction of
horizontal turbulent motion as any other direction. Provided
that a sufficient number of echoes randomly disposed in azi-
muth is observed over a sufficiently long period of time, the
RMS values of the turbulent velocity components in the NS and
EW directions determined by the foregoing method will be a
good approximation to the true values.

The hour by hour turbulent velocity components for
December, 1960, are presented in Fig. 37, together with the
mean wind for the height range 85 - 94 km. The curves are
the result of a Fourier analysis truncated at the second har-
monic, i.e. mean plus 24 hour and 12 hour components.

The RMS turbulent velocity has its maximum value in the
early morning, and is a minimum during the late evening. If
the turbulent and mean wind velocities are compared on the
basis of magnitude alone, there is no correlation, as was
found by Greenhow (see Chapter 3 Section 4). If, however,
relative phases are considered also, then some dependence is
evident. The maximum turbulent velocity is associated with
the change in mean wind from meridional to zonal, and the
minimum turbulence with a mean wind change from zonal to

DECEMBER 1960
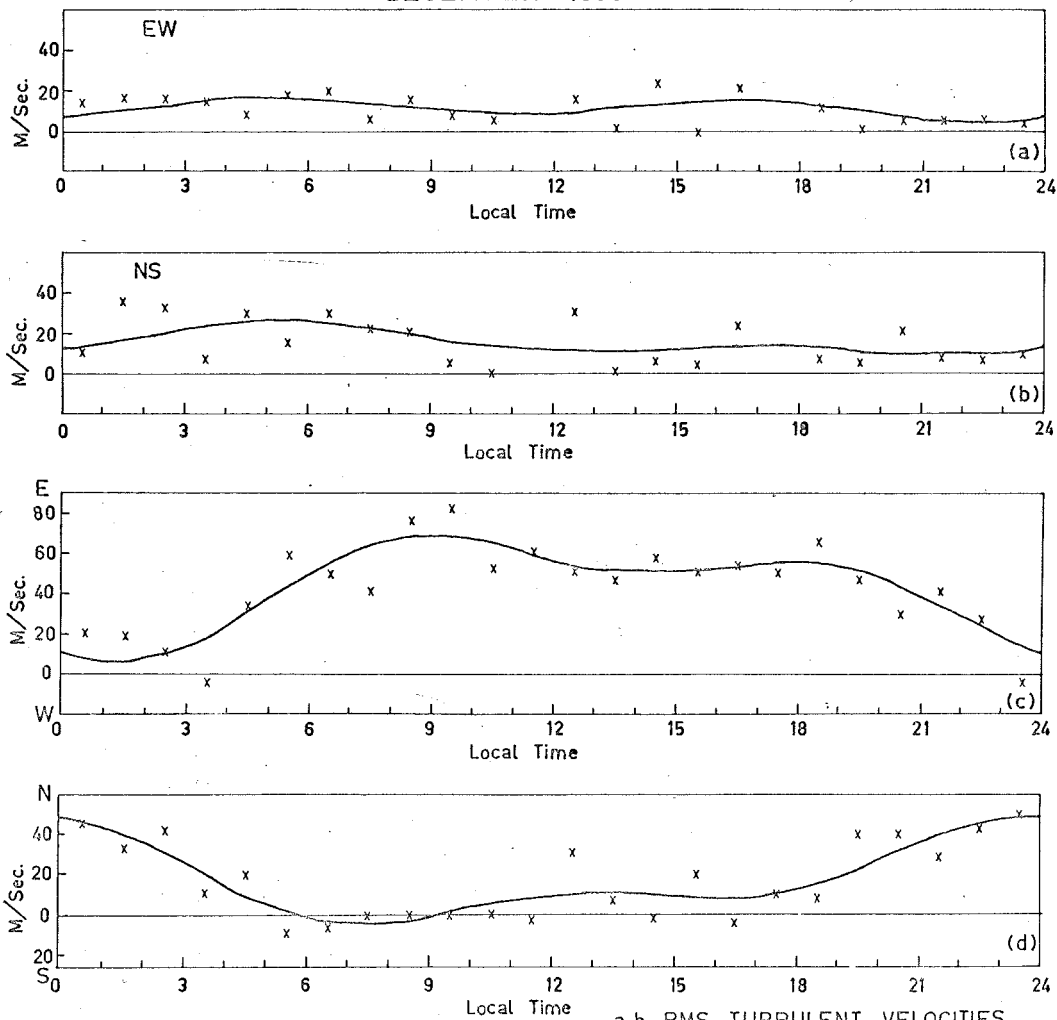
FIG. 37   a,b RMS TURBULENT VELOCITIES
          c,d MEAN WIND, 85-94 KM.

meridional.

Further comments are made on the time dependent nature of the turbulent flow field in Chapter XI, after consideration of the 1961 results for January to December inclusive.

9.9   The Characteristic Dissipation Length λ.

The characteristic dissipation length λ can be estimated by solving the equation

$$\epsilon = - \frac{15\nu U_0^2}{\lambda^2}.$$

(2.7.1)

For $\epsilon = 300$ ergs/gm/sec

$U_0 = 25$ metres/sec

and $\nu = 10^5$ sq.cm/sec

$\lambda = 1.7$ km

A similar value was obtained from Greenhow's velocity correlation function in Chapter III Section 3. This is somewhat surprising, since Greenhow's correlation function does not describe the total turbulent flow field, but only the scales to 6km. Because of this, and the time dependent nature of the turbulence, it is felt that no great significance should be attached to this agreement.

9.10   The Reynolds Number.

The value of λ determined in Section 9 is probably accurate to within a factor of 2, and it is of interest to calculate the value of the turbulence Reynolds Number defined in

Chapter II Section 8 as

$$R_\lambda = \frac{U_o \lambda}{\nu}$$

Substitution of the appropriate value yields

$$R_\lambda = 4 \times 10^3$$

which is of the same order as the critical value en-
countered in laboratory turbulence.

CHAPTER X.

The Results for 1961.

This Chapter is devoted to a discussion of the seasonal variations of turbulence parameters as deduced from the data for each month of 1961, January to December inclusive.

10.1   The Velocity Differences.

The mean wind analysis has not as yet been completed for all months of the year.   Whereas the total turbulence survey involves some 1800 three station echoes spread over the thirteen months, the mean wind reduction requires at least 1000 single station echoes per month.   Once available, the processing of the data on the computer involves only a few hours for each month; the time consuming portions of the reduction are the initial film reading and the subsequent card punching.

Before any mean wind information was available, the velocity differences with separation for several months were computed on the basis of zero mean wind.   When the mean wind extraction was subsequently performed and the data reprocessed, the velocity difference/separation relation for each month was found to be almost identical to that obtained by assuming zero mean wind.   This is really not surprising when
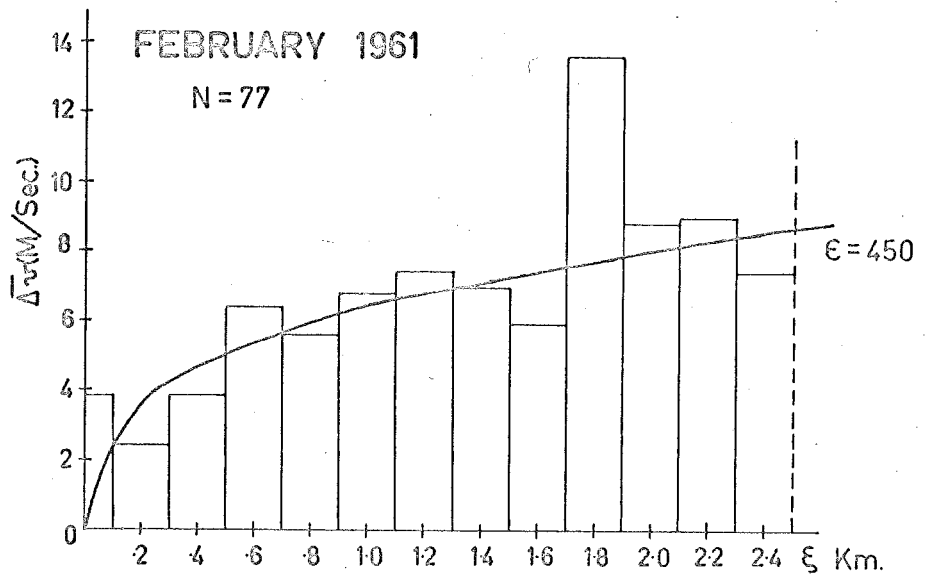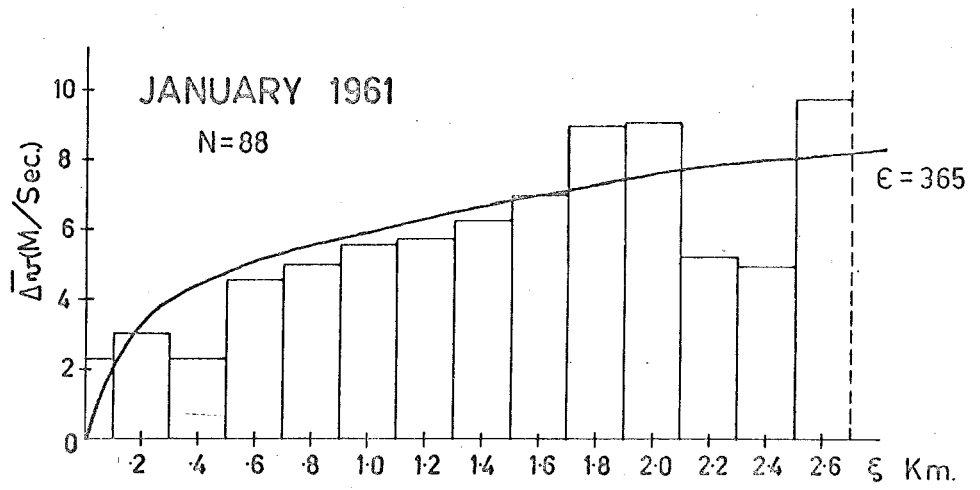
FIG. 38

one considers the factors which can influence this relation. The mean height gradient is always less than the turbulent gradient, and thus has only a small effect on the measured velocity differentials.

The value of the turbulent dissipation rates calculated from the velocity differences for January, February, April, May, October and November, for which the mean wind has not been taken into account, should be regarded as tentative, although no appreciable modification is expected in the final analysis.

The histograms of velocity differences against separations for the months January to December 1961 inclusive are presented in Figs. 38 to 44, together with the best fit theoretical curves determined as in Section 3 of Chapter IX. In comparing theory and experiment four factors must be taken into consideration:-

1. The size of the sample. At least 10 velocity differences are required for each separation to obtain a significant RMS value. This is usually achieved for values of separation up to 2.6km. In general, the total number of echoes in each sample has to exceed 80 (yielding 240 velocity differences) in order to obtain significant velocity differentials for a given month. For the early months of the year, the echo rate was reduced because of equipment troubles. This
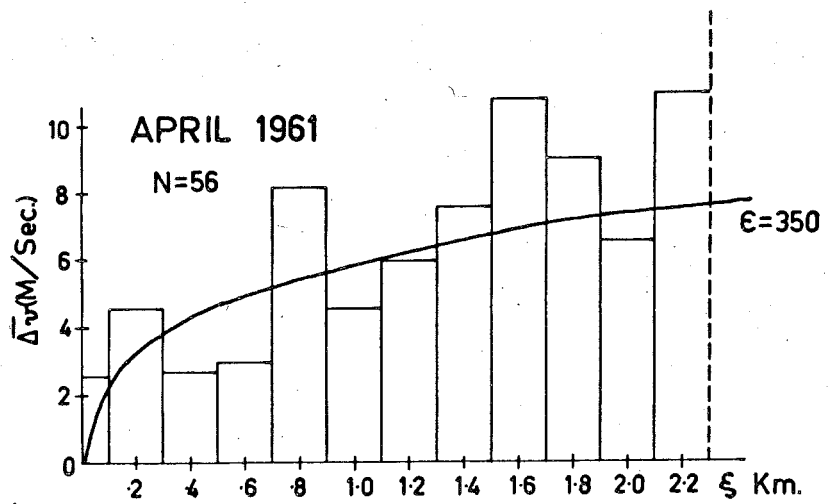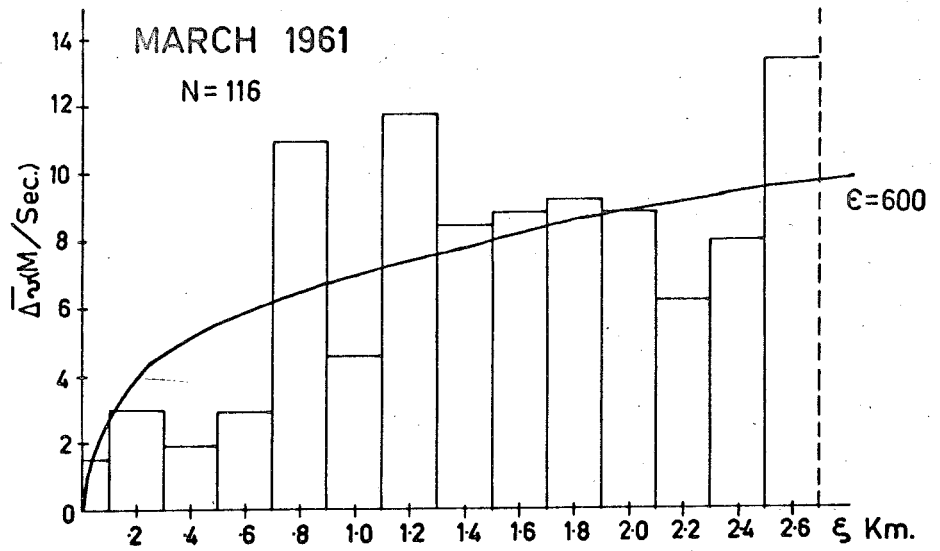
FIG. 39
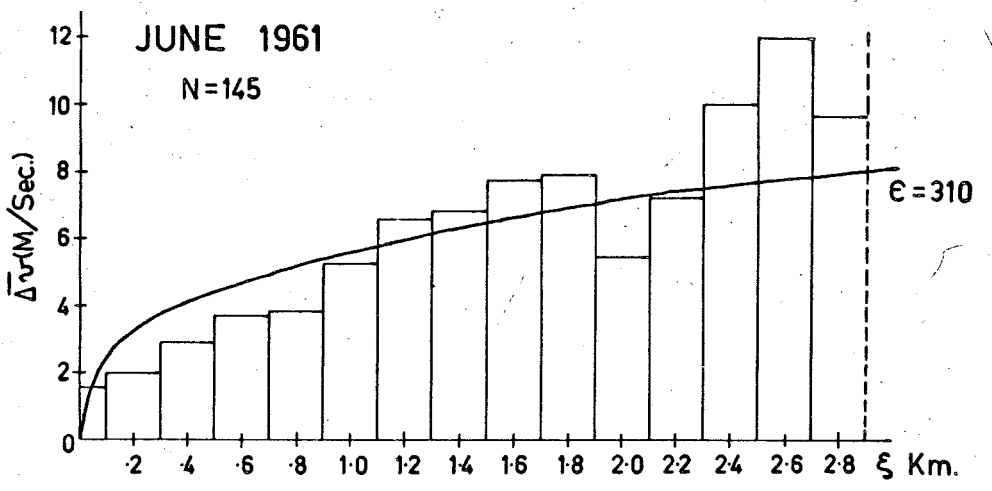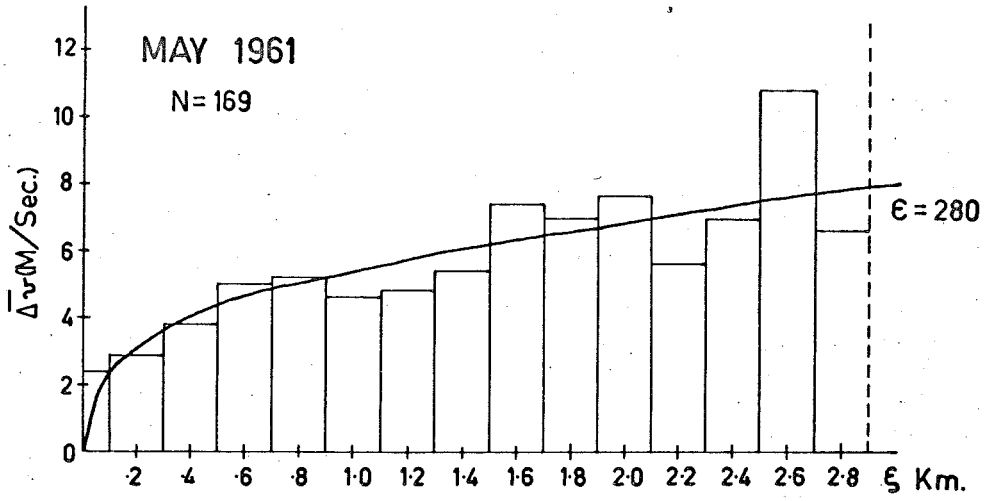
FIG. 40
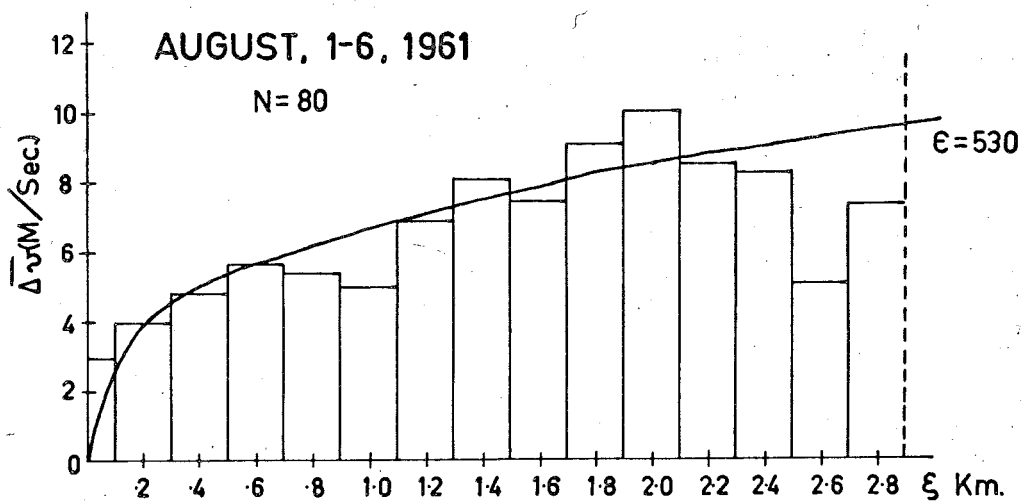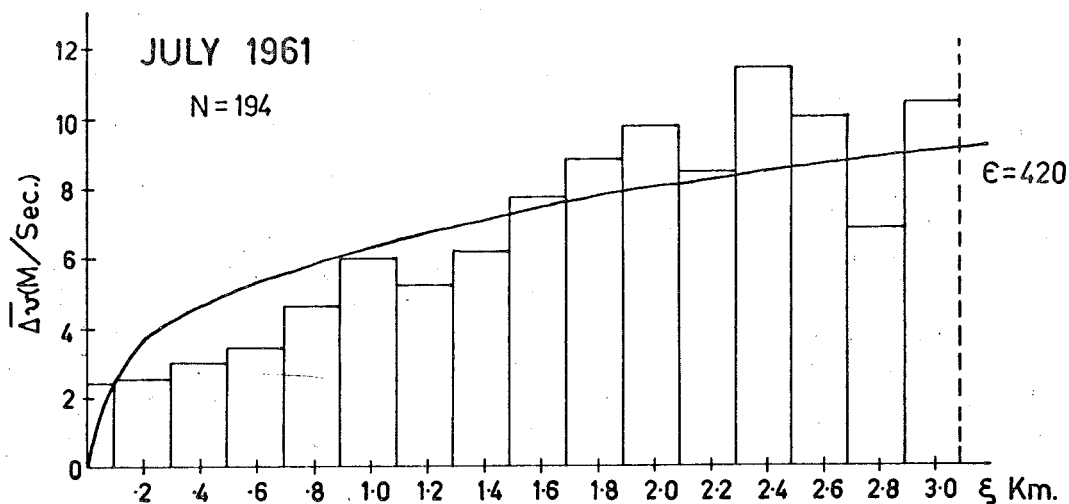
FIG. 41
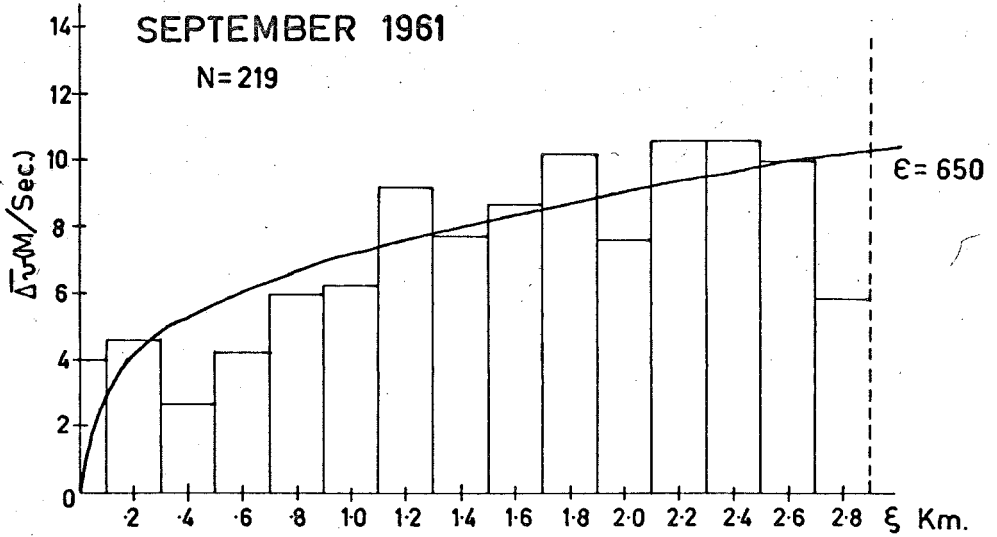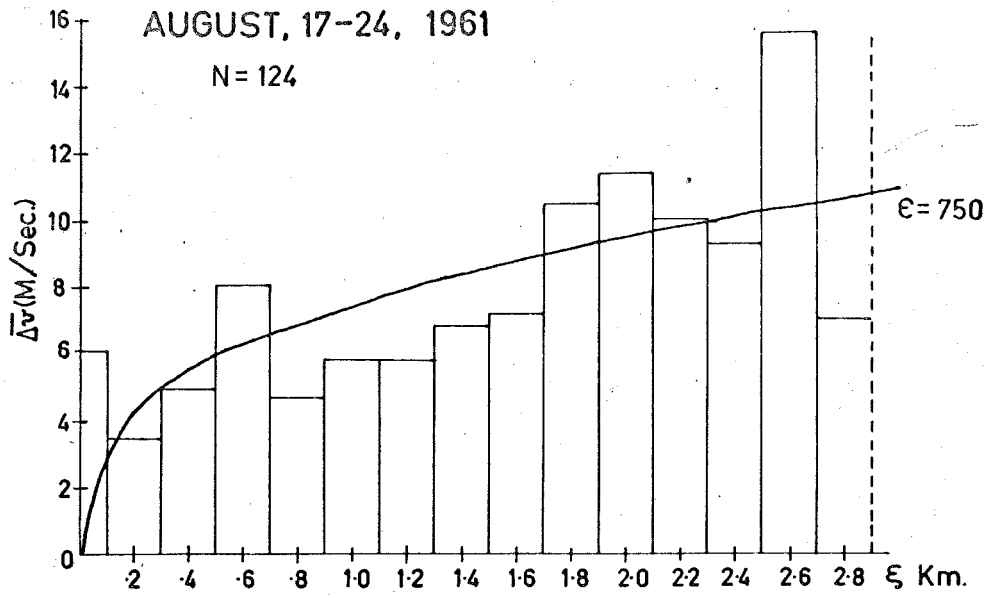
FIG. 42
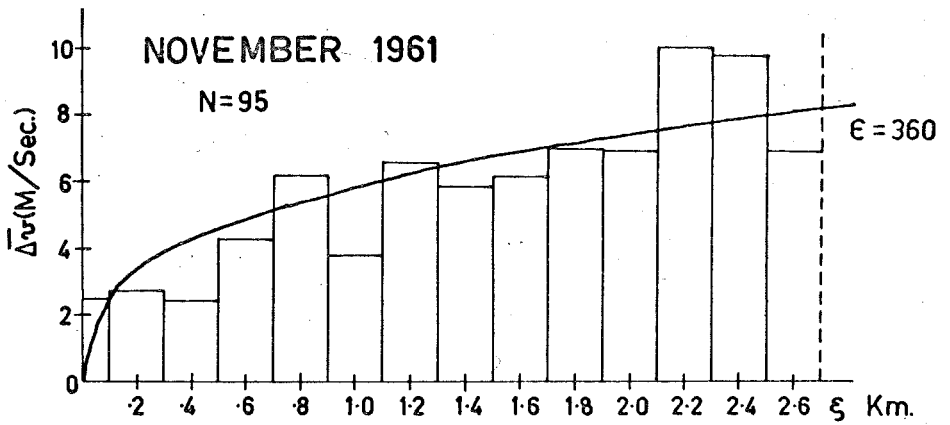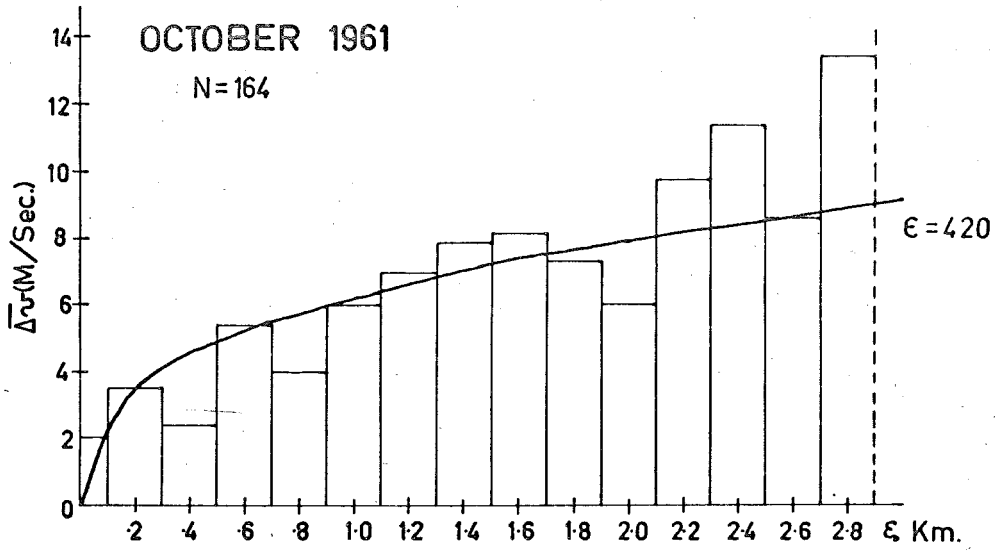
FIG. 43
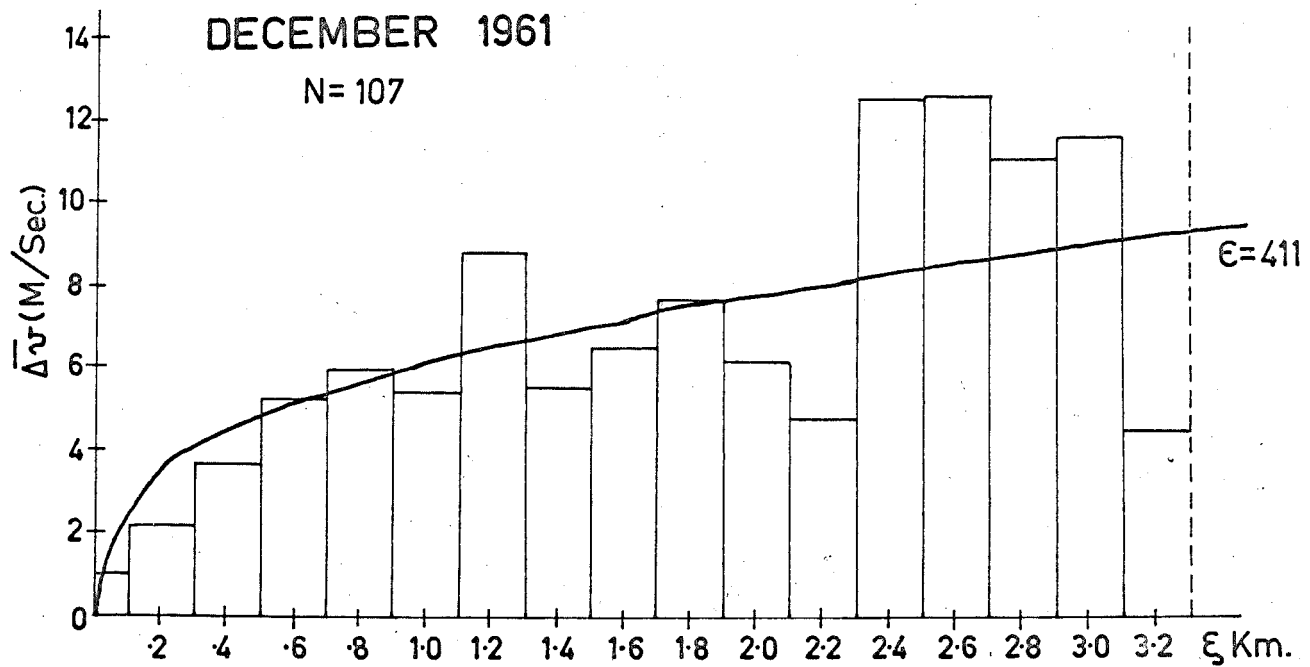
FIG. 44

is reflected in poor fits to the theoretical curves for these months.

2. At scales less than 200 metres anomalous velocity differentials are prevalent, due to the inaccuracy associated with the separation measurement brought about by the phenomenon of reflection point motion (see Chapter 6 Section 3).

3. The observations show a marked deviation from the theoretical curves at separations less than approximately 1km, and, to a lesser extent, an overall periodic fluctuation. This has already been explained in terms of the action of buoyancy forces. In general, these effects are greatest for the more disturbed months in which the turbulent dissipation rate exceeds 450 ergs/gm/sec. In fact, for August 17th to 24th it is almost impossible to decide on the best fit curve for the estimation of ϵ, and the actual dissipation rate for this month is probably somewhat less than that estimated.

4. The fourth factor involves the time dependence of the turbulent flow field, which has already been demonstrated for December, 1960, and which is confirmed by the other months analysed in Section 4 of this Chapter. The turbulent dissipation rate is expected to depend upon U_0, the velocity characteristic of the energy bearing eddies. The diurnal variation in U_0 is of the order of 2:1. Thus the turbulence

spectrum will be time dependent, and the histograms of Figs.
38 to 44 representative of an average over the characterist-
ically different turbulent flow fields which exist throughout
the day. If, for any reason, the sampling rate is not uni-
form, the spectrum determined will be biased towards the con-
ditions pertaining during the high rate hours. In general,
these will be the early morning hours, since the earth
"sweeps up" more meteors at 0600 hours than it does at 1800
hours.

10.2 The Seasonal Variation of the Turbulent Dissipation
Rate ϵ.

The ϵ values of the theoretical curves fitted to the re-
sults of Section 1 are considered to be the best estimates
yet determined of the turbulent dissipation in the 80 to 100km
region of the upper atmosphere.

In determining these values, the value of α, the constant
of proportionality in the expression

$$E(\kappa) = \alpha \epsilon^{\frac{2}{3}} \kappa^{-\frac{5}{3}}$$

has been taken as 2/3 (see Chapter II Section 10).

The value of ϵ determined from the velocity difference/
separation relation

$$\overline{\Delta v^2} = 4.82\alpha(\epsilon \xi)^{\frac{2}{3}}$$
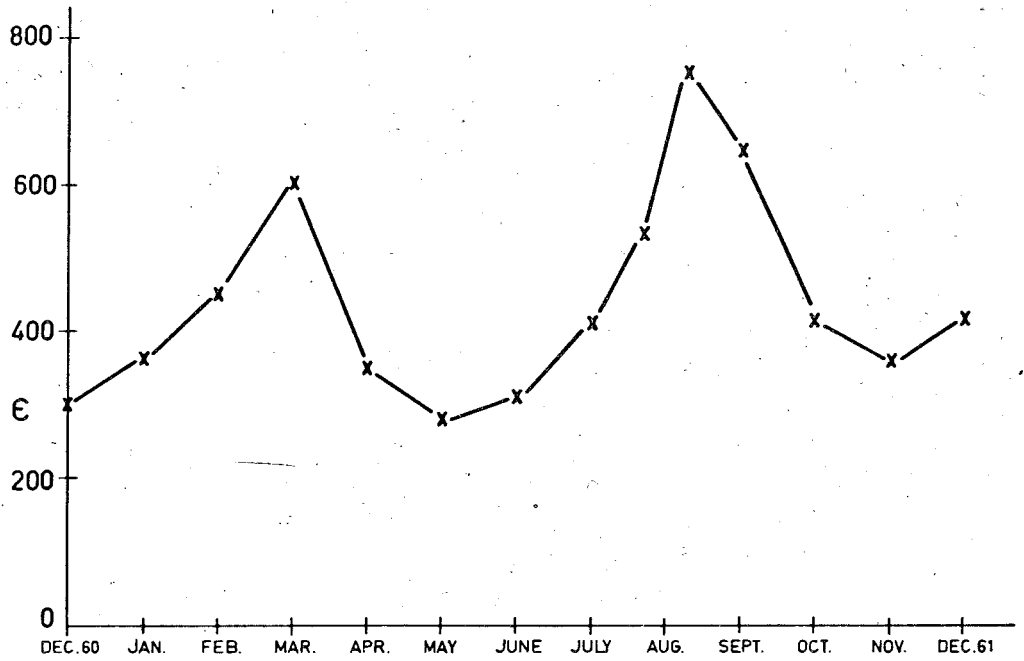
FIG. 45a – SEASONAL VARIATION OF THE TURBULENT DISSIPATION RATE.
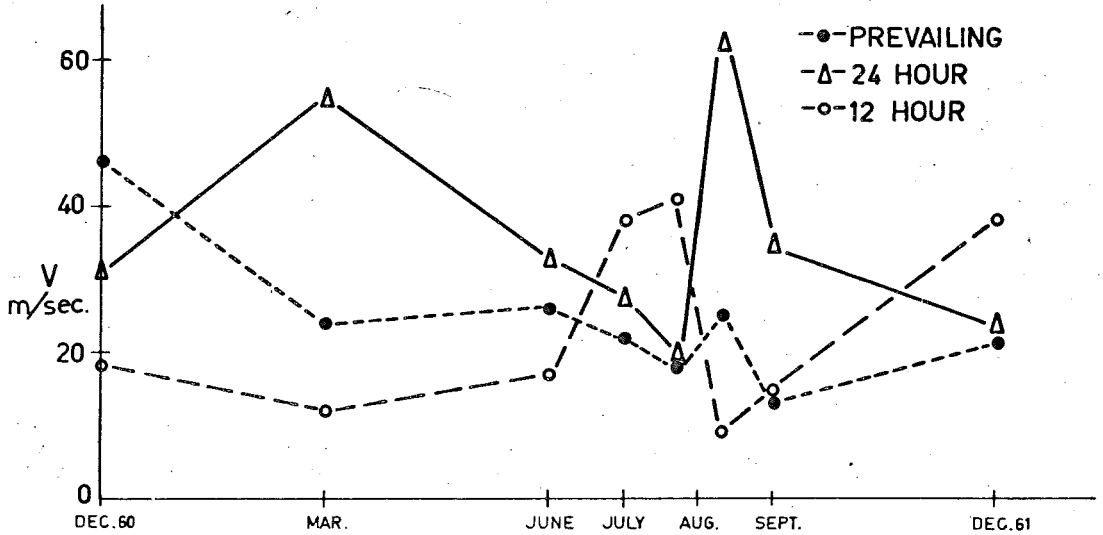
FIG. 45 b – SEASONAL VARIATION OF THE MEAN WIND COMPONENTS.

depends on $\alpha^{-\frac{3}{2}}$.

If α is taken as 1.0, then the resultant turbulent dissipation rates will be approximately half those given in Fig. 45a. (See Chapter XI, Section 7.)

Unfortunately, the upper limit of ϵ is not well established, since increased turbulence is accompanied by increased activity of the buoyancy subrange, and the velocity differences no longer follow the Kolmogoroff spectrum. Nevertheless, the relatively smooth rise in ϵ establishes the equinoxial maxima, and the maximum value of 750 ergs/gm/sec is probably a reasonable, if somewhat high, estimate.

It is of interest to compare the seasonal variations of ϵ and the three components of the mean wind as shown in Fig. 45. The prevailing and semidiurnal components do not appear to be in any way related to the turbulent dissipation, but the behaviour of the magnitude of the 24 hour component throughout the year is very similar. This suggests that the turbulent flow field may have its origin in the diurnal variation of the mean wind.

10.3 The Dependence of the Velocity Differentials on Height Differences.

The velocity differentials as a function of height difference have been calculated for those months for which the mean wind is available. The results are presented in Figs.

FIG. 46

FIG. 47

FIG. 48

165
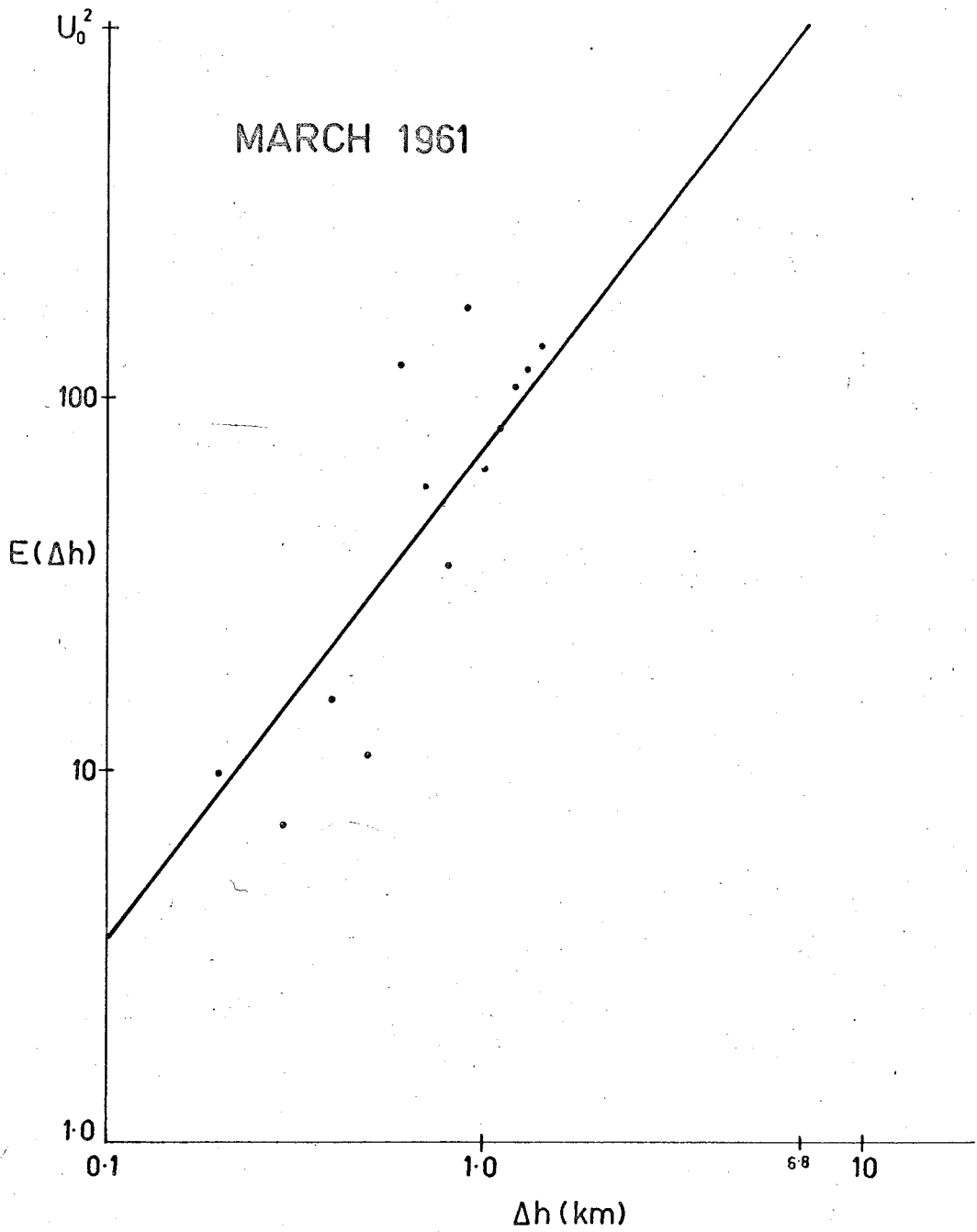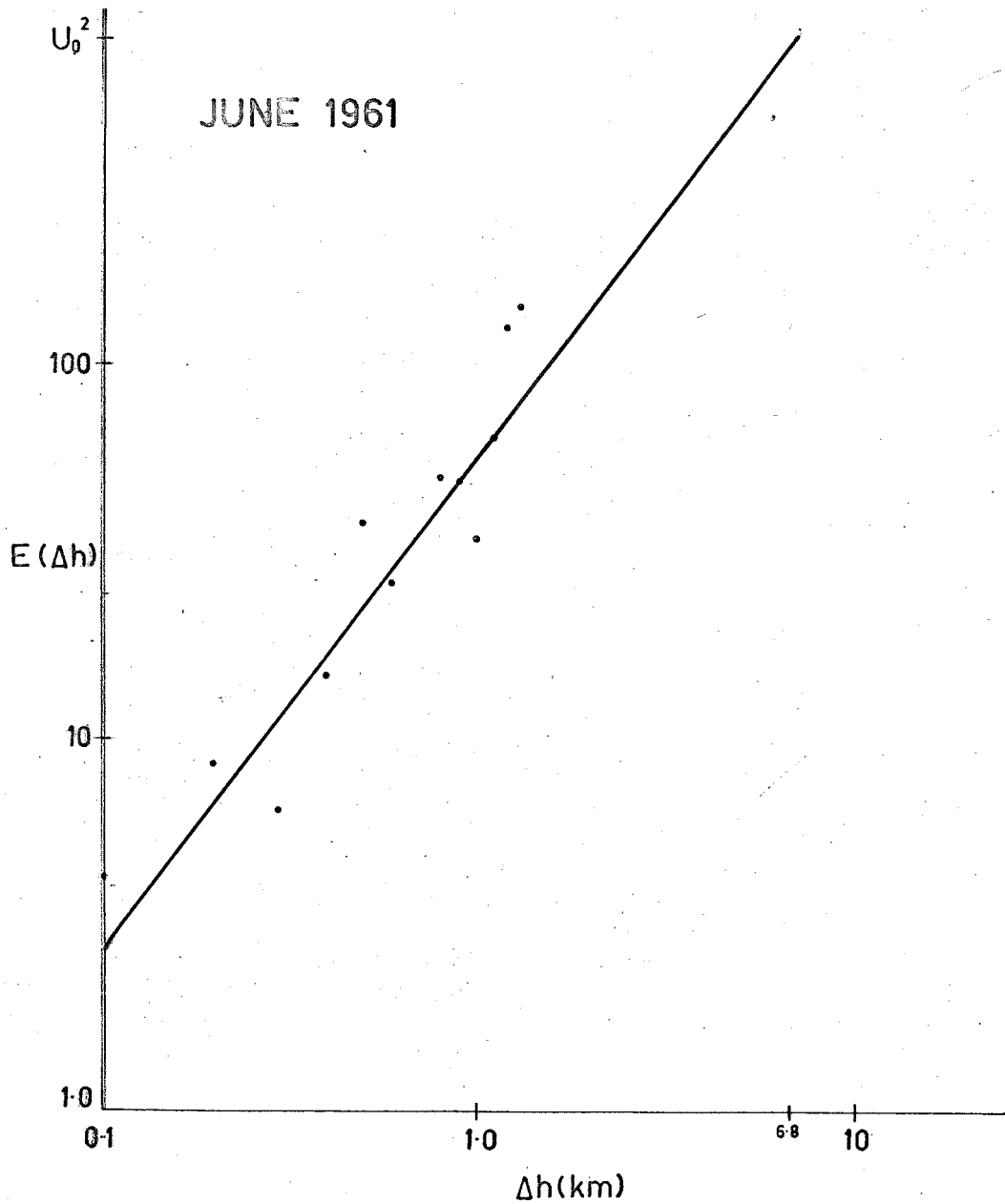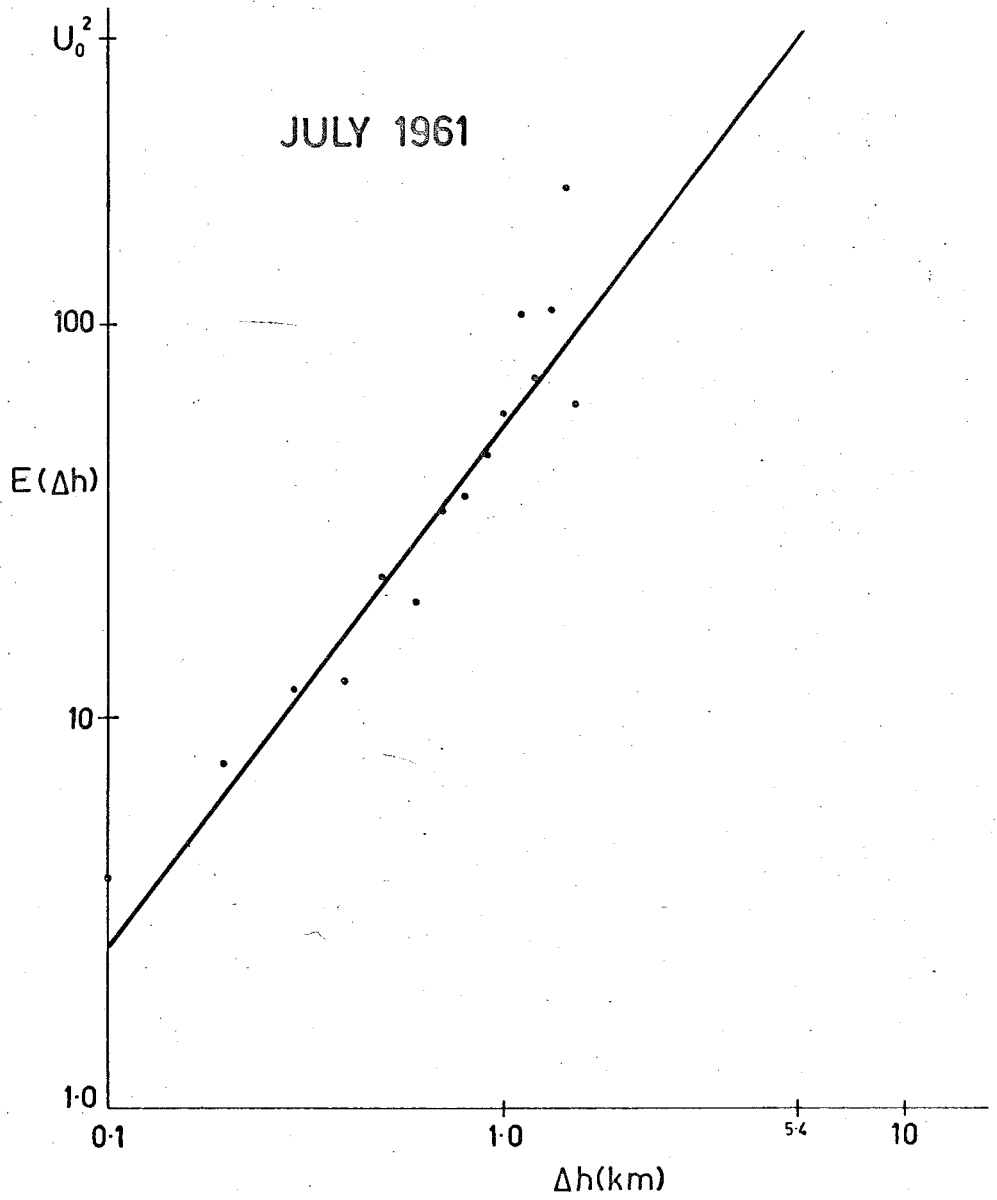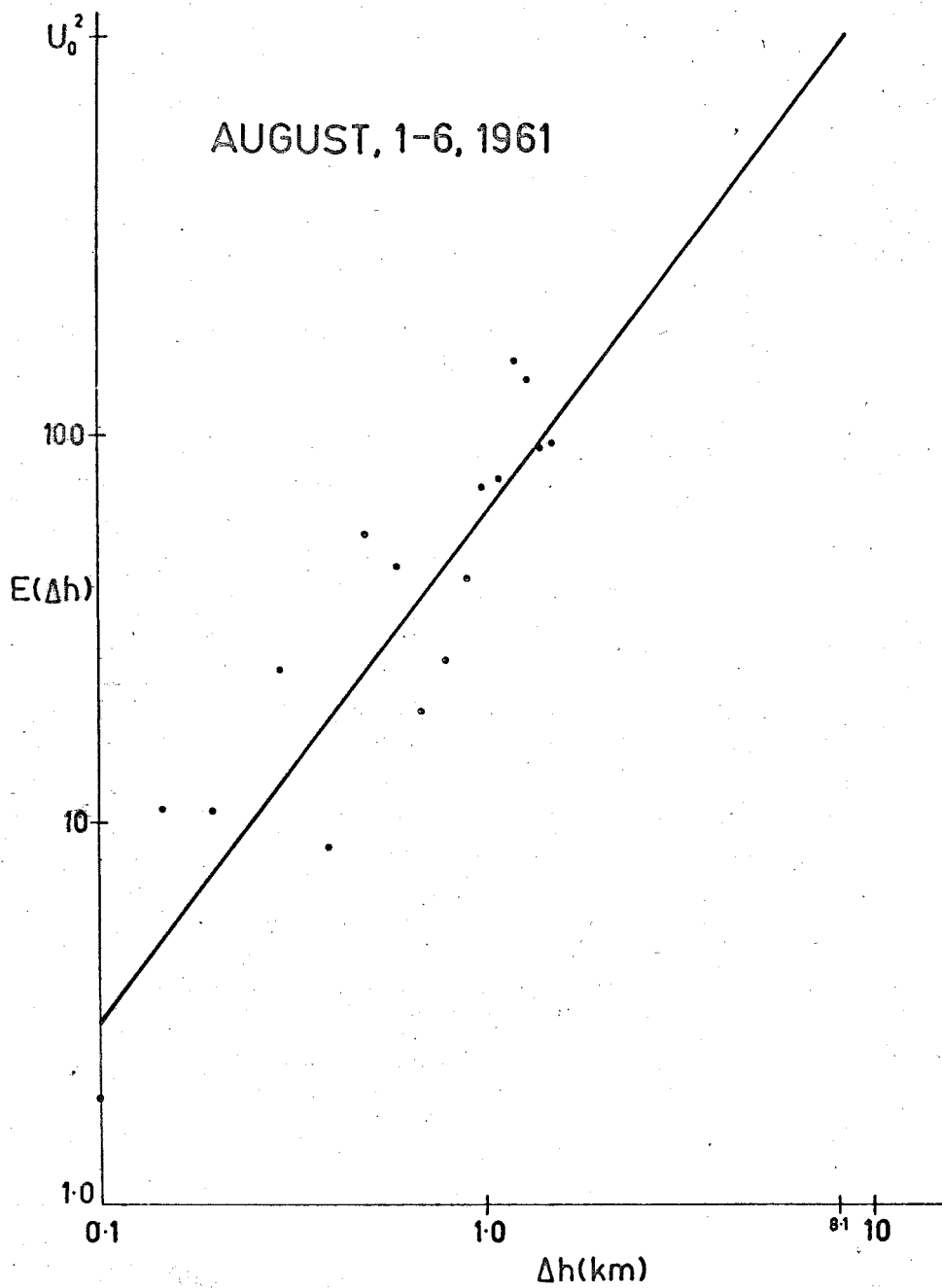
FIG. 49
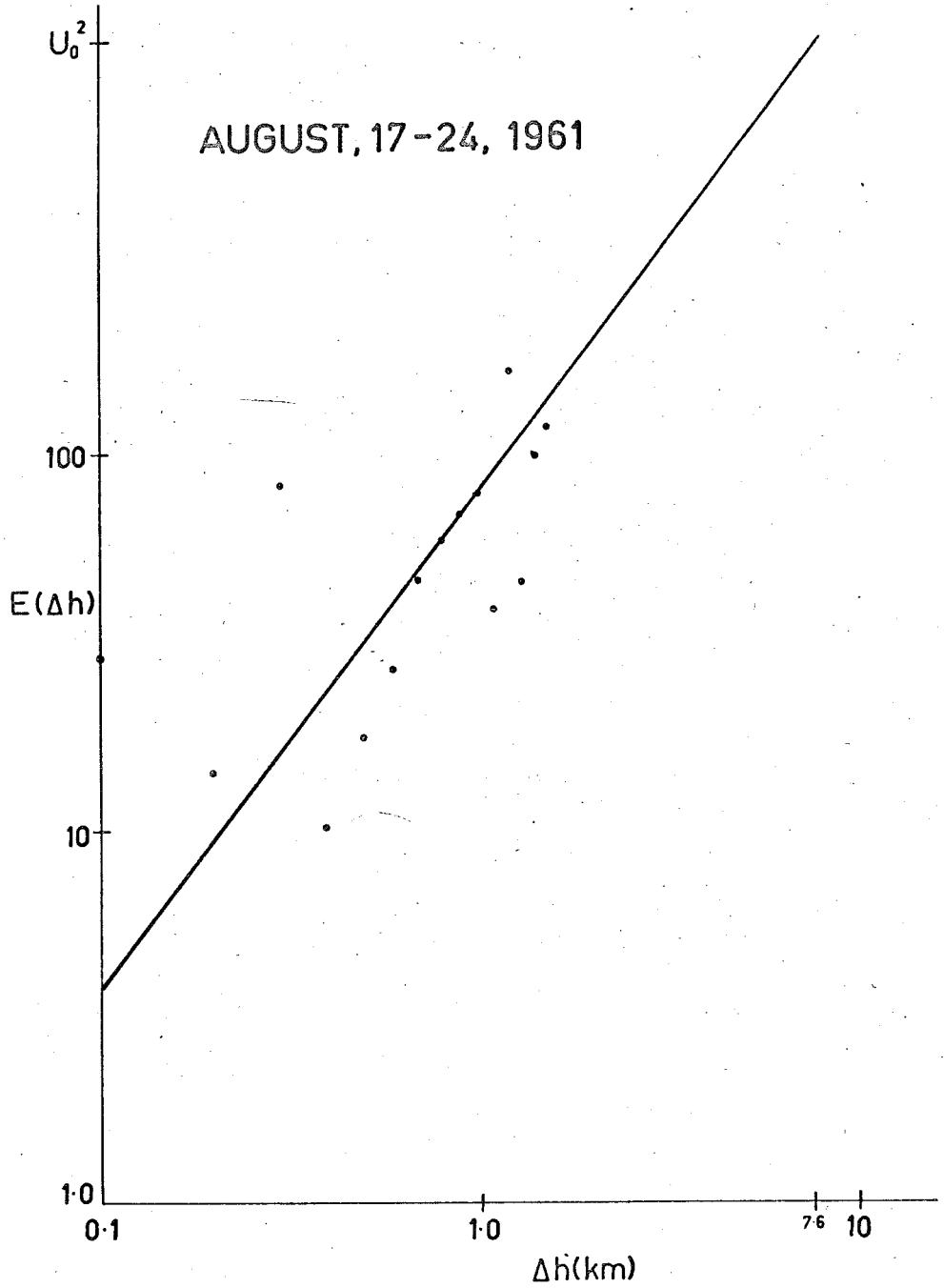
FIG. 50
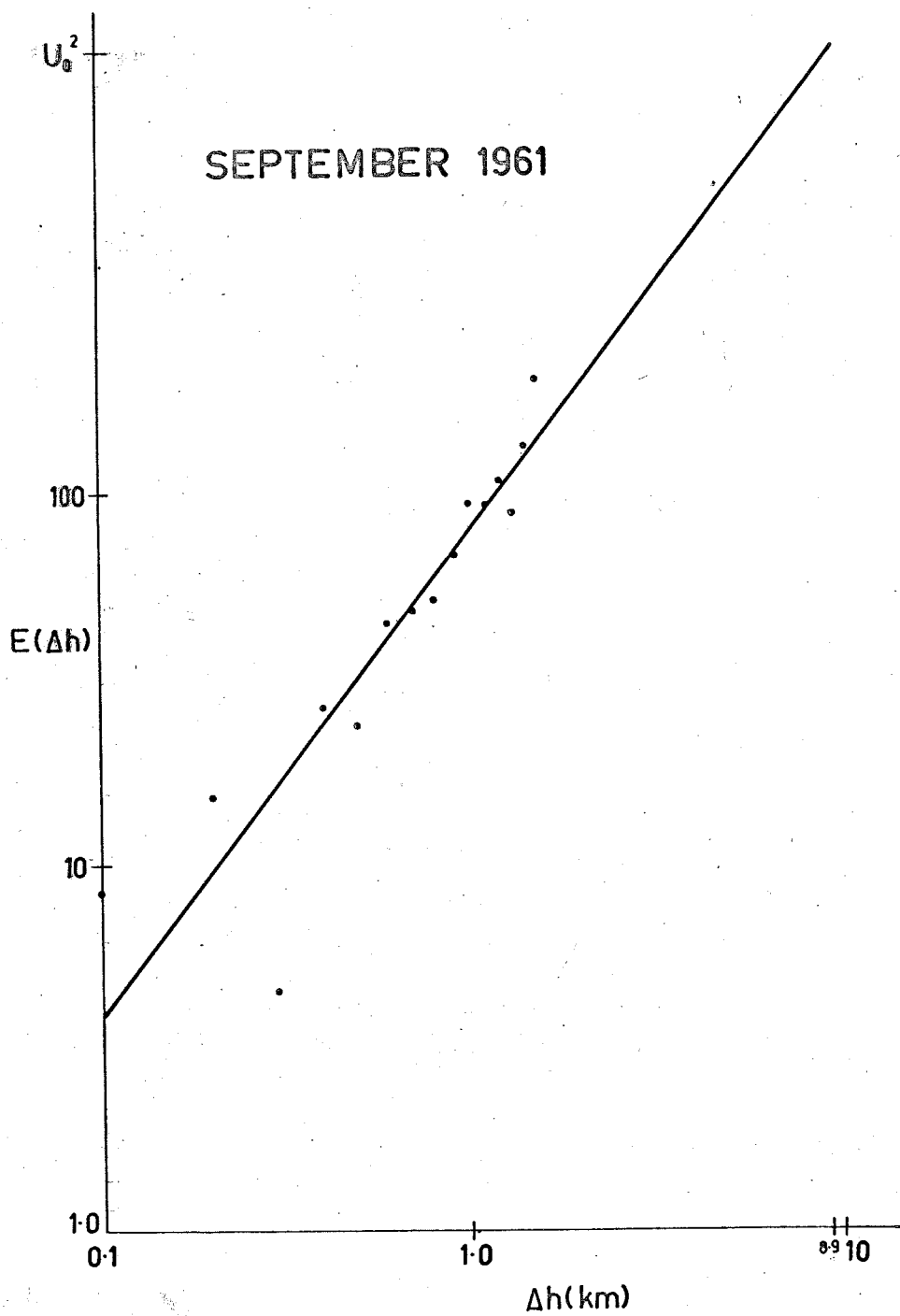
FIG. 51
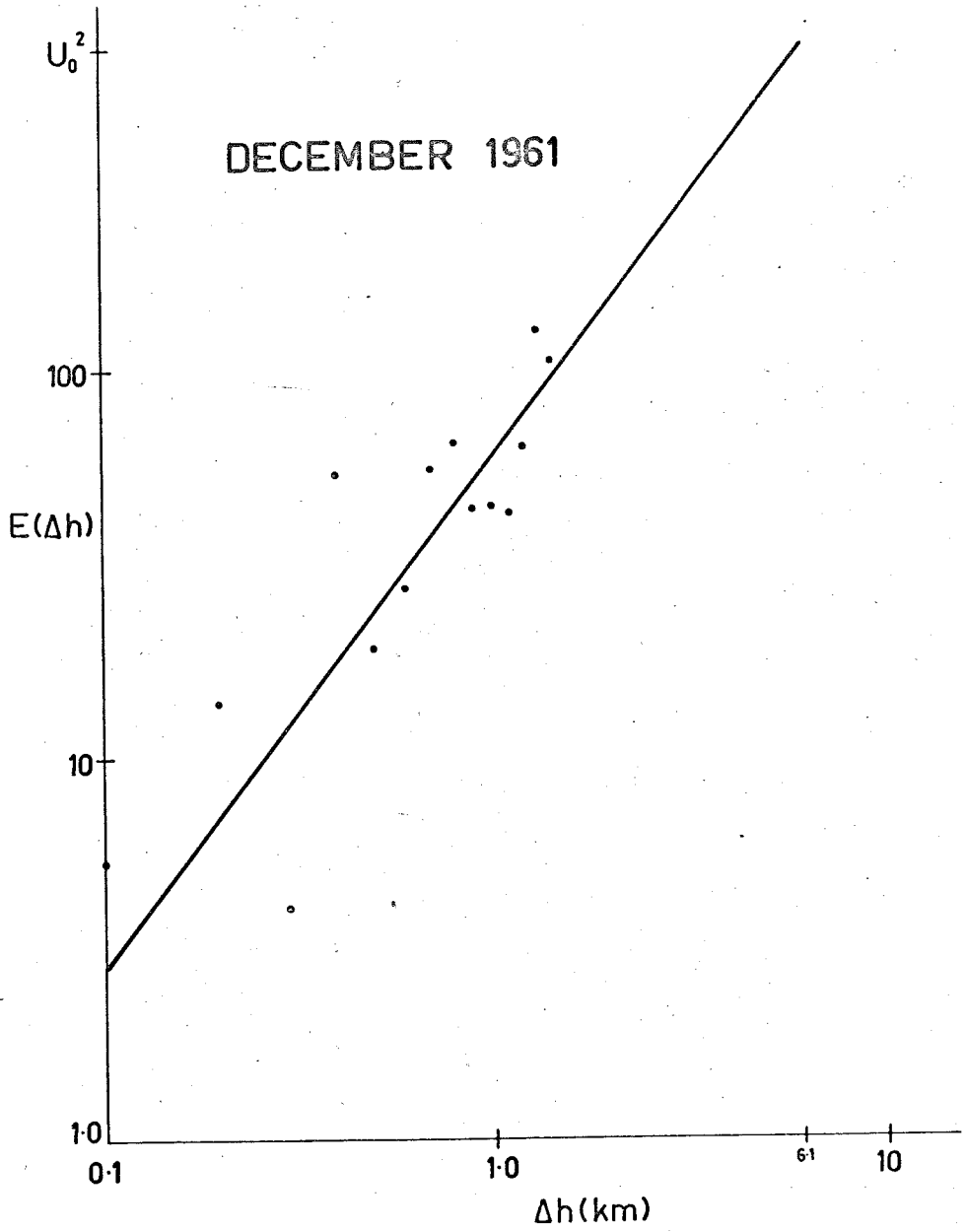
FIG. 52

46 to 52 inclusive. Most of the scatter in velocity differ-
ence for each month appears to be periodic and most prevalent
below height separations of 1km, due, at least in part, to
the action of the buoyancy subrange. Results for all months
tend to follow the 4/3 power law indicative of shear with
height. There is only a small variation throughout the year
in the turbulent velocity gradient as given by the RMS vel-
ocity difference measured over a height difference of 1km.
The best fit lines of slope 4/3 correspond to gradients rang-
ing from 7.5 metres/sec/km (June) to 9 metres/sec/km (Septem-
ber).

In an attempt to determine the vertical correlation dis-
tance, the plots of Figs. 46 - 52 have been extrapolated to
the values of $E(\Delta h)$ representative of the characteristic vel-
ocities of the energy bearing eddies. Because of the aniso-
tropic nature of the large eddies, the characteristic veloc-
ity U_o determined as the RMS over all the line of sight tur-
bulent velocities measured in a given month (see Chapter IX
Section 2) is not the actual velocity characteristic of the
predominantly horizontal large scale turbulent flow. How-
ever, the velocity U_o does characterize the flow as determ-
ined by line of sight observations.

The vertical correlation distances thus determined range
from 5.5km (July) to 8.9km (September). This variation in

scale may represent a seasonal change, but since the statistical significance of these values has not been examined, they are included only as substantiating evidence for the validity of the 4/3 power shear law at the scales measured, since extrapolation from these scales yields a vertical correlation distance similar to the value of 6.5km observed by other workers in this field.

10.4 The Seasonal Variation of the Turbulent Velocity.

The hour by hour turbulent velocity components, together with the mean wind for the height range 85 to 94km for the months of March, June, July, August, September and December, 1961, are presented in Figs. 53 to 59 inclusive.

The maximum turbulent velocity is, on the average, less than half the mean wind maximum. Hour by hour variation in the turbulent velocity is evident for all months; the maximum turbulent velocity occurs in the early morning in the summer, and in the late afternoon in the winter; in general the minimum value is attained some 8 hours before the maximum. It is encouraging, in considering these seasonal variations, to note that the results for December 1961 show all the general features of those for December 1960. The overall increase in the December 1961 turbulent velocity is presumably due to the increased complexity of variation of the mean flow.

MARCH 1961
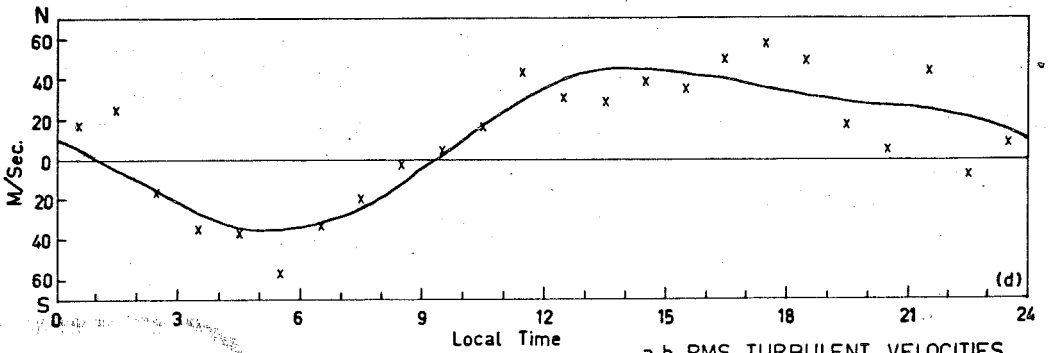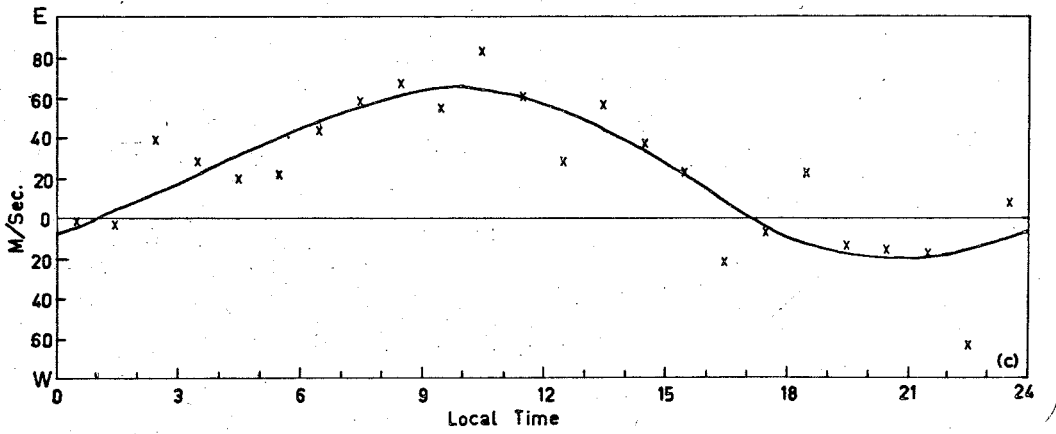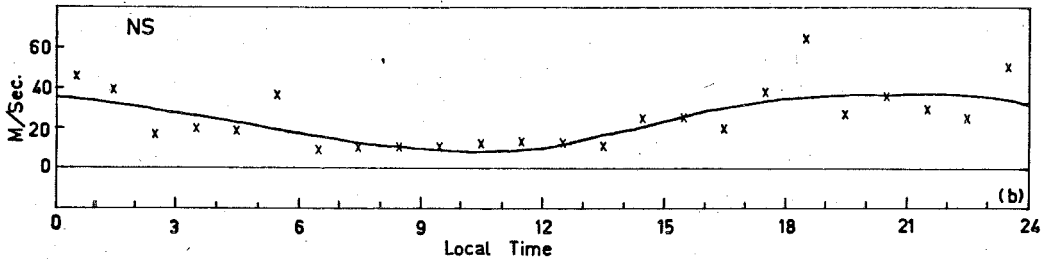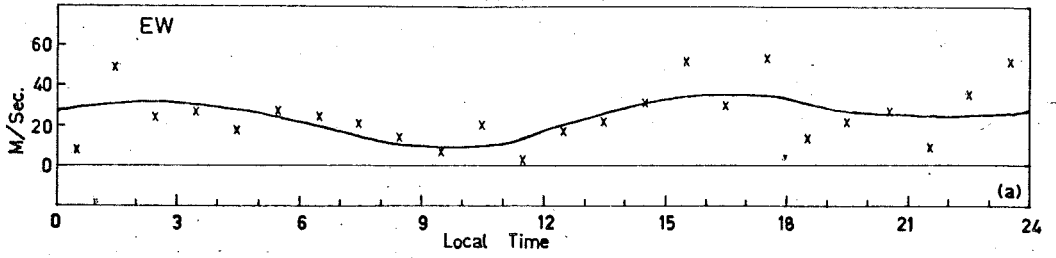
FIG. 53

a,b RMS TURBULENT VELOCITIES
c,d MEAN WINDS, 85-94 KM.

JUNE 1961
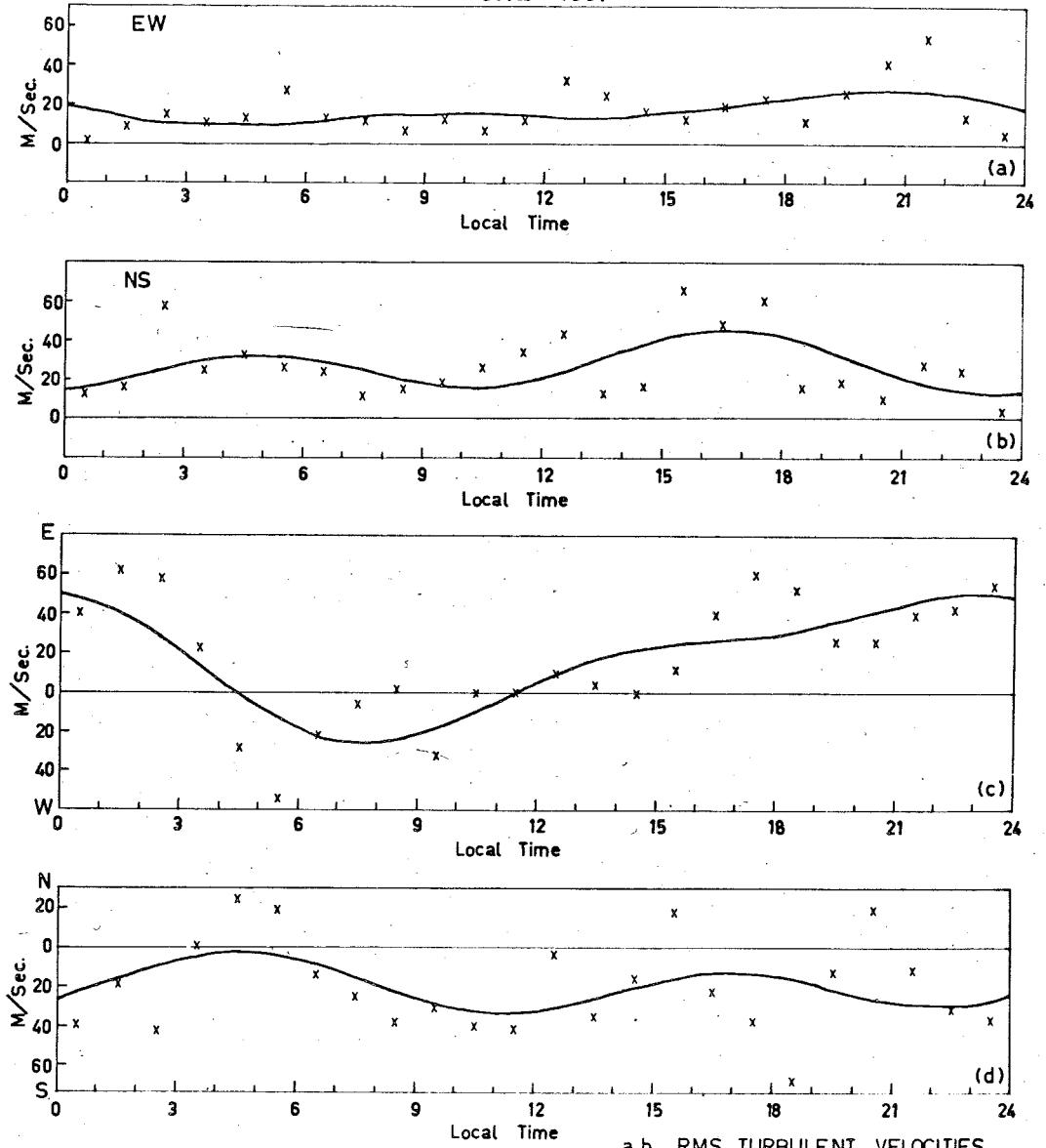
FIG. 54

a,b RMS TURBULENT VELOCITIES
c,d MEAN WIND, 85-94 KM.

JULY 1961
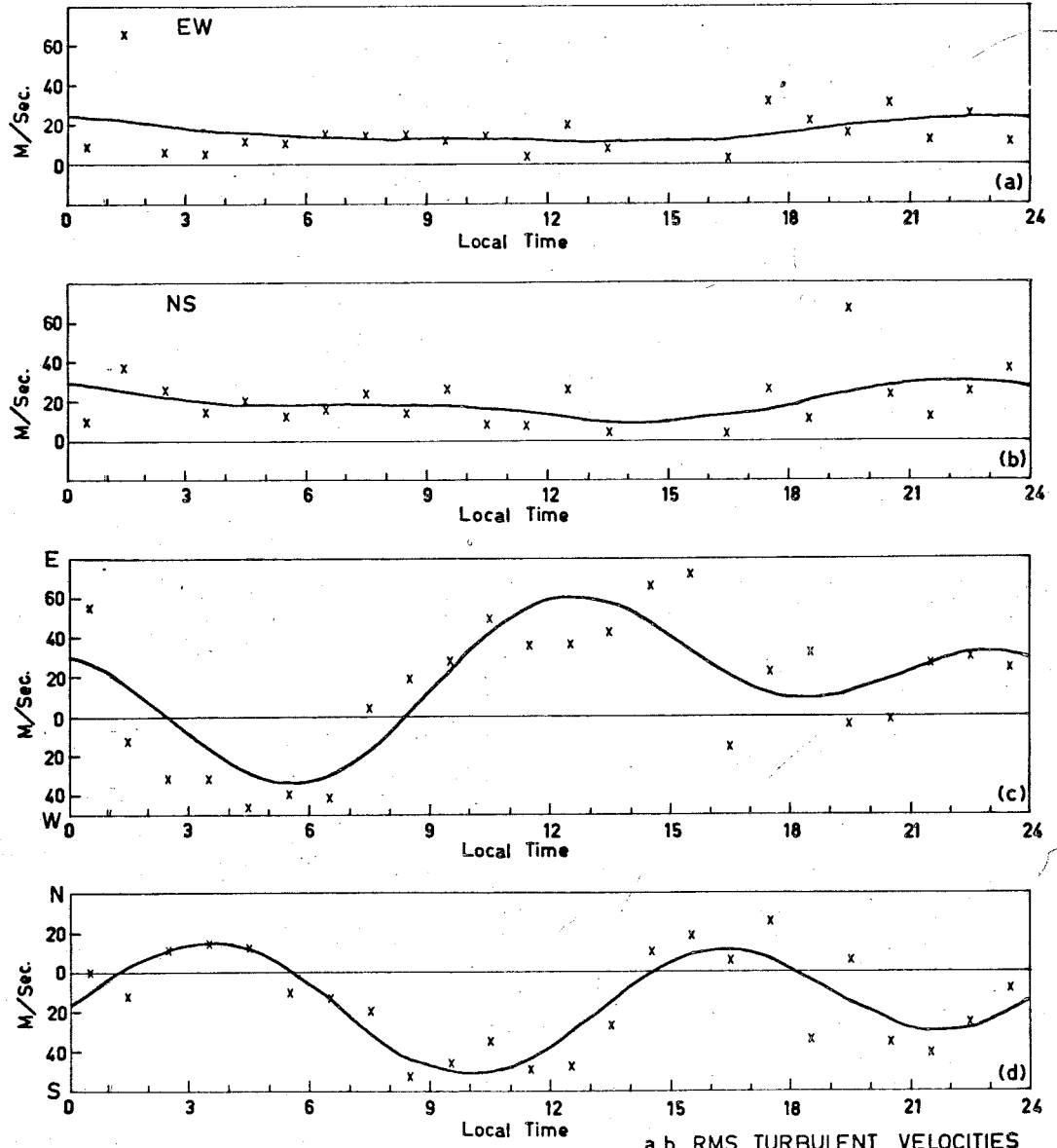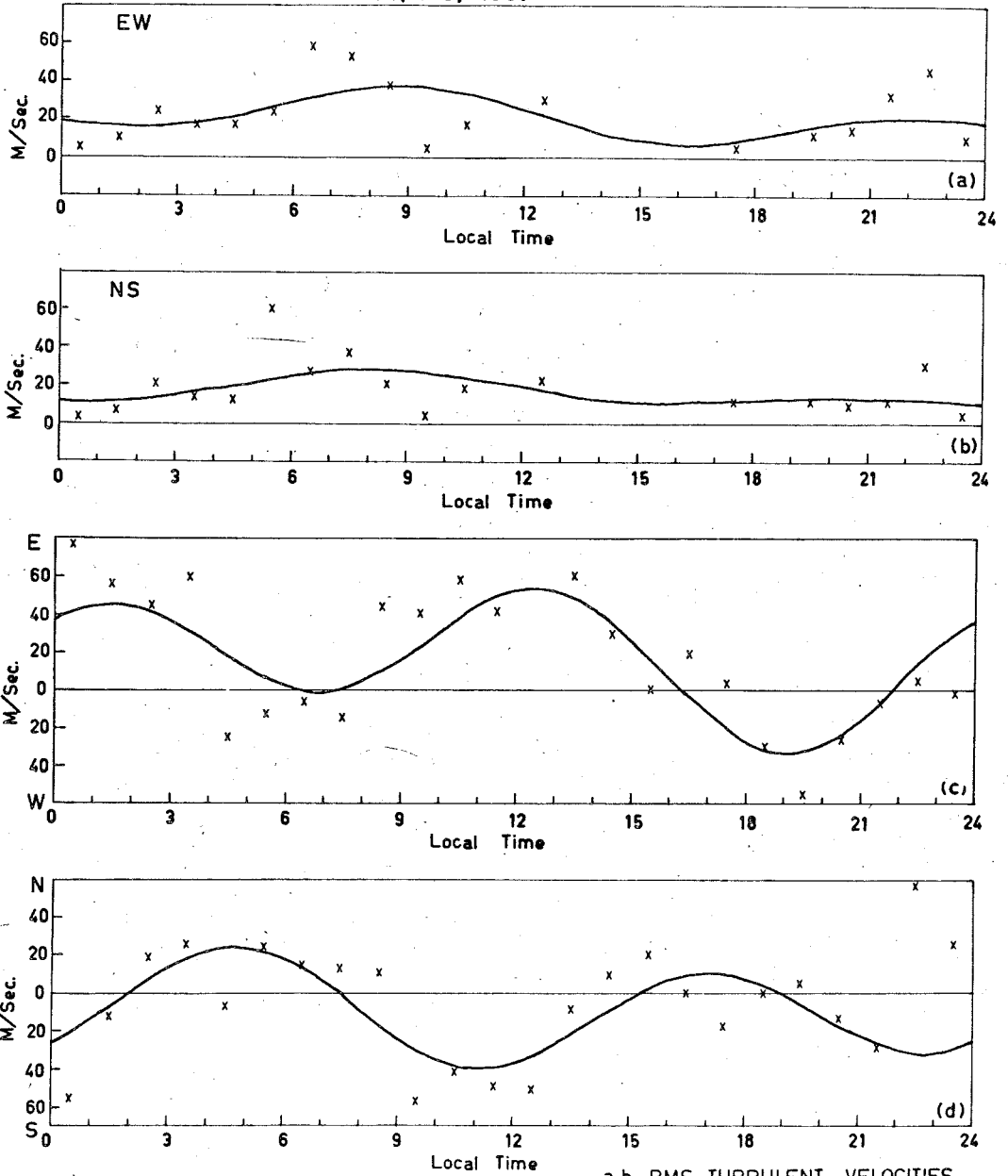
FIG. 55   a,b RMS TURBULENT VELOCITIES
           c,d MEAN WIND, 85-94 KM.

AUGUST, 1-6, 1961

(a) EW

(b) NS

(c)

(d)

a,b RMS TURBULENT VELOCITIES
c,d MEAN WIND, 85-94 KM.

FIG.56

AUGUST, 17 - 24, 1961
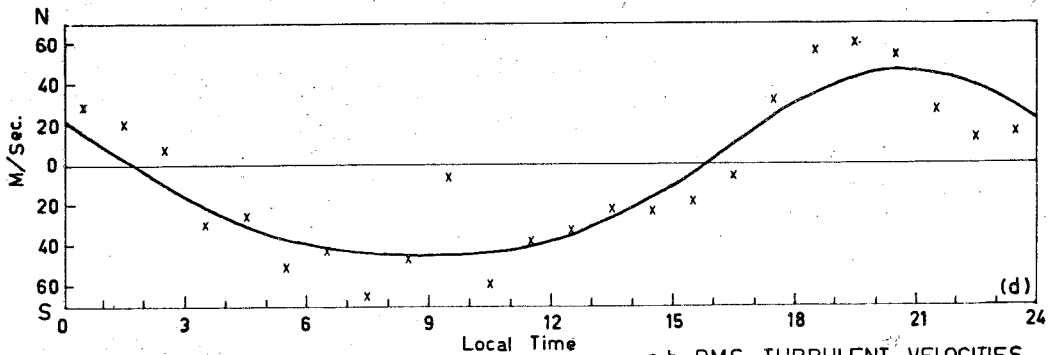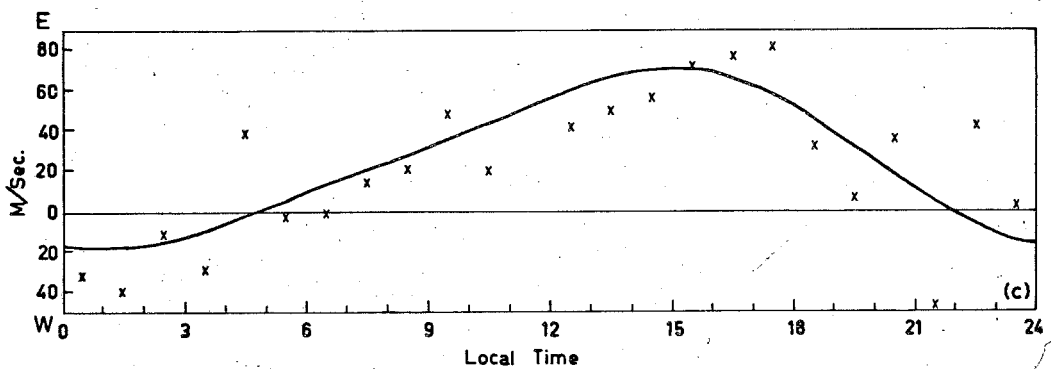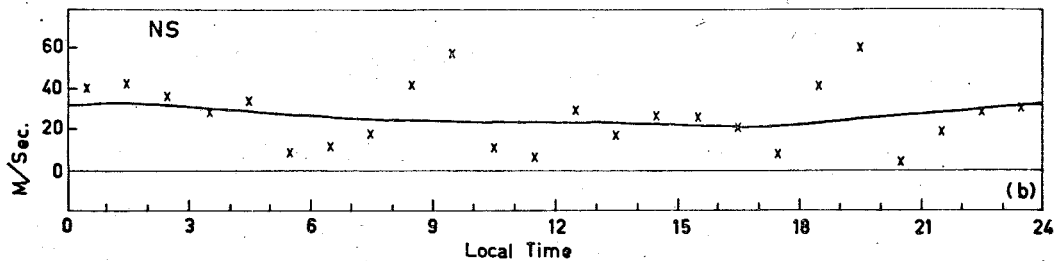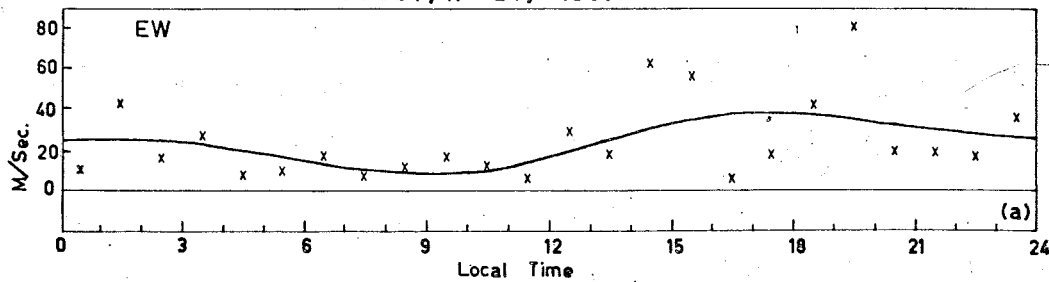
FIG.57

a,b RMS TURBULENT VELOCITIES
c,d MEAN WIND, 85-94KM.
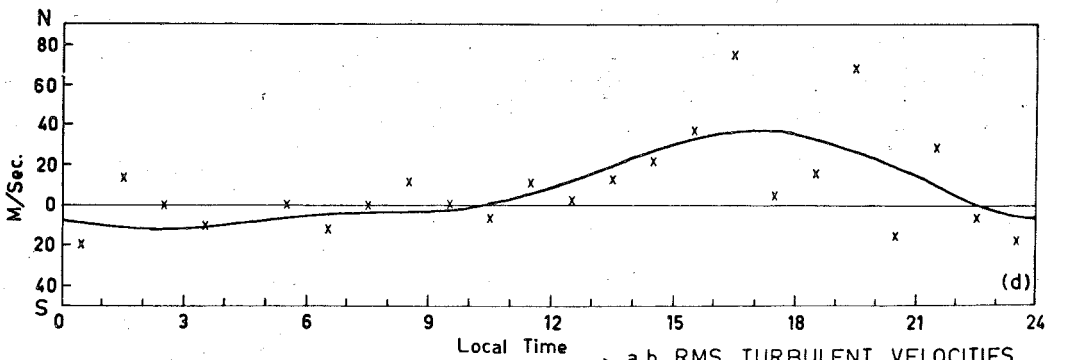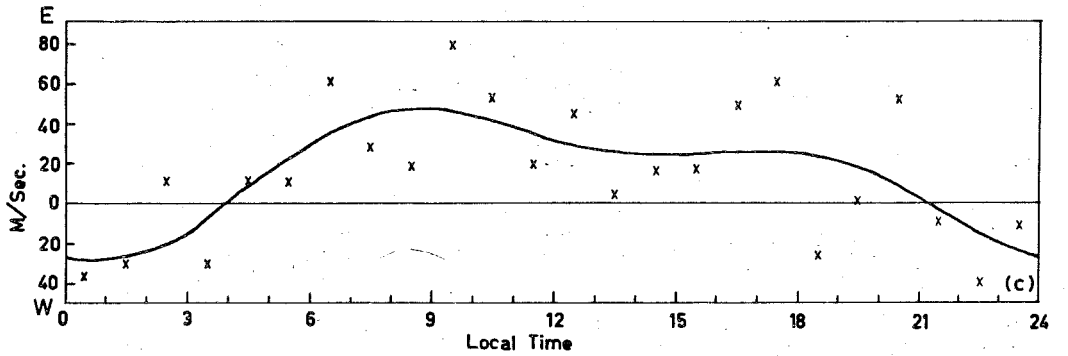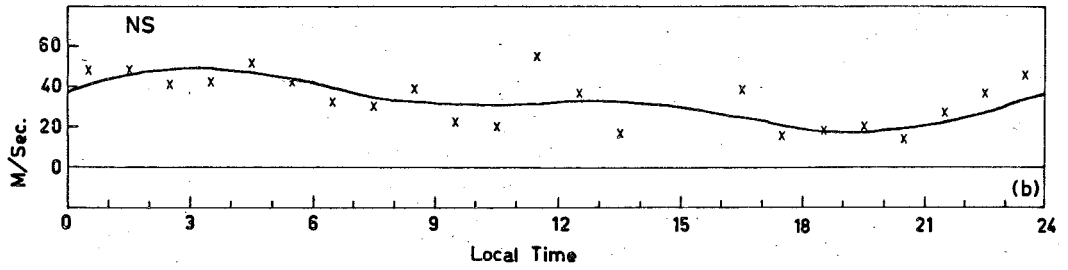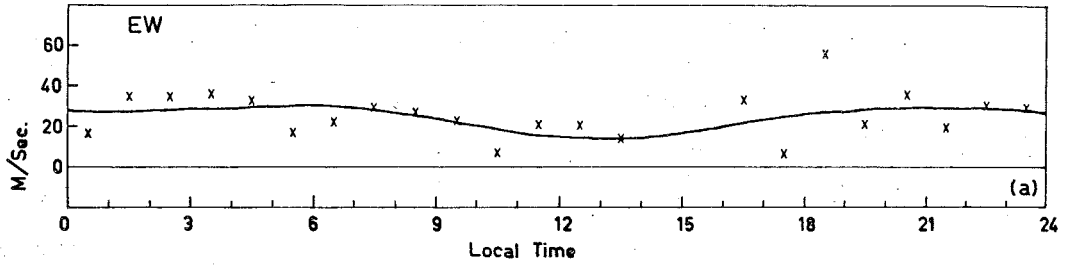
SEPTEMBER 1961

a,b RMS TURBULENT VELOCITIES
c,d MEAN WIND, 85-94 KM.

FIG. 58

DECEMBER 1961
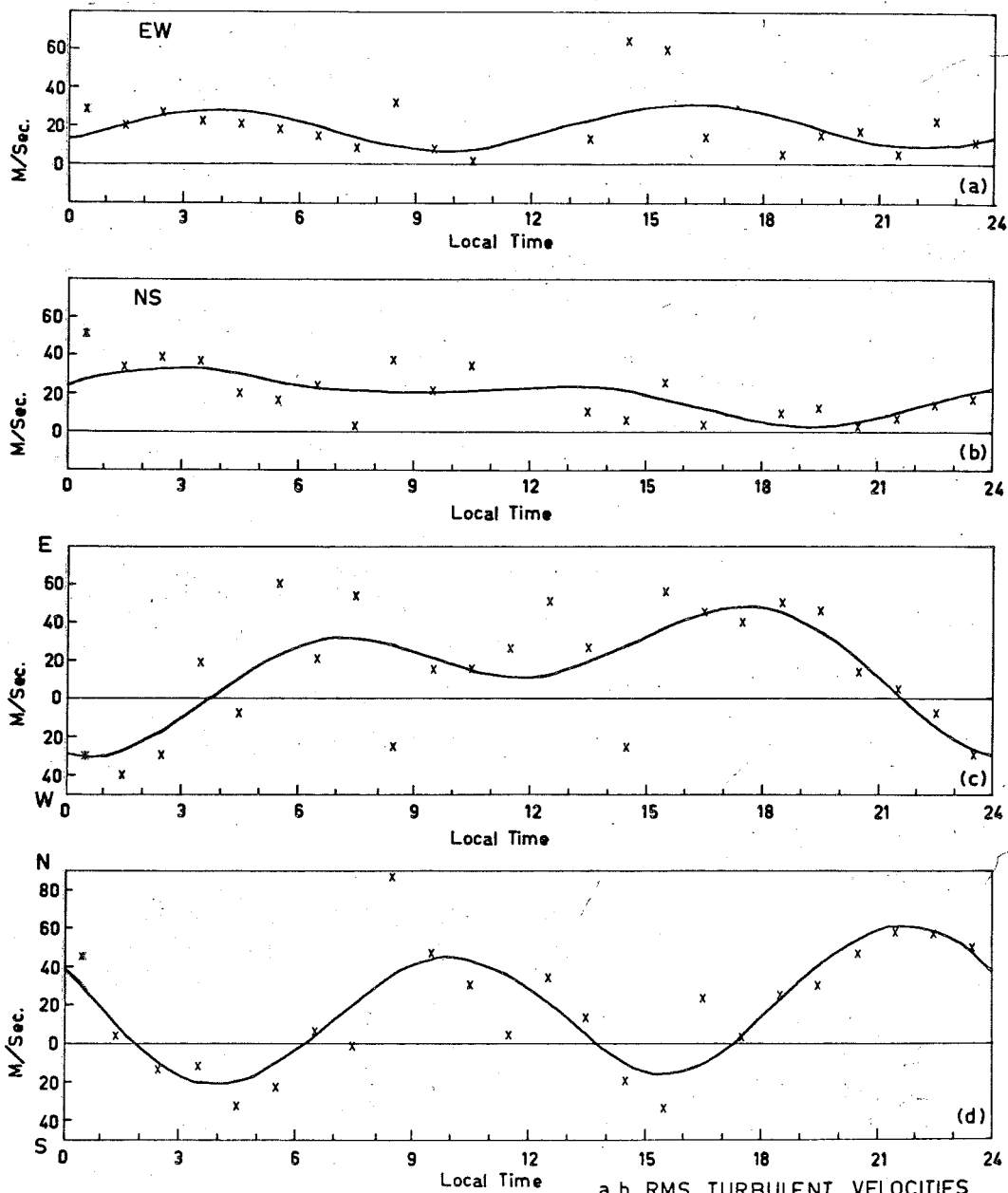
FIG. 59

a,b RMS TURBULENT VELOCITIES
c,d MEAN WIND, 85-94 KM.

10.5 Summary of the Seasonal Variations of the Parameters Specifying the Turbulent Flow Field.

A summary of the parameters of the turbulent flow field as determined for each month of the survey is given in Table I, under the following headings;

ϵ Turbulent dissipation rate, ergs/gm/sec.

U_0 Characteristic velocity of the energy bearing eddies, metres/sec.

L_0 Characteristic scale of the energy bearing eddies, km.

U_z RMS vertical velocity, metres/sec.

L_z Vertical correlation distance, km.

L_β Characteristic scale of the buoyancy subrange, metres.

T_{max} Maximum observed rate of reflection point motion along meteor trail, km/sec.

T_{rms} RMS value of

T_{mean} Arithmetic mean of

ς_{grad} RMS velocity difference across 1km of trail, m/sec/km.

Δh_{grad} RMS vel. difference across 1km height diff., m/sec/km.

λ Characteristic dissipation length associated with the energy bearing eddies, km.

R_λ Turbulence Reynolds number.

N No. of meteors observed during each month.

TABLE I

	ϵ	U_o	L_o	U_z	L_z	L_β	T_{max}	T_{rms}	T_{mean}	ξ_{grad}	Δh_{grad}	λ	R_λ	N
DEC 60	300	25	95	10	6.7	600	-3.2	0.70	0.05	5.6	7.1	1.6	4.2×10^3	104
JAN 61	365						-2.3	0.66	-0.04	5.8				88
FEB 61	450						-6.9	0.98	-0.00	6.4				77
MAR 61	600	30	66	13	6.8	900	-7.1	0.81	-0.09	7.0	8.6	1.5	4.6×10^3	116
APL 61	350						4.6	0.71	0.13	5.8				56
MAY 61	276						5.0	0.68	-0.00	5.4				169
JN 61	309	27	111	10	6.8	700	2.6	0.61	0.00	5.6	7.5	1.9	5.1×10^3	145
JY 61	416	23	50	12	5.4	600	4.3	0.66	0.00	6.2	7.4	1.4	3.2×10^3	194
A(1-6)	530	33	121	12	8.1	800	3.4	0.74	0.00	6.7	7.8	1.9	6.3×10^3	80
(17-24)	750	35	95	14	7.6	900	-7.3	0.85	0.04	7.5	9.0	1.5	5.1×10^3	124
SEP 61	642	40	177	13	8.9	1km	-4.6	0.83	-0.06	7.2	9.0	1.9	7.6×10^3	219
OCT 61	422						-3.1	0.73	-0.06	6.2				164
NOV 61	362						-2.1	0.63	-0.08	5.8				95
DEC 61	411	26	76	11	6.1	650	-4.0	0.74	-0.08	6.1	7.7	1.5	3.9×10^3	107

CHAPTER XI.

Atmospheric Turbulence at Meteor Heights

11.1   The Energy Bearing Eddies.

It has been shown in Chapters IX and X that the magnitude of the atmospheric turbulence encountered in the meteor region is time dependent; diurnal as well as seasonal variations are quite marked.   While no direct observations have been made of the large scale turbulent motions, other than the determination of their characteristic velocities, their properties as predicted by extrapolation from the smaller scales are in good agreement with the observations made at Jodrell Bank.   The observed monthly averages of the characteristic velocities of these eddies range from 20 m/sec. to 40 m/sec., and their predicted horizontal scales from some 60km to 200km; during individual months characteristic velocities as low as 15 m/sec. and as high as 60 m/sec. have been measured.

The vertical scale of these eddies has been predicted by extrapolation.   The vertical correlation distance of 7km thus determined is the same as that found from other radio and

photographic observations of meteor trails, and also from
the results of rocket experiments.

Whereas the large scale eddies have been shown to be a
possible extension of the inertial subrange, their relation-
ship to the mean flow at meteor heights has not been clearly
established. These large scale motions may have as their
origin some type of gravity wave, as has been proposed by
Hines (1959) and Long (1959). Gossard (1962) has established
that there is a mechanism whereby an upward escape of energy
from the turbulent motions in the troposphere is possible,
and that the gravity wave thus propagated will produce in the
meteor region anisotropic "eddies" of the scale and velocity
observed. However, there is some doubt that this energy loss
from the troposphere is of a continuous nature, as would be
required to sustain the always observable turbulence in the
meteor region.

11.2   The Small Scale Structure.

The turbulence investigation at Adelaide has concen-
trated particularly on scales less than 3km, since the eddies
in this range have, in the past, been the subject of consid-
erable controversy. It has been shown that the theories of
homogeneous turbulence can be successfully applied to the
data obtained from the radio echo observations of meteors,
and that these results can be reconciled with the photographic

meteor and rocket results by assuming the presence of what
has been termed a buoyancy subrange of eddy scales. The ex-
istence of such a subrange was first proposed by Bolgiano in
1959; his theory as applied by Dougherty (1961) to Greenhow's
results, however, produced a range of scales less than 100
metres and did nothing to resolve the difficulties associated
with the interpretation and reconciliation of radio and
photographic observations. The approach adopted in Chapter
IX Section 4 predicts that the characteristic eddy of the
buoyancy subrange at 95km is simply given by

$$L_B = 25 U_0 \qquad\qquad (9.4.1)$$

where U_0 is the characteristic velocity of the energy
bearing eddies of the Kolmogoroff turbulence spectrum. Since
U_0 varies from some 15 m/sec. to 60 m/sec., then

$$400 \text{ metres} < L_B < 1.5\text{km},$$

which is of the right scale to qualitatively explain the
small scale anomaly.

An interesting comparison can be made with the results
obtained by Rofe from rocket borne grenades (see Chapter III
Section 6). The size of the "cells" responsible for the
vertical fluctuations observed has been given by Rofe as 500
metres at 90km and 1km at 100km. If Rofe's "cells" are the
characteristic eddies of the buoyancy subrange, then according
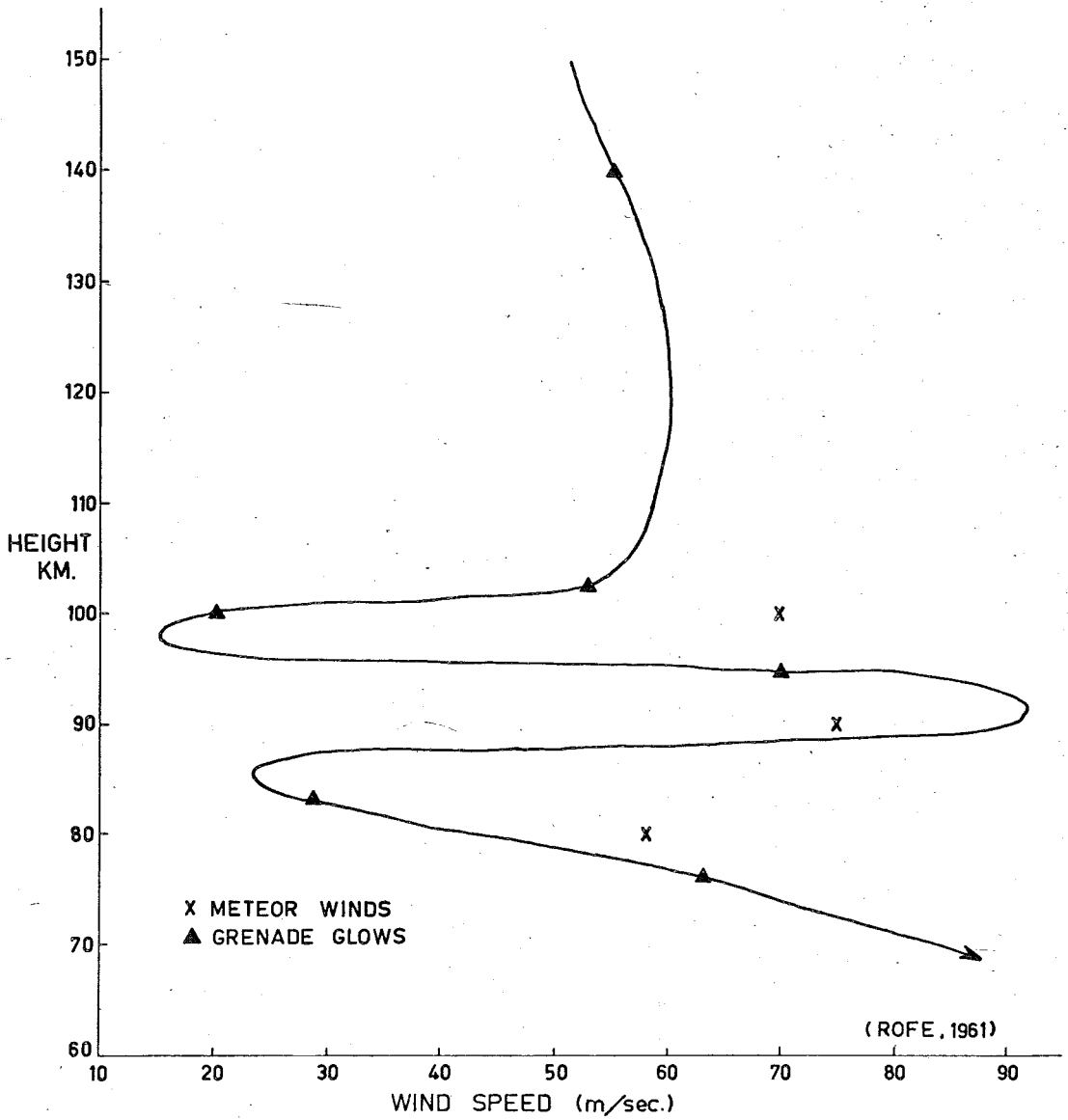
FIG. 60 - WIND SPEED PROFILE. WOOMERA, 17.11.60

to 9.4.1, they would be expected to be associated with turbulent winds of 20 m/sec. and 40 m/sec. respectively. The random wind components at the time of the firing from which Rofe's values are derived can be roughly estimated from Fig. 60 as the deviation of the measured windspeed profile from the mean wind determined by the meteor method. The relevant turbulent velocities are 15 m/sec. and 50 m/sec. The agreement with the predicted values is surprisingly good.

11.3   The Isotropic Inertial Region.

Once allowance is made for the buoyancy subrange, the velocity differentials closely follow the Kolmogoroff isotropic inertial spectrum up to the 3km separation limit imposed by the three station geometry. Since the extrapolation of this spectrum to 6km gives the observed RMS vertical velocity (Chapter IX Section 6) one would expect the isotropic inertial region to extend out to this scale. This is confirmed by the behaviour of the height correlation of Greenhow and Neufeld as treated in Chapter III Section 2, and by the results of Blamont and De Jager as revised by Zimmerman (Chapter III Section 7).

11.4   The Height Shear.

The velocity shear with height is one of the most interesting properties of the meteor region. The vertical correlation distance has been established almost conclusively as

being 6 to 7km. The most unusual feature of this correlation distance is the fact that it appears to define an actual, stable stratification of the region. Evidence of this comes from the high power pulse soundings of the lower ionosphere by Gregory (1961), who has shown that the maximum fluctuations in the electron density profile in the 55km to 95km region occur throughout the year at preferred heights approximately 10km apart, with the greatest fluctuation located at 80km. The reason for the stability of this stratification is as yet unknown.

The rocket investigations carried out by Rofe and others show a turbulence cutoff at just over 100km, which is probably due to the rapid increase in the kinematic viscosity above this level. Whitehead (1961) has explained the stratified nature of sporadic E ionization in terms of the occasional extension into the E region of the turbulent motions observed at meteor heights. Unfortunately, because of the rapid diffusion of meteor trails above 100km, no data pertaining to atmospheric motions at these heights is available from the Adelaide turbulence survey of 1961.

11.5 The Turbulent Dissipation Energy ϵ.

In the dimensionally derived expression for the turbulent energy spectrum of the inertial subrange, viz.

$$E(\kappa) = \alpha \epsilon^{\frac{2}{3}} \kappa^{-\frac{5}{3}} \qquad (2.6.5)$$

the value of α has been taken as $\frac{2}{3}$ (see Chapter II, Section 6). This leads via the velocity difference/separation relation of 2.10.3 to values for the turbulent dissipation rate ϵ of from 300 to 600 ergs/gm/sec, with an average for the thirteen months December 1960 to December 1961 of 430 ergs/gm/sec (Chapter X Section 2).

Since the completion of the main body of this work, an alternative expression for ϵ has been derived from the two equations defining the characteristic eddy of the buoyancy subrange contained in Chapter II (Section 12) and Chapter IX (Section 4), viz.

$$ Ri^* = \left[\frac{L_\beta}{\lambda} \right]^2 \frac{g}{T} \left[\frac{dT}{dh} + \Gamma \right] \left[\frac{d\bar{v}}{dh} \right]^{-2}, \qquad (2.12.2) $$

and

$$ \tfrac{1}{2}U_o{}^2 = L_\beta{}^2 \frac{g}{T} \left[\frac{dT}{dh} + \Gamma \right] \qquad\qquad 11.5.1 $$

The expression 2.12.2 differs from that proposed by Blamont and De Jager in that the characteristic dissipation length λ has been substituted for the momentum mixing length.

Batchelor gives

$$ \epsilon = \frac{15\nu U_o{}^2}{\lambda^2} \qquad\qquad (2.7.1) $$

which yields

$$\lambda = \sqrt{\frac{15\nu}{\epsilon}} \, U_0 \qquad\qquad 11.5.2$$

For the characteristic eddy of the buoyancy subrange $Ri^* = 1$, and on substitution of 11.5.2 for λ in 2.12.2

$$L_\beta = \sqrt{\frac{15\nu}{\epsilon}} \, U_0 \left[\frac{g}{T} \left(\frac{dT}{dh} + \Gamma \right) \right]^{\frac{1}{2}} \frac{d\bar{v}}{dh} \qquad 11.5.3$$

Rearrangement of 11.5.1 gives

$$L_\beta = \frac{U_0}{\sqrt{2}} \left[\frac{g}{T} \left(\frac{dT}{dh} + \Gamma \right) \right]^{-\frac{1}{2}} \qquad 11.5.4$$

Equating 11.5.3 and 11.5.4 we have

$$\sqrt{\frac{15\nu}{\epsilon}} \, \frac{d\bar{v}}{dh} = \frac{1}{\sqrt{2}}$$

i.e.

$$\epsilon_z = 30\nu \left(\frac{d\bar{v}}{dh} \right)^2 \qquad\qquad 11.5.5$$

Since the height gradient is not linear, but follows the 4/3 power law of a turbulence subjected to shear (Chapter X Section 3) the expression 11.5.5 cannot be regarded as providing an absolute value for ϵ. The equation also relies on the existence of a buoyancy subrange. However, substitution of actual values does lead to some interesting results. Since the scale of the buoyancy subrange

averages approximately 700 metres, the gradient is taken as
the velocity differential across this height difference. The
average gradient measured across a height difference of 700
metres for the 13 months Dec. 1960 to Dec. 1961 is 9 metres/
sec/km. The average echo height for the survey was 95km, at
which height the kinematic viscosity is 10^5 cm^2/sec.

Thus

$$\epsilon_{z(av)} = 30 \times 10^5 \times (9 \times 10^{-3})^2$$
$$= 240 \text{ ergs/gm/sec.}$$

If the α of 2.6.5 is taken as 1.0 instead of $\frac{2}{3}$, substitu-
tion of the measured data in equation 2.10.3 leads to an
average dissipation rate for the year of

$$\epsilon_{(av)} = 270 \text{ ergs/gm/sec.}$$

The revised seasonal variation of the turbulent dissipa-
tion rate for the thirteen months of the Adelaide survey is
presented in Fig. 61a. This plot has been produced by a more
refined weighted mean velocity difference programme using the
value $\alpha = 1.0$. The characteristics of the seasonal variation
presented in Fig. 45 remain, but the turbulent dissipation
rates for the low echo rate months have undergone some
modification.

Also plotted are the values of ϵ_z determined from the
height shear across the scale characteristic of the buoyancy
subrange for each month. With the exception of the values of

turbulent dissipation calculated for March and August 1st to 6th the seasonal variation follows a similar, although somewhat smoother, pattern. The comparison with the mean wind components of Fig. 61b serves to further substantiate the correlation between the turbulent dissipation rate and the 24 hour component of the mean wind at 90km.

A programme is being developed to determine an average mean wind speed weighted towards the high rate hours for the typical day of each month. Comparison of the seasonal variation of this wind speed with that of the turbulent dissipation rate should settle the question of whether or not the turbulent energy has its source in the mean flow.

Table II presents the revised parameters associated with the turbulent flow fields for each month.

11.6   The Reynolds Number R_λ:

The investigation of the significance of the variation in Reynolds Number is proceeding. However, the median value of 7×10^3 is considered to be as good an estimate as any yet proposed for this region of the atmosphere.

Note re Fig. 61b :- The magnitudes of the 24 and 12 hour components have been taken as the average of the respective hour by hour values,* not as the RMS of the maximum and minimum values, as was done in Fig. 45b.
*magnitudes
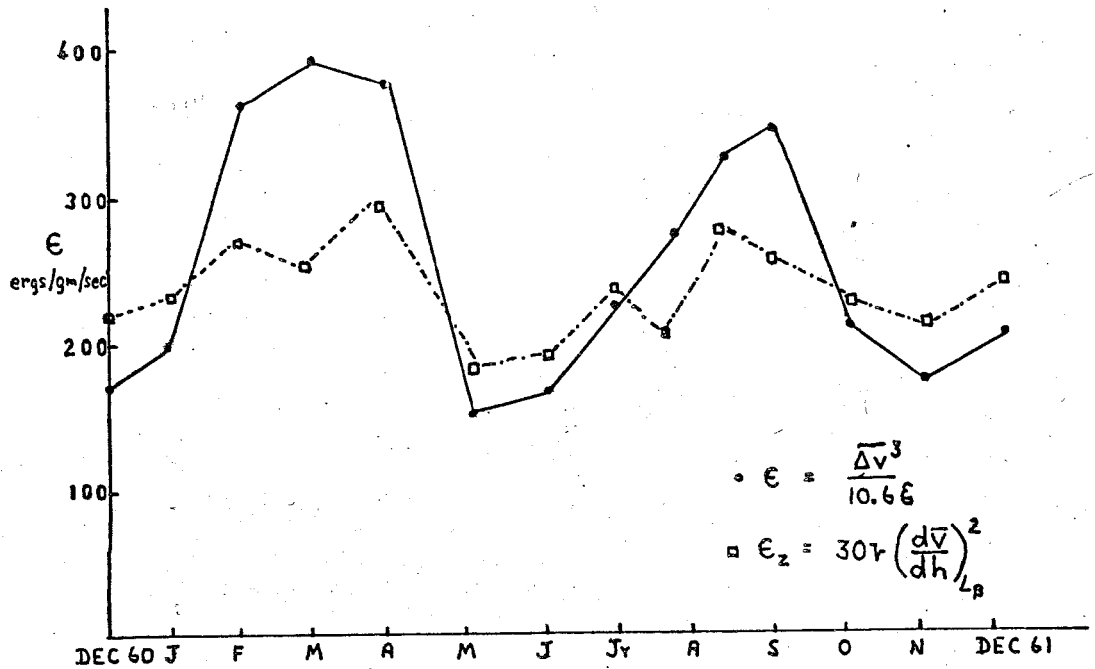
FIG. 61a SEASONAL VARIATION OF THE TURBULENT DISSIPATION RATE AT 90 KM
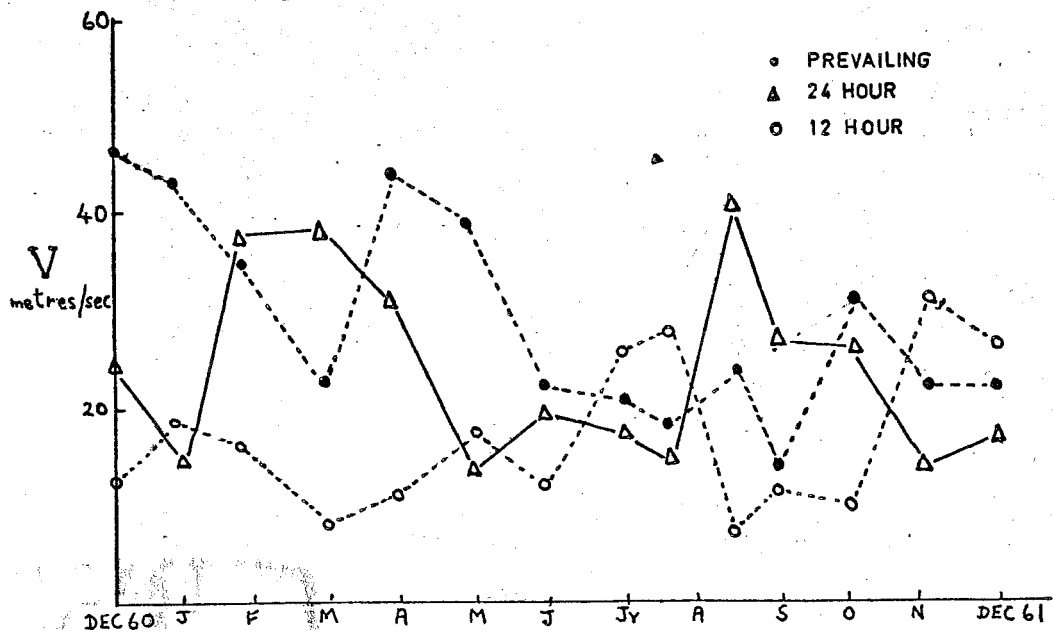
FIG. 61b COMPONENTS OF THE MEAN WIND, 85-94 KM

TABLE II

	ϵ	U_o	L_o	U_z	L_z	L_β	T_{max}	T_{rms}	T_{mean}	ξ_{grad}	Δh_{grad}	λ	R_λ	N
DEC 60	180	26	92	9	6.8	670	-3.2	0.70	0.05	5.6	7.2	2.1	5.2×10^3	104
JAN 61	200	36	230	10	9.0	950	2.0	0.65	0.02	5.8	8.4	3.2	1.1×10^4	88
FEB 61	360	30	74	11	6.1	790	-6.6	0.99	0.09	7.1	9.0	2.0	6.0×10^3	77
MAR 61	398	31	70	12	6.8	800	-6.6	0.79	-0.05	7.3	8.5	1.9	5.9×10^3	113
APL 61	363	28	55	10	5.4	720	4.6	0.75	0.12	7.1	8.9	1.8	4.9×10^3	57
MAY 61	160	29	145	9	7.8	760	5.0	0.69	0.00	5.4	7.3	2.8	8.2×10^3	169
JUN 61	187	27	99	9	6.8	700	2.6	0.61	0.00	5.7	7.4	2.4	6.5×10^3	145
JLY 61	242	23	47	9	5.0	590	4.3	0.66	0.00	6.2	7.7	1.8	4.1×10^3	194
A(1-6)	286	33	120	11	8.3	860	3.4	0.74	0.00	6.6	8.0	2.4	8.0×10^3	80
(17-24)	326	34	118	11	6.9	890	-7.3	0.85	0.04	6.9	9.4	2.3	8.1×10^3	124
SEP 61	345	40	177	12	8.5	1km	-4.6	0.83	-0.06	7.0	9.5	2.6	1.0×10^4	219
OCT 61	207	32	145	10	7.8	820	-3.3	0.71	-0.04	5.9	7.9	2.7	8.5×10^3	164
NOV 61	174	27	102	9	6.8	690	2.2	0.64	-0.05	5.6	7.3	2.5	6.6×10^3	95
DEC 61	214	26	78	9	5.9	680	-4.0	0.74	-0.08	6.0	7.9	2.2	5.7×10^3	107

Legend as for Table I, P178.

The Future

As presented in the foregoing chapters, the treatment of the data obtained from the 1961 survey is by no means exhaustive. An attempt has been made to overcome the fundamental difficulty of ascribing absolute values to the turbulent dissipation rate, but this relies heavily on the existence of the proposed buoyancy subrange. A correlation analysis which endeavours to derive the characteristic scale of the buoyancy subrange from the measured velocity shears is proceeding. However, the rocket borne grenade experiment would seem to be the best for direct observation of the buoyancy subrange, and analysis of more data from this source could prove profitable.

As has been mentioned in Chapter IV Section 5 the decay time of meteor echoes can be used to measure the coefficient of ambipolar diffusion at meteor heights. Such measurements of diffusion coefficient show considerable scatter which, to date, has not been explained satisfactorily. Pressure fluctuations arising from the turbulent shears could contribute to this scatter.

An attempt is being made to apply the Hines/Long theory of gravitational waves to the motions observed during the 1961 survey. The energy spectrum predicted by Hines is generally similar to that observed, but the discrepancies are more readily explicable in terms of the Kolmogoroff spectrum

modified by the influence of shearing and buoyancy forces.

A further investigation of the random motions at these heights is contemplated, using much higher transmitter power. A pulsed transmitter with a measured peak power output of 40KW has already been built, and a 1.5KW CW transmitter is in the process of construction. At this power level, the echo rate will be several times higher than that of the 1961 survey; this should enable several velocity difference/separation histograms to be produced each "typical" day, and provide further insight into the diurnal variations of the turbulence parameters.

The use of highly directive antennae is also contemplated, since these will allow direct measurement of the time constant of the energy bearing eddies and simultaneous spacial correlations to be determined. It is proposed to incorporate a fourth station at much greater separation to verify the isotropy of the eddies of scale 6 to 7km. The results obtained from this project should also determine whether or not the seasonal change in the vertical scale is significant.

The fact that the mean flow is latitude dependent has been established by simultaneous observations using the meteor method carried out at Mawson (68° S), Adelaide (35° S) and Jodrell Bank (53° N). Three-station measurements have also been made at Jodrell Bank, but not on a seasonal basis.

Under the Harvard Meteor Project a multi-station orbit survey is in progress, but unfortunately no provision has been made for wind measurement.   Several multi-station experiments carried out simultaneously at different latitudes would significantly increase our knowledge of this very interesting region of the Upper Atmosphere.

APPENDIX   I

IBM 1620 FORTRAN programmes for Mean Wind Reduction.

List of input/output variables as they appear in

Programme 1190A.

ERORX, ERORC	Maximum allowable errors between traces as read from Mean Wind Film.
SCALE	Allows for camera and film reader optics in conversion of distance between adjacent doppler maxima to line of sight trail drift velocity
MY	Year
MO	Month
JO	Day
LH	Local time, hours
LM	Local time, mins
UR	Echo number
KM	Midpoint echo range (St. Kilda) as read from film
WAVE	Distance between adjacent doppler maxima

MA, MB, MC, LA, LB, LC, LD

	Distances measured between doppler maxima on the DF traces, subsequently used in the direction finding routine.
ML	Checks that input data is of the correct format.

LHLM   Local time, hours and mins

EL, EM   Direction cosines of reflection point from

St. Kilda, Adelaide-St. K as Y axis.

EL3, EM3   Midpoint direction cosines, including aerial

corrections and rotation to NS-EW axes

KHT   Echo height, km.

LEVEL   Height group, 1   75-84km

                                    2   85-94km

                                    3   95-104km

LT   Local mean solar time, hours

NFL   EW drift responsible for line of sight

component

NFM   NS ditto.

MVEL, VEL   Measured line of sight drift velocity

MCS, MX   Errors involved in determination of EL, EM

This is the first of three programmes designed to convert
the data read from the mean wind recording display film to
a mean, diurnal and semidiurnal components of the wind at
meteor heights. Data is processed in monthly batches, and the
final result (output of 1190C) gives the winds for a
typical day of each month. This first programme involves
processing card by card, each input card producing one
output card.

```
C       1190A UNIVERSITY ADELAIDE ROPER 313
C       UPPER ATMOSPHERE WIND ANALYSIS,                  (METEOR GROU
P)
C       FILM READER DATA PROCESSOR, PUNCHES CARDS, PRINTS ERRORS

        READ270,ERORX,ERORC
  270 FORMAT(F4.2,F4.2)
        READ272,SCALE
  272 FORMAT(F6.0)
    8 READ11
   11 FORMAT(31H                                )
        PRINT11
  256 READ210,MY,MO,JO,LH,LM,UR,KM,WAVE,MA,MB,MC,MD,LA,LB,LC,L
D,ML
  210 FORMAT(I2,I3,I3,I3,I2,F6.0,I4,F5.0,I4,I4,I4,I4,I4,I4,I4
,I4,I2)
        LHLM=100*LH+LM
        IF(MO)301,10,262
   10 PRINT43
   43 FORMAT(41HLOAD MORE DATA, SET PAGE, THEN PUSH START)
        PAUSE
        GOTO8
  301 PRINT302
  302 FORMAT(1H 20HEND OF METEOR DATA  )
        STOP
  262 MB=MB+LA-LB
        MC=MC+LA-LC
        MD=MD+LA-LD
        A=MA
        B=MB
        C=MC
        D=MD
        VEL=SCALE/WAVE
        ALAMB=ABSF(WAVE)
        AL=A/ALAMB
        BL=B/ALAMB
        CL=C/ALAMB
        DL=D/ALAMB
  204 IF(AL-1.0)201,202,202
  202 AL=AL-1.0
        GOTO204
  201 IF(BL-1.0)205,203,203
  203 BL=BL-1.0
        GOTO201
  205 IF(CL-1.0)207,206,206
  206 CL=CL-1.0
        GOTO205
```

```
207 IF(DL-1.0)203,209,209
209 DL=DL-1.0
    GOTO207
203 CONTINUE
    IF(CL-DL)211,212,212
211 XL=1.0+CL-DL
    GOTO213
212 XL=CL-DL
213 CONTINUE
    MASS=VEL
    MVEL=VEL
    EL=-AL
    EM=-BL
    XLC=(EL/2.0)-(EM/2.0)+0.5
    NEXT=1
 99 NIX=0
    X=XL
    X1=XLC
    ELL=ERORX
100 CONTINUE
102 IF(X)101,103,104
101 X=X+1.0
    GOTO102
104 IF(X-1.0)103,103,105
105 X=X-1.0
    GOTO104
103 IF(X1)106,107,108
106 X1=X1+1.0
    GOTO103
108 IF(X1-1.0)107,107,109
109 X1=X1-1.0
    GOTO108
107 IF(ABSF(X-X1)-ELL)115,115,112
112 IF(ABSF(X-X1+1.0)-ELL)116,116,113
113 IF(ABSF(X-X1-1.0)-ELL)117,117,118
115 AMISS=X-X1
    GOTO110
116 AMISS=X-X1+1.0
    GOTO110
117 AMISS=X-X1-1.0
    GOTO110
118 AMISS=X-X1
    GOTO111
110 MZ=+1
    GOTO114
111 MZ=-1
114 AMISS=AMISS*100.0
```

```
      MISS=AMISS
      IF(NIX)499,499,50
  499 XL=X
      XLC=X1
      MXZ=MZ
      MX=MISS
      GOTO501
  500 CL=X
      CLC=X1
      MCZ=MZ
      MCS=MISS
  501 GOTO(214,219,229,237,243,251),NEXT
  214 NSTAT=1
      IF(MXZ)216,215,217
  216 EL=1.0-AL
      XLC=(EL/2.0)-(EM/2.0)+0.5
      NEXT=2
      GOTO99
  219 NSTAT=2
      IF(MXZ)218,215,221
  217 IF(MASS)224,215,225
  224 EL=AL
      EM=BL
      CLC=0.75-(1.25*EM)
      GOTO314
  225 CLC=(1.25*EM)+0.25
  314 NEXT=3
   98 NIX=1
      X=CL
      X1=CLC
      ELL=ERORC
      GOTO10
  229 NSTAT=3
      IF(MCZ)226,215,238
  226 IF(MASS)230,215,232
  230 EL=AL-1.0
      EM=BL-1.0
      CLC=0.75-(1.25*EM)
      GOTO313
  232 EL=1.0-AL
      EM=1.0-BL
      CLC=(1.25*EM)+0.25
  313 NEXT=4
      GOTO98
  237 NSTAT=4
      IF(MCZ)234,215,238
  221 IF(MASS)239,215,241
```

```
239 EL=AL-1.0
    EM=BL
    CLC=0.75-(1.25*EM)
    GOTO242
241 EL=1.0-AL
    EM=-BL
    CLC=(1.25*EM)+0.25
242 NEXT=5
    GOTO98
243 NSTAT=5
    IF(MCZ)245,215,238
245 IF(MASS)247,215,249
247 EL=AL
    EM=BL-1.0
    CLC=0.75-(1.25*EM)
    GOTO250
249 EL=-AL
    EM=1.0-BL
    CLC=(1.25*EM)+0.25
250 NEXT=6
    GOTO98
251 NSTAT=6
    IF(MCZ)252,215,238
238 CONTINUE
    RANGE=KM
    EL1=EL+0.04
    EM1=EM
    ZENTH=(EL1**2)+(EM1**2)
    IF(0.95-ZENTH)312,255,255
255 CONTINUE
    EL2=EL1*(1.0-EM1*(5.725/RANGE))
    EM2=EM1+(1.0-EM1**2)*(5.725/RANGE)
    EL3=(EL2*0.9774)-(EM2*0.2115)
    EM3=(EL2*0.2115)+(EM2*0.9774)
    EN3=SQRTF(1.0-EL3**2-EM3**2)
    HITE=2.0*RANGE*EN3
    IF(LM-45)1,2,2
  1 LT=LH
    GOTO9
  2 LT=LH+1
  9 NSTAT=7
    IF(LT)215,3,4
  3 LT=LT+24
  4 KHT=HITE
    IF(KHT-75)220,12,12
 12 IF(KHT-85)14,15,15
 14 LEVEL=1
```

```
        GOTO13
   15   IF(KHT-95)16,17,17
     16 LEVEL=2
        GOTO13
     17 IF(KHT-105)18,220,220
     18 LEVEL=3
     13 EL2M2=EL3**2+EM3**2
        E2L2M=1.0/EL2M2
        FL=-(VEL*EL3*E2L2M)
        FM=-(VEL*EM3*E2L2M)
        NFL=FL+0.5
        NFM=FM+0.5
PUNCH306,UR,MY,MO,JO,LHLM,EL,EM,EL3,EM3,KHT,LEVEL,LT,NFL,NFM,M
VEL,MCS,MX
306 FORMAT(F7.0,I3,I3,I3,I5,F5.2,F5.2,F5.2,F5.2,I4,I3,I3,I5,I
5,I5,I3,I3)
        GOTO256
    215 PRINT273,UR,NSTAT,LHLM
    273 FORMAT(F7.0,16HFAULT FOR NSTAT=I3,8H, TIME =I5,4H HRS)
        GOTO256
    218 PRINT275,UR,LHLM
    275 FORMAT(F7.0,14HNO CHECK FOR X,8H, TIME =I5,4H HRS)
        GOTO256
    220 PRINT274,UR,KHT,LHLM
    274 FORMAT(F7.0,25HHEIGHT UNACCEPTABLE. HT =I4,10HKM, TIME
=I5,4H HRS)
        GOTO256
    234 PRINT280,UR,LHLM
    280 FORMAT(F7.0,20HNO CHECK FOR C,L1,M1,8H, TIME =I5,4H HRS)

        GOTO256
    252 PRINT285,UR,LHLM
    285 FORMAT(F7.0,20HNO CHECK FOR C,L2,M2,8H, TIME =I5,4H HRS)

        GOTO256
    312 PRINT286,UR,LHLM
    286 FORMAT(F7.0,1X20HL2+M2 EXCEEDS 0.95   ,8H, TIME =I5,4H HR
S)
        GOTO256
        END
```

Programme 1190B

The cards punched by 1190A are fed into this programme, and
processed to produce a least squares fit wind for each of
the 24 hours at each level. Prints output, and punches cards
for processing by 1190C.

VCOS(LEVEL,LT) EW component for LEVEL at time LT

VSIN(LEVEL,LT) NS ditto.

MNO(LEVEL,LT) Number of meteors used to determine above.

Programme 1190C

Performs a Fourier Analysis of the winds punched out by 1190B
to produce mean, diurnal and semidiurnal wind components for
both NS and EW directions.

NGO   Control indicating type of data following
YE(J)   EW wind component for hour J
YN(J)   NS ditto.
AE   Prevailing component
COEFE(1)   Amplitude of 24 hour component
COEFE(2)   Ditto for 12 hour
ALPHE(1)   Phase of 24 hour component
ALPHE(2)   Ditto for 12 hour
A1, A2   EW 24hr, 12hr component at given time T
B1, B2   NS ditto
Y   Amplitude of the mean wind at time T

```
C       1190B   UNIVERSITY ADELAIDE ROPER  313
C       UPPER ATMOSPHERE WIND ANALYSIS,                    (METEOR GRO
UP)
C       PROCESSES OUTPUT CARDS FROM 1190A TO PRODUCE WINDS (PRI
NTS OUTPUT)
        DIMENSIONSUMC2(3,24),SUMS2(3,24),SUMSC(3,24),SUMFL(3,24
)
        DIMENSIONSUMFM(3,24),MNO(3,24),VCOS(3,24),VSIN(3,24)
        READ4
    4 FORMAT(30H                                  )
        DO26LEVEL=1,3
        DO26LT=1,24
        SUMC2(LEVEL,LT)=0
        SUMS2(LEVEL,LT)=0
        SUMSC(LEVEL,LT)=0
        SUMFL(LEVEL,LT)=0
        SUMFM(LEVEL,LT)=0
   26   MNO(LEVEL,LT)=0
1READ306,UR,MY,MO,JO,LHLM,EL,EM,EL3,EM3,KHT,LEVEL,LT,NFL,NFM,
MVEL,MCS,MX
306 FORMAT(F7.0,I3,I3,I3,I5,F5.2,F5.2,F5.2,F5.2,I4,I3,I3,I5,I
5,I5,I3,I3)
        IF(UR)8,8,13
   13 EL2M2=EL3*EL3+EM3*EM3
        E2L2M=1.0/EL2M2
        FL=NFL
        FM=NFM
        C2=EL3*EL3*E2L2M
        S2=EM3*EM3*E2L2M
        SC=EL3*EM3*E2L2M
        SUMC2(LEVEL,LT)=SUMC2(LEVEL,LT)+C2
        SUMS2(LEVEL,LT)=SUMS2(LEVEL,LT)+S2
        SUMSC(LEVEL,LT)=SUMSC(LEVEL,LT)+SC
        SUMFL(LEVEL,LT)=SUMFL(LEVEL,LT)+FL
        SUMFM(LEVEL,LT)=SUMFM(LEVEL,LT)+FM
        MNO(LEVEL,LT)=MNO(LEVEL,LT)+1
        GOTO1
    8 DO27LEVEL=1,3
        PRINT2
    2 FORMAT(1X////44H SET PAGE FOR NEXT LEVEL,    THEN PUSH S
TART./)
        PAUSE
        PRINT4
        PRINT34
   34 FORMAT(1X////40H LT LEVEL VCOS EAST  VSIN NORTH   METEOR
S//)
```

```
      DO27LT=1,24
      IF(MNO(LEVEL,LT)-1)35,35,25
  25    P=1.0/((SUMSC(LEVEL,LT)**2)-(SUMC2(LEVEL,LT)*SUMS2(L
EVEL,LT)))
      VSIN(LEVEL,LT)=P*(SUMFL(LEVEL,LT)*SUMSC(LEVEL,LT))
      VSIN(LEVEL,LT)=VSIN(LEVEL,LT)-P*SUMFM(LEVEL,LT)*SUMC2(L
EVEL,LT)
      VCOS(LEVEL,LT)=P*SUMFM(LEVEL,LT)*SUMSC(LEVEL,LT)
      VCOS(LEVEL,LT)=VCOS(LEVEL,LT)-P*SUMFL(LEVEL,LT)*SUMS2(L
EVEL,LT)
      GOTO28
  35    VCOS(LEVEL,LT)=999.0
      VSIN(LEVEL,LT)=999.0
  28 PUNCH42,LT,LEVEL,VCOS(LEVEL,LT),VSIN(LEVEL,LT),MNO(LEVE
L,LT)
  27    PRINT42,LT,LEVEL,VCOS(LEVEL,LT),VSIN(LEVEL,LT),MNO(LEVE
L,LT)
  42 FORMAT(I4,I3,6XF5.0,5XF5.0,4XI4)
      STOP
      END
```

```
C      1190C  UNIVERSITY OF ADELAIDE  ROPER  313
C      FOURIER ANALYSIS,  24 POINT INPUT      MEAN PLUS 2 HARM
ONICS
       DIMENSIONYE(24),YN(24)
       DIMENSIONSE(12),DE(12),DIFE(10),SUME(4),COEFE(2),ALPHE(
2)
  100 READ101,NGO
  101 FORMAT(I6)
       IF(NGO)19,21,20
   19 STOP
   21 PRINT22
   22 FORMAT(25HNEW PAGE, THEN PUSH START)
       PAUSE
   20 READ 20
  200 FORMAT(38H                                          )
       DO201J=1,24
  201 READ202,LEVEL,YE(J),YN(J)
  202 FORMAT(4XI3,6XF5.0,5XF5.0)
       IF(LEVEL-2)1,2,3
    1 LOW=75
      LHI=84
      GOTO4
    2 LOW=85
      LHI=94
      GOTO4
    3 LOW=95
      LHI=104
    4 NEXT=0
      GO TO 30
   31 DO32J=1,24
   32 YE(J)=YN(J)
      NEXT=1
      PRINT22
      PAUSE
   30 PRINT5,LOW,LHI
    5 FORMAT(10X34HFOURIER ANALYSIS FOR HEIGHT RANGE I4,2H -I
4,3H KM)
      PRINT20
      DO6J=1,11
      K=J+12
      SE(J)=YE(J)+YE(K)
    6 DE(J)=YE(J)-YE(K)
      SE(12)=YE(24)+YE(12)
      DE(12)=YE(24)-YE(12)
      AE=0
      DO7J=1,12
```

```
    7 AE=AE+SE(J)
      AE=AE/24.
      DO8J=1,5
      K=12-J
      DIFE(J)=DE(J)-DE(K)
    8 DIFE(J+5)=DE(J)+DE(K)
      SUME(1)=SE(1)-SE(5)-SE(7)+SE(11)
      SUME(2)=SE(2)-SE(4)-SE(8)+SE(10)
      SUME(3)=SE(1)+SE(5)-SE(7)-SE(11)
      SUME(4)=SE(2)+SE(4)-SE(8)-SE(10)
      AE24=DE(12)+0.966*DIFE(1)+0.866*DIFE(2)+0.707*DIFE(3)+0
.5*DIFE(4)
      AE24=(AE24+0.259*DIFE(5))/12.
      BE24=DE(6)+0.259*DIFE(6)+0.5*DIFE(7)+0.707*DIFE(8)+0.86
6*DIFE(9)
      BE24=(BE24+0.966*DIFE(10))/12.
      AE12=(SE(12)-SE(6)+0.866*SUME(1)+0.5*SUME(2))/12.
      BE12=(SE(3)-SE(9)+0.5*SUME(3)+0.866*SUME(4))/12.
      COEFE(1)=SQRTF(AE24*AE24+BE24*BE24)
      COEFE(2)=SQRTF(AE12*AE12+BE12*BE12)
      ALPHE(1)=ATANF(ABSF(BE24/AE24))
      ALPHE(2)=ATANF(ABSF(BE12/AE12))
      PI=3.1416
      IF(AE24)40,40,41
   41 IF(BE24)43,43,42
   43 ALPHE(1)=2.*PI-ALPHE(1)
      GOTO42
   40 IF(BE24)44,44,45
   44 ALPHE(1)=ALPHE(1)+PI
      GOTO42
   45 ALPHE(1)=PI-ALPHE(1)
   42 IF(AE12)50,50,51
   51 IF(BE12)53,53,52
   53 ALPHE(2)=2.*PI-ALPHE(2)
      GOTO52
   50 IF(BE12)54,54,55
   54 ALPHE(2)=ALPHE(2)+PI
      GOTO52
   55 ALPHE(2)=PI-ALPHE(2)
   52 IF(NEXT)34,34,35
   34 PRINT11
   11 FORMAT(10X25HEAST-WEST WIND COMPONENTS//)
      GOTO36
   35 PRINT16
   16 FORMAT(10X27HNORTH-SOUTH WIND COMPONENTS//)
   36 PRINT9,AE
```

```
    9 FORMAT(10X3HY =F7.1)
      ALPHE(1)=ALPHE(1)*(12./PI)
      PRINT10,COEFE(1),ALPHE(1)
   10 FORMAT(13XF7.1,13H*COS(PI/12(T-F6.2,2H ))
      ALPHE(2)=ALPHE(2)*(6./PI)
      PRINT18,COEFE(2),ALPHE(2)
   18 FORMAT(13XF7.1,12H*COS(PI/6(T-F6.2,2H )///)
      PRINT12
   12 FORMAT(10X48HTIME A24COST B24SINT A12COS2T B12SIN2T MEA
 N    Y//)
      DO301J=1,24
      T=J
      A1=AE24*COSF((PI/12.)*T)
      B1=BE24*SINF((PI/12.)*T)
      A2=AE12*COSF((PI/6.)*T)
      B2=BE12*SINF((PI/6.)*T)
      Y=AE+A1+B1+A2+B2
  301 PRINT302,J,A1,B1,A2,B2,AE,Y
  302 FORMAT(10XI3,2XF6.1,2XF6.1,2XF6.1,3XF6.1,F7.1,F7.1)
      IF(NEXT)31,31,10
      END
```

APPENDIX   II

IBM FORTRAN programmes for the Turbulence Reduction.

Programme E5 200   (written in 7090 FORTRAN)

Reads output of Orbit Programme from tape, and punches data required for Turbulence Analysis.

NUMBRI	Echo number
MYEARI	Year
MONTHI	Month
JOURI	Day
LMSTHI	Local mean solar time, Hours
LMSTMI	Local mean solar time, Mins
IWAZ	Azimuth of reflection point from St. Kilda
IWZ	Zenith angle of ditto
IWH	Echo height
IRAZ	Azimuth of meteor radiant
IRZ	Zenith angle of ditto
IU(I)	Line of sight component of trail drift as observed from station I
IEPS1	Separation of reflection points, St. K to Sheedys farm
IEPS2	Ditto, St. Kilda to Direk
IRA	Right ascencion of meteor radiant
IDEC	Declination of ditto
IVEL	Velocity of the meteor particle

```
*      E5   200  UNIVERSITY OF ADELAIDE   ROPER  313
*      DATE 13/8/62
*      EXEQ TIME 19 MINS
*      XEQ
       DIMENSION JUMP(3),ITEM(3),MOVE(3),DEVN(3),VELOC(3),TIME
(3),
     1WIND(3),TOPHAS(3)
       DIMENSIONNUMBRI(1500),MYEARI(1500),MONTHI(1500),JOURI(
1500),
     1         LMSTMI(1500),IWAZ(1500),IWZ(1500),IWH(1500), IRAZ
(1500), IRZ
     2(1500),              IU(3,1500),IEPS1(1500),IEPS2(1500),L
MSTHI(1500)
       DIMENSIONIVEL(1500),IRA(1500),IDEC(1500)
       COMMONNUMBRI,MYEARI,MONTHI,JOURI
       PRINT1
    1 FORMAT(1X56H THIS PROGRAMME PUNCHES APPROXIMATELY 2000
OUTPUT CARD
     1S./1X60H LOAD UNI TAPE NILSSON NO. 2. ONTO B7. PUSH STA
RT WHEN REA
     2DY//////)
       PAUSE
       CALLDNSHI(17)
       REWIND17
       NSTART=7416
       NSTOP=76459
    2 I=0
    3 READ TAPE 17,NUMBR,MYEAR,MONTH,JOURA,LMSTH,LMSTM,JUMP,I
TEM,MOVE,
     1DEVN,VELC,VELOC,TIME,WH,SKIP,NWOP,WZ,WAZ,RZ,RAZ,EPS1,EP
S2,TLAM,
     2TMU,TLAM3,TMU3,RNEW,HAR,RA,DEC,VEL,DRAG,VGE,NQ,WIND,SMA
,E,EYE,AGP,
     3ANL,TAN,RLG,RLT,TLG,TLT,ALG,AEL,TEL,VHE,LENGTH,TOPHAS
       IF(NUMBR-NSTART)3,5,3
    4 READ TAPE 17,NUMBR,MYEAR,MONTH,JOURA,LMSTH,LMSTM,JUMP,I
TEM,MOVE,
     1DEVN,VELC,VELOC,TIME,WH,SKIP,NWOP,WZ,WAZ,RZ,RAZ,EPS1,EP
S2,TLAM,
     2TMU,TLAM3,TMU3,RNEW,HAR,RA,DEC,VEL,DRAG,VGE,NQ,WIND,SMA
,E,EYE,AGP,
     3ANL,TAN,RLG,RLT,TLG,TLT,ALG,AEL,TEL,VHE,LENGTH,TOPHAS
       IF(NUMBR-NSTOP)5,6,5
    5 I=I+1
       NUMBRI(I)=NUMBR
       MYEARI(I)=MYEAR
       MONTHI(I)=MONTH
```

```
      JOURI(I)=JOURA
      LMSTHI(I)=LMSTH
      LMSTMI(I)=LMSTM
      IWAZ(I)=WAZ+0.5
      IWZ(I)=WZ+0.5
      IWH(I)=WH+0.5
      IRAZ(I)=RAZ+0.5
      IRZ(I)=RZ+0.5
      IU(1,I)=WIND(1)
      IU(2,I)=WIND(2)
      IEPS1(I)=1000.0*EPS1
      IEPS2(I)=1000.0*EPS2
      IU(3,I)=WIND(3)
      IRA(I)=RA
      IDEC(I)=DEC+SIGNF(0.5,DEC)
      IVEL(I)=VEL+0.5
      GOTO4
    6 NI=I+1
      NUMBRI(I)=NUMBR
      MYEARI(I)=MYEAR
      MONTHI(I)=MONTH
      JOURI(I)=JOURA
      LMSTHI(I)=LMSTH
      LMSTMI(I)=LMSTM
      IWAZ(I)=WAZ+0.5
      IWZ(I)=WZ+0.5
      IWH(I)=WH+0.5
      IRAZ(I)=RAZ+0.5
      IRZ(I)=RZ+0.5
      IU(1,I)=WIND(1)
      IU(2,I)=WIND(2)
      IU(3,I)=WIND(3)
      IEPS1(I)=1000.0*EPS1
      IEPS2(I)=1000.0*EPS2
      IRA(I)=RA
      IDEC(I)=DEC+SIGNF(0.5,DEC)
      IVEL(I)=VEL+0.5
      DO7I=1,NI
    7 PUNCH8,NUMBRI(I),MYEARI(I),MONTHI(I),JOURI(I),LMSTHI(I)
,LMSTMI(I),
     1IWAZ(I),IWZ(I),IWH(I),IRAZ(I),IRZ(I),IU(1,I),IU(2,I),IU
(3,I),
     2IEPS1(I),IEPS2(I),IRA(I),IDEC(I),IVEL(I)
    8 FORMAT(1X15,4I3,I2,8I4,2I5,2I3,I4)
      N=N+1
      IF(N-2)10,9,11
```

```
10  NSTART=76734
    NSTOP=76448
    GOTO2
 9  NSTART=47363
    NSTOP=63666
    GOTO2
11  CALLEXIT
    END
```

```
C      1200   UNIVERSITY OF ADELAIDE   ROPER   313
C      PROCESSES OUTPUT 7090   200   TO PRODUCE INPUT FOR 1200A

C      CONVERTS LINE OF SIGHT AND RADIANT AZIMUTHS AND ZENITH
ANGLES TO
C      DIRECTION COSINES ( L, EAST.   M, NORTH.)
1READ8,UR,MY,MO,JO,LH,LM,WAZ,WZ,WH,RAZ,RZ,IU1,IU2,IU3,EPS1,EP
S2
   8 FORMAT(F6.0,4I3,I2,2F4.0,F4.0,2F4.0,3I4,2F5.3)
     IF(UR)3,4,5
   4 PRINT6
   6 FORMAT(9HMORE DATA)
     PAUSE
     GOTO1
   5 LTHM=100*LH+LM
     IWH=WH+0.5
     D1=11.45
     R=WH/COSF(WZ/57.3)
     RL=-SINF(WZ   /57.3)*SINF(WAZ   /57.3)
     RM=SINF(WZ   /57.3)*COSF(WAZ   /57.3)
     R1=SQRTF(R*R+D1*D1-2.0*RL*R*D1*0.2115+2.0*RM*R*D1*0.977
4)
     M3=1000.0*(RM*R+D1*0.9774)/R1
     L3=1000.0*(RL*R-D1*0.2115)/R1
     LR=-SINF(RZ/57.3)*SINF(RAZ/57.3)*1000.0
     MR=SINF(RZ/57.3)*COSF(RAZ/57.3)*1000.0
PUNCH9,UR,MY,MO,JO,LTHM,L3,M3,IWH,LR,MR,IU1,IU2,IU3,EPS1,EPS
2
   9 FORMAT(F7.0,3I3,I5,5I4,3I4,   2F6.3)
     GOTO1
   3 STOP
     END
```

212

```
C       1200A   UNIVERSITY OF ADELAIDE   PHYSICS DEPT.   ROPER   31
3
C       PROCESSES OUTPUT OF 1200 TO PUNCH INPUT TO 1200B
C       SUBTRACTS MEAN WIND COMPONENTS FROM MEASURED LINE OF SI
GHT DRIFTS
C       TO GIVE TURBULENT VELOCITIES.
C       REJECTS ECHOES WITH REFLECTION POINT HEIGHTS LYING OUTS
IDE THE
C       RANGE   74KM - 106KM.
C       INCORPORATES OPTIONAL PRINTOUT OF MEASURED AND MEAN WIN
DS OF
C       OPPOSITE SIGN.                    SWITCH 1 ON IGNORES PR
INT OUT
        DIMENSIONV(24),W(12)
        DIMENSIONVE1(24),VE2(24),VE3(24),VN1(24),VN2(24),VN3(24
)
        DIMENSIONH(3),DELH(3),X(3),U(3),UT(3),UMEAN(3)
     10 READ10
    100 FORMAT(48H
     )
        PRINT10
        DO49J=1,6
READ7,V(1),V(2),V(3),V(4),V(5),V(6),V(7),V(8),V(9),V(10),V(11
),V(12)
      7 FORMAT(12F4.0)
READ7,W(1),W(2),W(3),W(4),W(5),W(6),W(7),W(8),W(9),W(10),W(11
),W(12)
        DO48K=1,12
     48 V(K+12)=W(K)
        GOTO(30,31,32,33,34,35),J
     30 DO50K=1,24
     50VE1(K)=V(K)
        GOTO49
     31 DO51K=1,24
     51 VE2(K)=V(K)
        GOTO49
     32 DO52K=1,24
     52VE3(K)=V(K)
        GOTO49
     33 DO53K=1,24
     53 VN1(K)=V(K)
        GOTO49
     34 DO54K=1,24
     54 VN2(K)=V(K)
        GOTO49
     35 DO55K=1,24
     55 VN3(K)=V(K)
     49 CONTINUE
```

```
1READ2,UR,MY,MO,JO,LT,TL,TM,WH,RL,RM,U(1),U(2),U(3),X(1),X(2
)
      2 FORMAT(F7.0,3I3,I5,2F4.3,F4.0,2F4.3,3F4.0,2F6.3)
        IF(UR)3,4,5
      4 PRINT6
      6 FORMAT(9HMORE DATA)
        PAUSE
        GOTO10
      5 LTH=LT/10
        LTM=LT-LTH*10
        TN=SQRTF(1.0-TL*TL-TM*TM)
        RN=SQRTF(1.0-RL*RL-RM*RM)
        DO8K=1,3
      8 U(K)=-U(K)
        IR=WH/TN+0.5
        IH=WH+0.5
        M=LTH+1
        MP1=M+1
        IF(MP1-25)45,46,46
     46 MP1=1
     45 TIN=LTM
        TIN=TIN/60.0
        DELH(1)=-X(1)*RN
        DELH(2)=0
        DELH(3)=-X(2)*RN
        INUM=0
        K=1
     18 H(K)=WH+DELH(K)
        IF(H(K)-74.)75,72,72
     72 IF(H(K)-106.)73,73,75
     75 PRINT80,UR,H(K)
     80 FORMAT(F7.0,2X22HHEIGHT UNACCEPTABLE ATF6.0,3H KM)
        GOTO1
     73 IF(H(K)-90.)20,19,19
     19 VGE=(VE3(M)-VE2(M))*0.1
        VGE=VGE+(VE3(MP1)+VE2(M)-VE2(MP1)-VE3(M))*TIN*0.1
        VGN=(VN3(M)-VN2(M))*0.1
        VGN=VGN+(VN3(MP1)+VN2(M)-VN2(MP1)-VN3(M))*TIN*0.1
        GOTO21
     20 VGE=(VE2(M)-VE1(M))*0.1
        VGE=VGE+(VE2(MP1)+VE1(M)-VE1(MP1)-VE2(M))*TIN*0.1
        VGN=(VN2(M)-VN1(M))*0.1
        VGN=VGN+(VN2(MP1)+VN1(M)-VN1(MP1)-VN2(M))*TIN*0.1
     21 DELHM=H(K)-90.
        VE=VE2(     M)+VGE*DELHM+(VE2(    MP1)-VE2(     M))*TIN
        VN=VN2(     M)+VGN*DELHM+(VN2(    MP1)-VN2(     M))*TIN
        UMEAN(K)=VE*TL+VN*TM
```

```
      IF(SENSESWITCH1)304,299
  299 IF(UMEAN(K))300,301,301
  300 IF(U(K))304,304,302
  301 IF(U(K))302,304,304
  302 INUM=INUM+1
      IF(INUM- 3)304,303,303
303PRINT902,UR,UMEAN(1),UMEAN(2),UMEAN(3),U(1),U(2),U(3),LTH

  902 FORMAT(F7.0,2X6F5.0,I5)
  304 UT(K)=U(K)-UMEAN(K)
      K=K+1
      IF(K- 3)18,18,22
   22 L=TL*100.
      M=TM*100.
      LR=100.0*RL
      MR=100.0*RM
      X(3)=X(2)-X(1)
 PUNCH9,UR,MY,MO,JO,LT,UT(1),UT(2),UT(3),L,M,LR,MR,IR,IH,X(1
),X(2),X(3)
    9 FORMAT(F7.0,3I3,I5,3F5.0,4I3,2I4,3F5.2)
      GOTO1
    3 STOP
      END
```

```
C      1200B   UNIVERSITY OF ADELAIDE  PHYSICS DEPT    ROPER  31
3
C      PROCESSES 1200A OUTPUT TO PRINT OUT VELOCITY DIFFERENCE
S AND
C      TURBULENT VELOCITIES AS A FUNCTION OF SEPARATION.
C      CALCULATES THE SCALE OF THE ENERGY BEARING EDDIES.
C      CALCULATES THE PARAMETERS OF REFLECTION POINT MOTION.
DIMENSIONUT(3),X(3),A(20),DELSE(20),USEP(3),SUSEP(20),ATUR(3
),BTUR(3)
DIMENSIONSATUR(20),SBTUR(20),NUM(20)
  199 READ50
  500 FORMAT(30H                                   )
      PRINT50
      DO41J=1,20
      A(J)=0.
      DELSE(J)=0.
      SUSEP(J)=0.
      SATUR(J)=0.
      SBTUR(J)=0.
   41 NUM(J)=0
      DIV=0.0
      EROR1=0.0
      EROR2=0.0
      NO=0
      ROTMA=0.
      ROTME=0.
      ROTSQ=0.
      S=0.
      SERGS=0.
      SOROT=0.
      SUMG=0.0
      TOTUR=0.
      READ400,CALEH
  400 FORMAT(F6.1)
    1 READ2,UR,LT,UT(1),UT(2),UT(3),R,X(1),X(2),X(3)
    2 FORMAT(F7.0,9X15,3F5.0,12XF4.0,4X3F5.2)
      IF(UR)3,4,5
    5 USEP(1)=UT(2)-UT(1)
      USEP(2)=UT(2)-UT(3)
      USEP(3)=UT(1)-UT(3)
      ATUR(1)=UT(2)
      ATUR(2)=UT(2)
      ATUR(3)=UT(1)
      BTUR(1)=UT(1)
      BTUR(2)=UT(3)
      BTUR(3)=UT(3)
      L=1
```

```
115 J=1
118 A(J)=1+2*(J-1)
    IF(ABSF(X (L))-0.1*A(J))119,119,120
119 DELSE (J)=DELSE (J)+USEP(L)**2
    SUSEP(J)=SUSEP(J)+ATUR (L)*BTUR (L)
    SATUR (J)=SATUR (J)+ATUR (L)**2
    SBTUR (J)=SBTUR (J)+BTUR (L)**2
    NUM(J)=NUM(J)+1
    TOTUR=TOTUR+UT(L)**2
    S=S+1.0
    IF(J-3)121,123,123
123 ROTIO=R*(USEP(L)/X(L))*1.E-3
    IF(ABSF(ROTMA )-ABSF(ROTIO ))70,70,71
 70 ROTMA =ROTIO
 71 ROTME=ROTME+ROTIO
    ROTSQ=ROTSQ+ROTIO **2
    SOROT=SOROT+1.0
    GOTO121
120 J=J+1
    IF(J-20)118,118,121
121 L=L+1
    IF(L-   3)115,115,122
122 NO=NO+1
    GOTO1
  4 PRINT820,NO
820 FORMAT(13HNO OF METEORS16//)
    PRINT30
 30 FORMAT(39HSEPARATION DELV  G    DELG  RMSGRAD    NO/)
    AMAX=0.
    DO663J=1,20
    IF(AMAX-A(J))664,664,663
664 AMAX=A(J)
663 JA=AMAX/2.0+0.55
    DO700J=1,JA
    AUM=NUM(J)
    IF(NUM(J))200,200,201
200 RMSDE=0.
    GOTO202
201 RMSDE=SQRTF(DELSE(J)/AUM)
202 C=J
    A(J)=0.1*(1.0+2.0*(C-1.0))
    GRAD=RMSDE/A(J)
    IF(NUM(J)-9)240,240,241
240 G=0.
    DELG=0.0
    GOTO70
241 G    =SUSEP(J)/SQRTF(SATUR (J)*SBTUR (J))
```

```
      DELG=(1.0-G*G)/SQRTF(AUM-1.0)
      IF(J-12)243,243,70
243   IF(J-3)700,244,244
244   ERGS    =((RMSDE    /0.83)**3)/A(J)
      SERGS=SERGS+ERGS    **2
      SUMG=SUMG+(A(J)-0.1)/(1.0-G)**1.5         .
      EROR1=EROR1+(A(J)-0.1)/(1.0-G+DELG)**1.5
      EROR2=EROR2+(A(J)-0.1)/(1.0-G-DELG)**1.5
      DIV=DIV+1.0
700   PRINT31,A(J),RMSDE,G,DELG,GRAD,NUM(J)
 31   FORMAT(1XF6.2,2XF6.2,F5.2,F5.3,1XF6.2,I7)
      IF(DIV)199,199,755
755   ENERG=SQRTF(SERGS/DIV)
      TYD=EXP(LOG(ENERG*CALEH)/3.0)*0.83
      ENVEL=SQRTF(TOTUR/S)
      SIZE=ENVEL**3/(ENERG *0.57)
      ROTME=ROTME/SOROT
      ROTSQ=SQRTF(ROTSQ/SOROT)
      SUMG=SUMG/DIV
      EROR1=EROR1/DIV
      EROR2=EROR2/DIV
      PRINT35,ENVEL,SIZE,CALEH
35FORMAT(3HUO=F8.2,6H M/SEC,//3HLO=F7.1,3H KM//6HSCALE F6.1,
3H KM//)
      PRINT34,ENERG,        TYD,ROTME,ROTMA,ROTSQ
34FORMAT(5HERGS=F6.0,11HERGS/GM/SEC,   //3HVZ=F6.2,5HM/SEC//3
HRM=3F8.2//)
      PRINT36,SUMG,EROR1,EROR2
 36   FORMAT(//11HLO FROM G =F7.1,5H KM (2F7.1,2H )//)
      PAUSE
      GOTO199
  3   STOP
      END
```

```
C       1200C  UNIVERSITY OF ADELAIDE  PHYSICS DEPT.   ROPER  313
C       READS OUTPUT FROM 1200A AND PRINTS ZENITH DEPENDENCE
  DIMENSION         ZUTUR(20),NN(20),TGZ(20),NNG(20),UT(3),X(3),US
  EP(3)
  199 READ50
  500 FORMAT(30H                              )
      PRINT50
      DO41J=1,20
      TGZ(J)=0.
      NN(J)=0
      ZUTUR(J)=0.
   41 NNG(J)=0
      NIXZ=0
      NO=0
 1 READ2,UR,LT,UT(1),UT(2),UT(3),WL,WM,R,X(1),X(2),X(3)
    2 FORMAT(F7.0,9XI5,3F5.0,2F3.2,6XF4.0,4X3F5.2)
      IF(UR)3,4,5
    5 COZR=SQRTF(1.-WL*WL-WM*WM)
      USEP(1)=UT(2)-UT(1)
      USEP(2)=UT(2)-UT(3)
      USEP(3)=UT(1)-UT(3)
      J=1
  128 C=J
      IF(ABSF(COZR)-0.05*C)129,129,131
  129 DO130K=1,3
      ZUTUR (J)=ZUTUR (J)+UT(K)**2
  130 NN(J)=NN(J)+1
      GOTO132
  131 J=J+1
      IF(J-20)128,128,132
  132 L=1
  447 IF(ABSF( X(L))-0.3)448,449,449
  448 NIXZ=NIXZ+1
      GOTO450
  449 TGZ(J)=TGZ(J)+(USEP(L)/X (L))**2
      NNG(J)=NNG(J)+1
  450 L=L+1
      IF(L-    3)447,447,451
  451 NO=NO+1
      GOTO1
    4 PRINT820,NO
  820 FORMAT(13HNO OF METEORSI6//)
      PRINT33
   33 FORMAT(22H COZR RMSVT RMSTG  NO./)
      DO701J=1,20
      ANG=NNG(J)
      IF(NNG(J))250,250,251
```

```
250 RMSTG=0.
    GOTO252
251 RMSTG=SQRTF(TGZ(J)/ANG)
252 CONTINUE
    AN=NN(J)
    IF(NN(J))210,210,211
210 RMSZU=0.
    GOTO212
211 RMSZU      =SQRTF(ZUTUR (J)/AN)
212 CONTINUE
    C=J
    C=C/20.0
701 PRINT32,C,RMSZU,RMSTG,NN(J)
 32 FORMAT(F5.2,2F6.2,I4)
    PRINT777,NIXZ
777 FORMAT(//5HNIXZ=I6//)
    PAUSE
    GOTO199
  3 STOP
    END
```

```
C      1200D  UNIVERSITY OF ADELAIDE  PHYSICS DEPT  ROPER  313

C      PROCESSES 1200A OUTPUT TO PRODUCE HEIGHT DEPENDENCE
C      CALCULATES VERTICAL CORRELATION DISTANCE FROM THE TCHEN
SHEAR LAW
       DIMENSIOND(20),HDEL(3),VLESS(3),USEP(3),HUSEP(3),DELUH(20
),VERTA(3)
       DIMENSIONVERTB(3),SATH(20),SBTH(20),NUMH(20),SUH(20),UT(
3),X(3)
       DIMENSIONATURB(3),BTURB(3)
    10 READ10
   100 FORMAT(30H                                       )
       PRINT10
       DO41J=1,20
       DELUH(J)=0.0
       SUH(J)=0.0
       SATH(J)=0.0
       SBTH(J)=0.0
       NUMH(J)=0
    41 CONTINUE
       A=0.0
       DMAX=0.0
       CALEM=0.0
       SUMC=0.0
       NO=0
       READ500,ERGS,ENVEL,TYD,CALEH
   500 FORMAT(4F8.1)
       PRINT500,ERGS,ENVEL,TYD,CALEH
     1 READ2,UR,UT(1),UT(2),UT(3),TL,TM,RL,RM,WH,X(1),X(2),X(3
)
     2 FORMAT(F7.0,14X3F5.0,4F3.2,4XF4.0,3F5.2)
       IF(UR)3,4,5
     5 RNU=SQRTF(1.0-RL*RL-RM*RM)
       COZR=SQRTF(1.0-TL*TL-TM*TM)
       SNZ=SQRTF(1.0-COZR*COZR)
       USEP(1)=UT(2)-UT(1)
       USEP(2)=UT(2)-UT(3)
       USEP(3)=UT(1)-UT(3)
       ATURB(1)=UT(2)
       ATURB(2)=UT(2)
       ATURB(3)=UT(1)
       BTURB(1)=UT(1)
       BTURB(2)=UT(3)
       BTURB(3)=UT(3)
       L=1
    85 HDEL(L)=X(L)*RNU
```

```
          J=1
    88  D(J)=1+2*(J-1)
        IF(ABSF(HDEL(L))-.05*D(J))89,89,90
    89  DELUH(J)=DELUH(J)+ USEP(L)* USEP(L)
        VERTA(L)=(ABSF(ATURB(L))-TYD*COZR)/SNZ
        VERTB(L)=(ABSF(BTURB(L))-TYD*COZR)/SNZ
        SUH(J)=SUH(J)+VERTA(L)*VERTB(L)
        SATH(J)=SATH(J)+VERTA(L)*VERTA(L)
        SBTH(J)=SBTH(J)+VERTB(L)*VERTB(L)
        NUMH(J)=NUMH(J)+1
        GOTO91
    90  J=J+1
        IF(J-20)88,88,91
    91  L=L+1
        IF(L-    3)85,85,92
    92  NO=NO+1
        GOTO1
     4  PRINT599,NO
   599  FORMAT(13HNO OF METEORSI6)
        PRINT60
   600  FORMAT(5X20HDELH  DELV     GH  NO/)
        DO161J=1,20
        IF(DMAX-D(J))165,165,161
   165  DMAX=D(J)
   161  CONTINUE
        JA=DMAX/2.0+0.55
        DO169J=1,JA
        D(J)=1+2*(J-1)
        D(J)=.05*D(J)
   169  CONTINUE
        DO700J=1,JA
        AUMH    =NUMH(J)
        IF(NUMH(J))400,400,401
   400  RMSDH=0.
        GOTO402
   401  RMSDH=SQRTF(DELUH(J)/AUMH)
   402  CONTINUE
        IF(SUH(J))411,410,411
   410  GH=0.
        GOTO412
   411  GH    =SUH(J)/SQRTF(SATH(J)*SBTH(J))
   412  A=(RMSDH/(D(J)**0.6667))*AUMH+A
        SUMC=SUMC+AUMH
700PRINT8,D(J),RMSDH,GH,NUMH(J)
     8  FORMAT(2XF7.2,F6.2,F6.2,I4)
        CALEM=(ENVEL*SUMC/A)**1.50
        PRINT777,CALEM,SUMC
```

```
777 FORMAT(//5X6HSCALECF7.1,3H KM,3X1H(F6.0,2H ))
    PAUSE
    GOTO10
  3 STOP
    END
```

```
C      1200E UNIVERSITY OF ADELAIDE  PHYSICS DEPT  ROPER  313

C      PROCESSES 1200A OUTPUT TO PRINT TIME DEPENDENCE
C      PRINTS AND PUNCHES NORTHERLY AND EASTERLY TURBULENT WIN
D
C      COMPONENTS HOUR BY HOUR.
       DIMENSIONSUTE(24),SUTN(24)
       DIMENSIONUT(3),X(3),AM(24),BM(24),STGM(24),USEP(3)
   199 READ50
   500 FORMAT(30H                                    )
       PRINT50
       DO10M=1,24
       BM(M)=0.0
       SUTE(M)=0.0
       SUTN(M)=0.0
       STGM(M)=0.0
    10 AM(M)=0.0
       NME=0
       NO=0
       READ100,ERGS,ENVEL,TYD,CALEH
   100 FORMAT(4F8.1)
       PRINT100,ERGS,ENVEL,TYD,CALEH
     1 READ2,UR,LT,UT(1),UT(2),UT(3),TL,TM,X(1),X(2),X(3)
     2 FORMAT(F7.0,9X15,3F5.0,2F3.2,14X3F5.2)
       IF(UR)3,4,5
     5 M=LT/10
       M=M+1
       USEP(1)=UT(2)-UT(1)
       USEP(2)=UT(2)-UT(3)
       USEP(3)=UT(1)-UT(3)
       COZR=SQRTF(1.0-TL*TL-TM*TM)
       SNZ=SQRTF(1.0-COZR*COZR)
       DO469K=1,3
       SUTE(M)=SUTE(M)+(((ABSF(UT(K))-TYD*COZR)/SNZ)*(TL/SNZ))
  **2
       SUTN(M)=SUTN(M)+(((ABSF(UT(K))-TYD*COZR)/SNZ)*(TM/SNZ))
  **2
       BM(M)=BM(M)+1.
   469 CONTINUE
       L=1
   470 IF(ABSF(X (L))-0.3)471,472,472
   471 NME=NME+1
       GOTO473
   472 STGM(M)=STGM(M)+(USEP(L)/X (L))**2
       AM(M)=AM(M)+1.
   473 L=L+1
```

```
      IF(L-    3)470,470,120
120 NO=NO+1
      GOTO1
  4 PRINT820,NO
820 FORMAT(//13HNO OF METEORSI6//)
      PRINT9
  9 FORMAT(8X40HTIME    RMSVTE  RMSVTN    NO  RMSTG    NO/)

      DO700M=1,24
      NBM    =BM(M)+0.5
      IF(BM(M))480,480,481
480 RSUTE=0.0
      RSUTN=0.0
      GOTO482
481 RSUTE=SQRTF(SUTE(M)/BM(M))
      RSUTN=SQRTF(SUTN(M)/BM(M))
482 CONTINUE
      NAM    =AM(M)+0.5
      IF(AM(M))483,483,484
483 RSTGM=0.0
      GOTO485
484 RSTGM    =SQRTF(STGM(M)/AM(M))
485 CONTINUE
      NIM=(M-1)*10
      NIME=M*10
      LEVEL=2
      PUNCH202,LEVEL,RSUTE,RSUTN
202 FORMAT(4XI3,6XF5.0,5XF5.0)
700 PRINT8,NIM,NIME,RSUTE,RSUTN,NBM,RSTGM,NAM
  8 FORMAT(2XI5,2H -I5,F7.2,F8.2,I6,F7.2,I6)
      PRINT777,NME
777 FORMAT(//5X3HNMEI7)
      PAUSE
      GOTO199
  3 STOP
      END
```

BIBLIOGRAPHY

Attree, V., H., Electronic Engineering, 27, 174, 1955.

Batchelor, G., K., The Theory of Homogeneous Turbulence, Cambridge University Press, 1953.

Blamont, J., E., and de Jager, C., Ann. de Geophys., 17, 134, 1961.

Booker, H., G., and Cohen, R., Jour. Geophys. Res., 61, 707, 1956.

Bolgiano, R., Jour. Geophys. Res., 64, 2226, 1959.

Chamanlal and Venkataraman, K., Electrotechnics, 14, 28, 1941.

Corrsin, S., Jour. Geophys. Res., 64, 2134, 1959.

Defant, A., Geograf. Ann., 3, 209, 1921.

Dougherty, J., P., Jour. Atmos. Terr. Phys., 21, 210, 1961.

Elford, W., G., and Robertson, D., S., Jour. Atmos. Terr. Phys., 4, 271, 1953.

Elford, W., G., Ph. D. Thesis, University of Adelaide, 1954.

Gossard, E., Jour. Geophys. Res., 67, 745, 1962.

Greenhow, J., S., and Neufeld, E., L., Proc. Phys. Soc., 74, 1, 1959.

Greenhow, J., S., and Neufeld, E., L., Jour. Geophys. Res., 64, 2129, 1959a.

Greenhow, J., S., and Neufeld, E., L., Jour. Atmos. Terr. Phys., 16, 384, 1959b.

Greenhow, J., S., and Neufeld, E., L., Proc. Phys. Soc., 482, 228, 1960.

Gregory, J., B., Jour. Geophys. Res., 66, 429, 1961.

Groves, G., V., Data Note 5, Dept. of Physics, University College, London, 1959.

Herlofson, N., Rep. Phys. Soc. Progr. Phys., 11, 444, 1948.

Hines, C., O., Jour. Geophys. Res. 64, 2210, 1959.

Hey, J., S., and Stewart, G., S., Proc. Phys. Soc., 59, 858, 1947.

Hutchings, J., W., Jour. Met., 12, 263, 1955.

Karman, T., von and Howarth, L., Proc. Roy. Soc. London, 164, 192, 1938.

Kaiser, T., R., and Closs, R., L., Phil. Mag., 43, 1, 1952.

Kaiser, T., R., Mon. Not. Roy. Astron. Soc., 114, 39, 1954.

Kaiser, T., R., Spec. Suppl. Jour. Atmos. Terr. Phys., 2, 55, 1955.

Kolmogoroff, A., C. R. Acad. Sci. U.R.S.S., 30, 301, 1941.

Liller, W., and Whipple, F., L., Spec. Suppl. Jour. Atmos. Terr. Phys., 1, 112, 1954.

Long, R., R., Jour. Geophys. Res., 64, 2151, 1959.

Lovell, A., C., B., and Clegg, J., A., Proc. Phys. Soc., 60, 491, 1948.

Mainstone, J., S., Mon. Not. Roy. Astron. Soc., <u>120</u>, 517, 1960.

Manning, L., A., Villard, O., G., and Peterson, A., M., Proc. Inst. Radio Engrs. N. Y., <u>38</u>, 877, 1950.

Manning, L., A., Jour. Geophys. Res., <u>64</u>, 1415, 1959.

McCready, P., B., Jour. Met., <u>10</u>, 434, 1953.

Ogura, Y., Jour. Met. Soc. Japan, <u>31</u>, 355, 1953.

Rao, M., S., Can. Jour. Phys., <u>36</u>, 840, 1958.

Rao, M., S., and Armstrong, R., L., Can. Jour. Phys., <u>36</u>, 1601, 1958.

Robertson, D., S., Liddy, D., and Elford, W., G., Jour. Atmos. Terr. Phys., <u>4</u>, 225, 1953.

Rofe, B., Tech. Memo. S. A. D. 125, Dept. of Supply, W.R.E., South Aust., 1961.

Sheppard, P., A., Jour. Geophys. Res., <u>64</u>, 2086, 1959.

Skellet, A., M., et al, Proc. Inst. Radio Engrs., <u>2</u>, 1935, 1932.

Stewart, R., W., Jour. Geophys. Res., <u>64</u>, 2112, 1959.

Taylor, R., J., Aust. Jour. Phys., <u>8</u>, 535, 1955.

Tchen, C., M., Phys. Rev., <u>94</u>, 4, 1954.

Weizsacker, C., F., von, Z. Phys., <u>124</u>, 614, 1948.

Whitehead, D., Jour. Atmos. Terr. Phys., <u>20</u>, 49, 1961.

Zimmerman, S., P., Ann. de Geophys., <u>18</u>, 116, 1962.